Design and Validation of a Hip and Quadriceps Assembly Mechanism for a Knee Squat Simulator

by
Ebard Joubert

Thesis presented in partial fulfilment of the requirements for the degree of Master of Engineering (Mechatronic) in the Faculty of Engineering at Stellenbosch University

Supervisor: Dr Johan van der Merwe
Co-supervisor: Dr Jacobus H. Müller

March 2020

Declaration

By submitting this thesis electronically, I declare that the entirety of the work contained therein is my own, original work, that I am the sole author thereof (save to the extent explicitly otherwise stated), that reproduction and publication thereof by Stellenbosch University will not infringe any third party rights and that I have not previously in its entirety or in part submitted it for obtaining any qualification.

Date: March 2020

Abstract

Given the prevalence of osteoarthritis, knee implants are continuously being improved. In vitro experiments can be used to evaluate the performance of an implant by investigating biomechanical behaviour of the knee joint inside a dynamic knee simulator that reproduces knee loading by inducing a force on the quadriceps muscles. This dissertation deals with the design and verification of such a knee simulator that can autonomously perform a squat motion. Artificial knees were constructed to be tested in the machine, with a posterior stabilised knee implant fixed to it. An optical position sensor was used to track the motion of the knee joint in order to describe the relative motion between components in the joint. Knee kinematics and the quadriceps forces were evaluated and validated against previous literature findings. The knee simulator was proved to deliver repeatable results and the artificial knees demonstrated accurate biomechanical behaviour while performing squat motions.

Uittreksel

Knie vervangings word voortdurend verbeter en bestudeer as gevolg van die algemene voorkoms van osteoartritis in die gewrig. In vitro eksperimente kan gebruik word om die werking van knie vervangings te evalueer deur die biomeganiese gedrag van die kniegewrig binne ‘n dinamiese kniesimulator te ondersoek. So ‘n simulator reproduseer die kniebelading deur ‘n krag op die quadriceps-spiere te induseer. Hierdie proefskrik handel oor die ontwerp en verifikasie van so ‘n kniesimulator wat automaties ‘n hurkbeweging kan uitvoer. Kunsmatige knieë met ‘n posterior gestabiliseerde knie-inplantaat is gebou om in die masjien getoets te word. ‘n Optiese posisiesensor is gebruik om die beweging van die kniegewrig te meet sodat die relatiewe beweging tussen komponente in die gewrig beskryf kon word. Knie kinematika en die quadriceps-kragte is geëvalueer en bevestig deur dit met vorige literatuurbevindings te vergelyk. Daar is bewys dat die kniesimulator herhaalbare resultate gelewer het, en dat die kunsmatige knieë akkurate biomeganiese gedrag getoon het terwyl hulle hurkbewegings uitgevoer het binne die simulator.

Acknowledgements

I would like to specially thank Dr Johan van der Merwe for all his time and guidance throughout this project. Thank you for allowing me to make mistakes and providing guidance when necessary. Dr Cobus Müller, thank you for all your guidance as well. Thank you for the financial support you two provided, it is much appreciated.

To Dr Pieter Erasmus, I appreciate your time, guidance and generosity. Thank you for always being willing to help.

To all my friends, thank you for being part of this journey, supporting me all the way. Thank you for all the office, corridor and Wombats cricket sessions when we actually should have worked. I would not have been who I am today without you guys.

To my wife, Jeanette, thank you for all your support, love and always believing in me! Thank you that I can always just be myself when I am with you. My appreciation for you cannot be expressed enough.

To my parents, thank you for making all of this possible! Thank you very much for your financial support, but more importantly, thank you for your love, compassion and believing in me. Thank you that you were always there from the start. Thank you for laying your lives down for your children so that we can make a success of our lives.

To the One who holds everything together, thank you Father for your love, favour and faithfulness. Thank you for new joy every day.

Table of Contents

List of Figures

List of Tables

Nomenclature

Abbreviations

3D – Three Dimensional

ACL – Anterior Cruciate Ligament

ACS – Anatomical Coordinate System

ANOVA – Analysis of Variance

AP – Anterior-Posterior

BW – Body weight

CAD – Computer-Aided Design

CoCr – Cobalt-Chromium

CR – Coefficient of Repeatability

CT – Computed Tomography

DCM – Direction Cosine Matrix

DOF – Degrees of Freedom

EMG – Electromyography

FE – Flexion-Extension

IE – Internal-External

IR – Infrared

LCL – Lateral Collateral Ligament

Max. – Maximum

MCL – Medial Collateral Ligament

MCU – Microcontroller

ML – Medial-Lateral

MR – Magnetic Resonance

NC – Normally Closed

NO – Normally Open

OA – Osteoarthritis

OKR – Oxford Knee Rig

PCL – Posterior Cruciate Ligament

PEEK – Polyether Ether Ketone

PFJ – Patellofemoral Joint

PID – Proportional, Integral, Derivative

PS – Posterior Stabilizing

PT – Patella Tendon

PTMA – Patella Tendon Moment Arm

RDOF – Rotational Degrees of Freedom

RKTS – Robotic Knee Testing Systems

ROM – Range of Motion

SD – Standard Deviation

SI – Superior/inferior

TFJ – Tibiofemoral Joint

Ti – Titanium

TKA – Total Knee Arthroplasty

TVS – Transient Voltage Suppressor

v/v – Volume-per-volume

VPP – Vertical Position of the Patella

VV – Varus-Valgus

w/w – Weight-per-weight

Chapter 1

1. Introduction

1.1. Background

The human knee is a complex and important joint consisting of multiple bones and soft tissue structures. The two articulating areas in the knee are the tibiofemoral joint (TFJ) and the patellofemoral joint (PFJ). According to Huberti and Hayes (1984), the reaction forces within the PFJ can be up to 6.5 times body weight. This shows the high demands placed on the contact surfaces in the knee joint for daily living.

The knee is one of the joints in the human body that is most affected by joint degradation (Anjum and Abbas, 2015). Osteoarthritis (OA), a major cause of joint degradation, occurs when the cushioning protective cartilage in joints wear down over time to cause discomfort. Joint replacement surgery, or arthroplasty, is a common surgical treatment for OA intended to relieve pain and restore a patient's quality of life by replacing the articulating surfaces of the knee with a prosthesis.

According to the Organization for Economic and Co-operation Development (OECD) health statistics for its 35 member countries, including South Africa, 2.6 million total knee arthroplasty (TKA) surgeries were performed in 2015. This is just a fraction of the worldwide figures and gives an indication of how many people rely on knee implants to reduce pain and increase mobility.

1.2. Motivation

Given the prevalence of OA, implants are continuously being improved and it is necessary to investigate their performance. This can be done by in vivo clinical trials or in vitro experiments. Knee replacement performance metrics include biomechanical parameters such as flexion range of motion, joint contact forces and muscle forces. These performance measures are typically evaluated during in vitro experimental trials. The performance of pre-TKA can be compared with post-TKA to directly see the improved or worsened performance as a result of the prosthesis. Implant performance can also be measured in terms of patient satisfaction on the basis of pain relief and functional outcomes. Clinical outcomes are typically evaluated during in vivo trials.

A dynamic knee simulator that reproduces knee loading by inducing a force on the quadriceps muscle can be used to evaluate in vitro performance and further expedite implant design. It is intended to help study the interaction between different anatomic components of the knee, the articulating forces between these

components, the performance of implants and to increase the understanding of knee biomechanics.

1.3. Objectives and Aims

A first iteration of the mechanical design of a squat simulating machine was developed at Stellenbosch University. The design was based on the Oxford Knee Rig (Zavatsky, 1997) with the intention to better simulate a natural squat. However, the machine was partially incomplete and non-functional.

The aim of this study was thus to complete and verify a squat simulator with which to facilitate further research in knee biomechanics and implants. The main objectives were as follows:

- Use literature to gain knowledge on the knee joint, existing squat simulators and bone cuts.
- Complete the existing squat simulator, including an effective controller, so that it can function with an artificial knee.
- Build an artificial knee.
- Implement a position sensor to describe relative motion of the knee joint.
- Verify the functioning of the squat simulator against previous literature findings for quadriceps forces, the effect of the position of the patella and knee joint motion.

Chapter 2

2. Literature Study

2.1. Knee Anatomy and Physiology

The knee is the largest and one of the most complex joints in the human body. It acts as a hinge that is located between the femur (upper leg) and tibia (lower leg). The knee must be able to transfer heavy loads while staying stable and endure a great deal of flexibility. It plays a vital role in human mobility and a wide range of everyday activities.

2.1.1. Anatomical Directional Reference System

To describe movement and locations in the human body, an anatomical reference system is required. This reference system is based on the anatomical planes in the human body as seen in Figure 1.

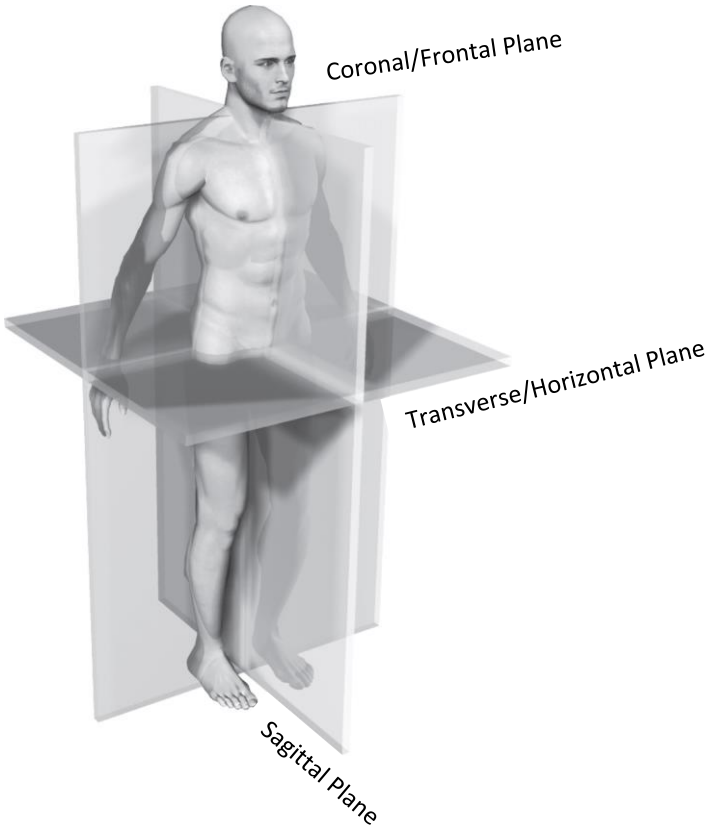

Figure 1: Human Anatomical Planes (Affatato, 2014)

The body is divided into three main planes, and are further divided to refer to the relative position of two different body parts (Platzer, Kahle and Leonhardt, 1986):

- The coronal plane divides the body in an anterior (front) and posterior (back) section.
- The sagittal plane divides the body into left and right. Medial is towards the midline/sagittal plane and lateral means away from the middle.
- The transverse plane divides the body into a superior (upper) and inferior (lower) section.

Two other common terms are proximal (closer to the centre) and distal (further away from the centre). The ankle is thus distal and the hip proximal to the knee joint, with the centre of the body as reference. Additionally, varus/adduction refers to the inward angulation of a limb (knock-kneed), where valgus/abduction means the opposite (bow-legged).

2.1.2. Bones

The three bones involved in the knee joint are the femur, tibia and patella. In addition, the fibula is located next to the tibia in the lower leg and is important for the insertion of some knee ligaments and muscles. Figure 2 shows an illustration of these bones as they form the two articulating joints: the patellofemoral joint (PFJ) and tibiofemoral joint (TFJ).

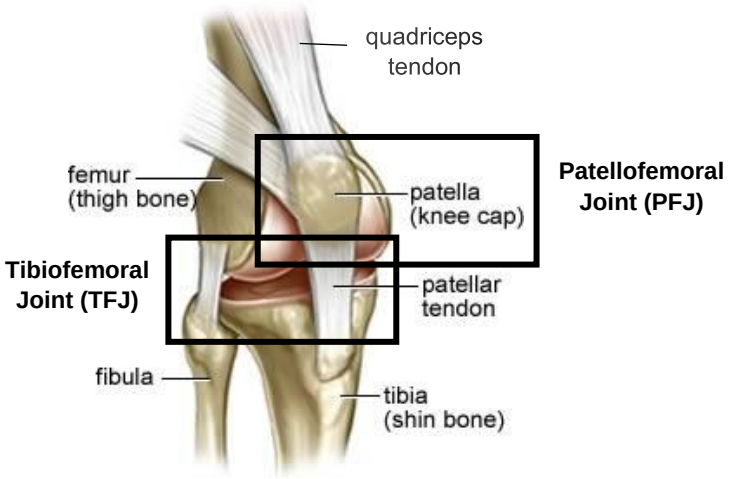

Figure 2: Knee Bones and the Articulating Surfaces (Adapted from: Carter, 2015)

The Femur

The femur is the longest, strongest and heaviest human bone, with a length varying from one fourth to one third of the human body (O'Rahilly, Müller, Carpenter and Swenson, 2008). The superior end of the femur is the ball part of the ball-and-socket hip joint and the inferior end is the top part of the knee joint. It consists of the medial and lateral condyles which are separated by the intercondylar notch. These condyles are covered by a cartilage layer and experience high contact forces (Saxby *et al.*, 2016). The condyles form a groove-like surface anteriorly, called the trochlear groove of the femur, that guides and articulates with the patella during flexion and extension. The epicondyles are the rounded eminence on the sides of the femoral condyles.

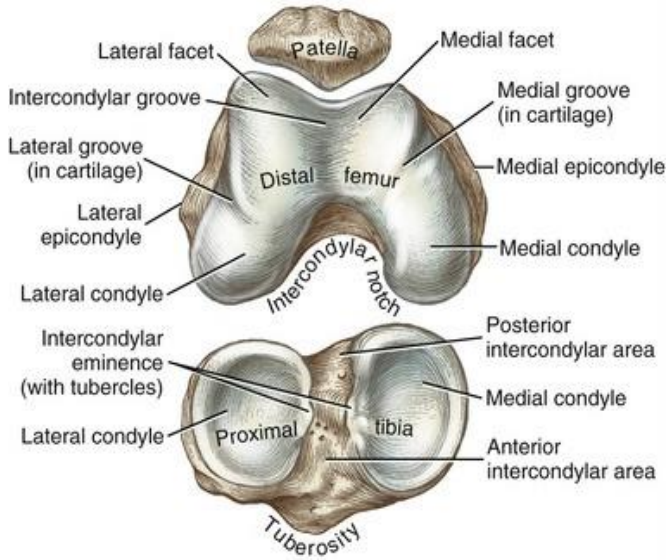

Figure 3: Articular Surfaces of the Inferior Femur and Superior Tibia (Neumann, 2015)

The Tibia

The tibia, or shin bone, transmits the weight from the femur to the foot and measures one fourth to one fifth of a body's total length (O'Rahilly *et al.*, 2008). The superior end of the tibia is the bottom part of the knee joint and articulates with the inferior end of the femur. The lateral and medial tibial condyles articulate with the corresponding femoral condyles. Figure 3 shows how the condyles fit into each other. The cruciate ligaments attach at the intercondylar eminence and the patellar tendon attaches to the tibial tuberosity.

The Fibula

The fibula is a slender bone that does not functionally contribute to the knee. It does however support the lateral tibia and superiorly serves as an attachment point for the lateral collateral ligament and one of the hamstrings, the biceps femoris muscle.

The Patella or Kneecap

The patella (meaning “small plate” in Latin) is an independent sesamoid bone fixed to the tendon of the quadriceps femoris muscle. It has a triangular-like shape having an apex and a base, as shown in Figure 4. The patella plays an important role in knee functioning as it increases the lever arm of the extensor mechanism. It thus reduces the required quadriceps force during knee extension.

The posterior surface of the patella is protected by articular cartilage that can be up to 5 mm thick (Neumann, 2015). The medial and lateral facets of the cartilage articulate with the trochlear groove of the femur. Compression forces up to 6.5 times body-weight have been measured at these articulating surfaces (Huberti and Hayes, 1984).

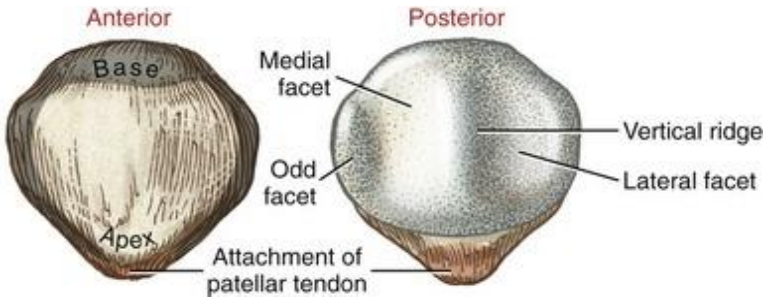

Figure 4: Anterior and Posterior Surfaces of the Patella (Neumann, 2015)

To define the position of the patella in the sagittal plane, the Insall-Salvati ratio was developed. This is a ratio of the length of the patellar tendon to the greatest diagonal length of the patella (Insall and Salvati, 1971). Although there are variations, the generally accepted definitions are that a ratio around 1.0 is normal, less than 0.8 is patella baja (low riding patella) and a ratio greater than 1.2 is patella alta (high riding patella) (Loudon, 2016).

The position of the patella plays an important role in the functioning of the knee. Patella alta can cause patellofemoral pain, patella dislocation and knee effusion

(Ali, Helmer and Terk, 2009). Patella baja restricts range of motion and results in greater quadriceps and patellofemoral forces (Nakamura *et al.*, 2017).

2.1.3. Articular Cartilage and Menisci

Articular cartilage is found where bone surfaces move against each other. It is a slippery and viscoelastic substance which facilitates motion in joints by reducing friction between sliding surfaces and functions as a damper to prevent bone-on-bone contact.

The menisci and some nearby ligaments are shown in Figure 5. The menisci provide additional protection against the heavy loads acting on the knee joint by further reducing compressive stresses across the tibiofemoral joint. Compression forces in the tibiofemoral joint can easily reach three times body weight just through normal walking (Neumann, 2015). The menisci nearly triples the joint contact area and thus significantly reduce the force per unit area on the articular cartilage. Other functions include stabilization, articular cartilage lubrication, providing proprioception (the awareness of a joint's position) and joint surface guidance during motion (Neumann, 2015).

These supporting and protective surfaces wear out with age and bone-on-bone contact can occur (osteoarthritis). This results in joint pain and limited range of motion.

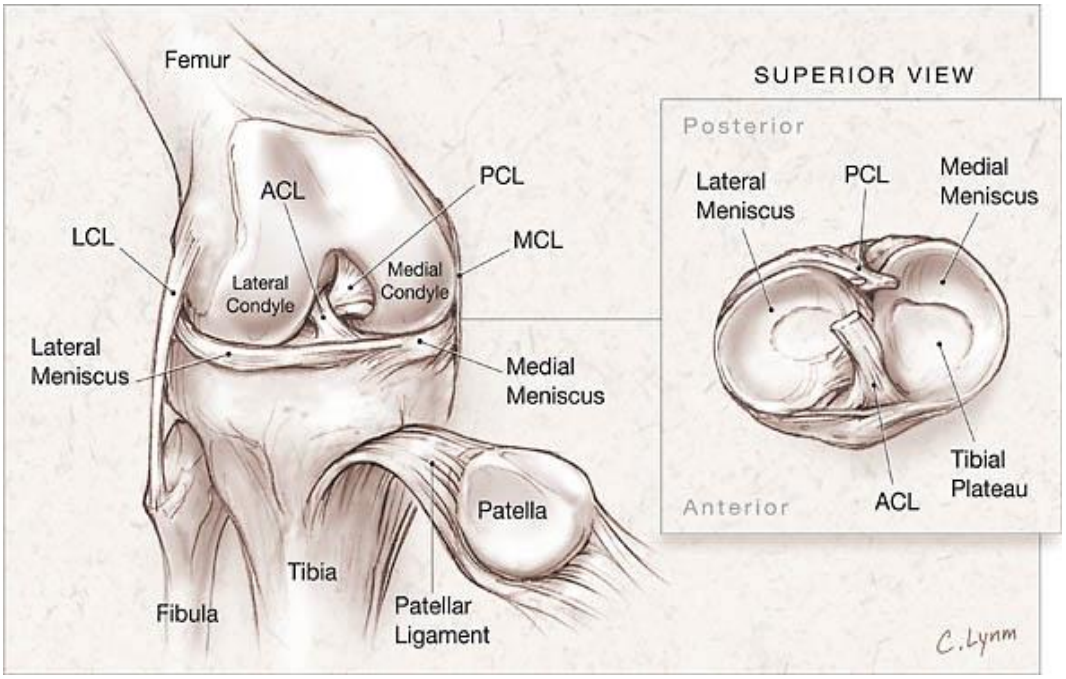

Figure 5: Right Knee with Ligaments and Menisci (Solomon *et al.*, 2006)

2.1.4. Ligaments and Tendons

Tendons and ligaments are often confused with one another. According to Mosby's Medical Dictionary, a ligament is an elastic and flexible fibrous tissue that bind joints together (bone to bone), whereas a tendon is inelastic and connect muscles to bone (Anderson, 2012). Both facilitate movement, serves as support and strengthen joints.

The length, shape and orientation of the knee ligaments all affect the joint kinematics. The two main ligament groups in the knee are the cruciate and the collateral ligaments. The anterior and posterior cruciate ligaments (ACL and PCL respectively) are located at the centre of the knee, while the medial and lateral collateral ligaments (MCL and LCL) are attached to the medial and lateral sides of the knee (Figure 5). The MCL is also called the tibial collateral ligament as it attaches to the tibia and the LCL is also called the fibular collateral ligament as it attaches to the fibula.

Anterior and Posterior Cruciate Ligaments

Cruciate, which means cross-shaped, describes the spacial relation of the ACL and PCL as they cross inside the femur's intercondylar notch. The anterior cruciate ligament starts at the tibia on the anterior end of the intercondylar eminence and attaches to the medial side of the lateral condyle of the femur. The ACL accounts for the primary constraint of the anterior tibial translation. The posterior cruciate ligament starts at the posterior end of the intercondylar eminence of the tibia. As it runs to the lateral side of the medial femoral condyle where it attaches, it crosses the ACL to form an 'X'. The PCL prevents the femur from sliding off the anterior edge of the tibia and prevents the tibia from shifting posteriorly to the femur. The PCL is about twice as thick as the ACL and consequently also much stronger (Peterson, 1994).

At any flexed knee position, at least one of the two cruciate ligaments are taut. This ensures the femur and tibia are held together and guides the knee during bending motion. Additionally, the ACL and PCL prevent hyperflexion and hyperextension, respectively.

Medial and Lateral Collateral Ligaments

The collateral ligaments are located on the inside and outside parts of the knee. They are called the medial (inside) collateral ligament (MCL) and the lateral (outside) collateral ligament (LCL) due to their anatomical locations as seen in Figure 5 and Figure 6.

The primary function of the collateral ligaments is to prevent the knee from excessive movement in the coronal plane. When the knee is fully extended, both

collateral ligaments are taut, with the MCL providing the primary resistance against abduction force and the LCL providing the primary resistance against adduction force (Neumann, 2015). The collateral ligaments thus stabilises the knee from sideways movement.

The MCL is a wide and flat band ligament with two attachment sites on the tibia, as seen in Figure 6 (b). As previously mentioned, the LCL distally attaches to the fibula. On the femur, the MCL and LCL attaches just anteriorly to the medial and lateral epicondyles respectively.

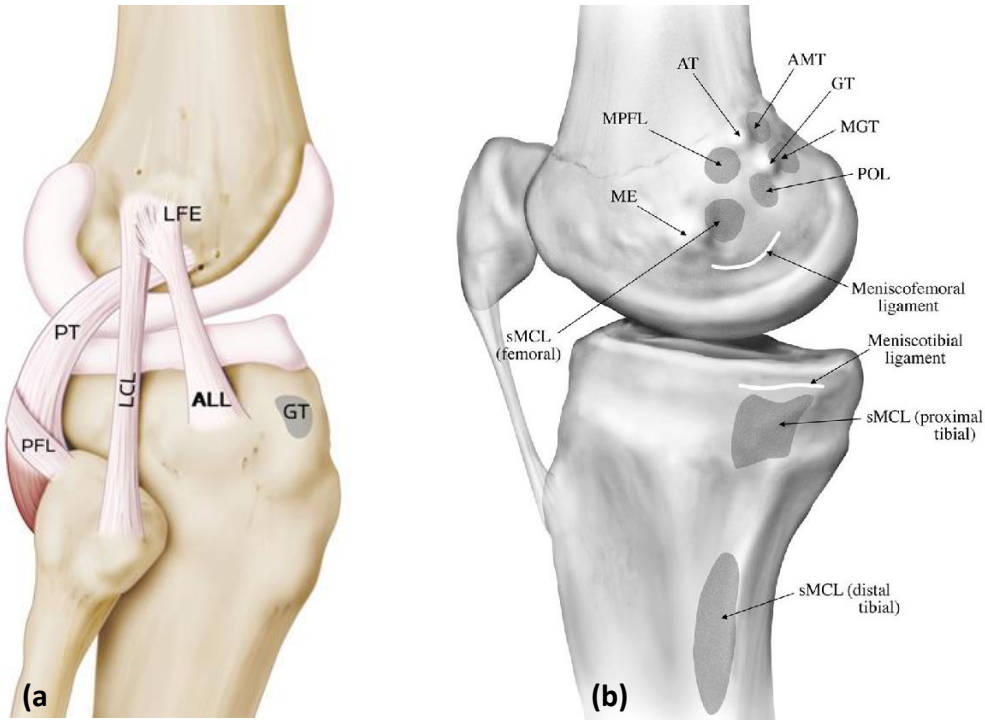

Figure 6: LCL and MCL Insertion Sites: a) Lateral View; b) Medial View (Adapted from: LaPrade et al., 2007; Claes et al., 2013)

Patellar and Quadriceps Tendons

The quadriceps tendon is proximal to the patella, with the patellar tendon distal to it. The quadriceps tendon transfers the quadriceps muscle's force to the patella to induce flexion and extension on the knee joint. A part of the quadriceps tendon covers the anterior surface of the patella and is continued as the patellar tendon until where it attaches at the tibial tuberosity. The patellar tendon is a strong and flat ligament with lengths ranging from 38 – 65 mm (Norman *et al.*, 1983). The

quadriceps muscle's force is transferred to the tibia via this ligament to extend the knee.

2.1.5. Muscles

Extensors and flexors are the two main muscle groups responsible for the knee-joint's movement and control. They work antagonistically to stabilise and move the knee joint.

Extensor Muscles

The quadriceps femoris is situated on the anterior side of the femur. It consists of four muscles, as apparent from its name, and is the principal extensor muscle of the knee. These muscles can be seen in Figure 7, with the vastus intermedius located under the rectus femoris.

The four quadriceps muscles are distally joined by the quadriceps tendon which is connected to the patella. The muscles have different insertion points at the hip joint which gives each muscle a distinctive line of action that applies different forces and moments at the knee joint (Palastanga and Soames, 2012).

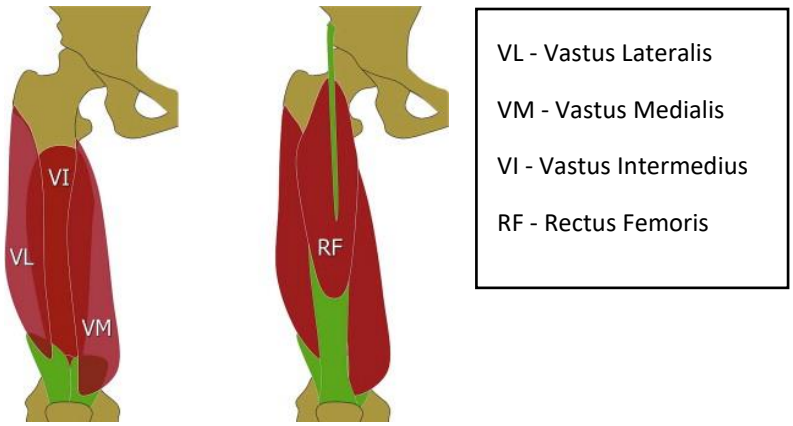

Figure 7: Quadriceps Muscles (Pasta *et al.*, 2010)

Flexor Muscles

The hamstring muscles are located at the posterior of the femur. It consists of three muscles and are the principal flexor muscles of the knee. It contains the biceps femoris (which has a long and a short arm), the semitendinosus and the semimembranosus as seen in Figure 8. The hamstring helps to regulate the effect of inertial forces when the leg is extended and it stabilizes the tibia against

rotational and anteroposterior (from front-to-back) movement (Palastanga and Soames, 2012).

The semitendinosus and the long arm of the biceps femoris attaches proximally to the pelvis with a combined tendon and the semimembranosus muscle attaches slightly above this. The shorter arm of the biceps femoris attaches to the lateral side of the femur.

Distally, the semitendinosus and the semimembranosus both attach to the medial condyle of the tibia and the biceps femoris attaches to the head of the fibula (Gilroy, MacPherson and Ross, 2012).

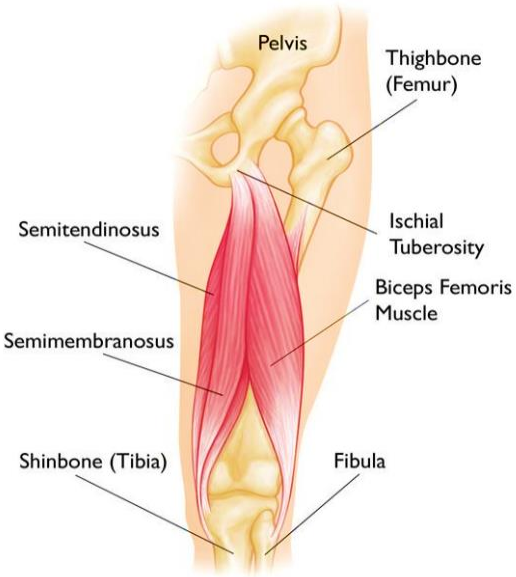

Figure 8: Hamstring Muscles
(Hamstring Muscle Injuries - OrthoInfo, 2015)

2.1.6. Q Angle

The quadriceps angle (Q-angle) can be seen in Figure 9. It is measured by drawing a line from the anterior superior iliac spine (ASIS) to the centre of the patella and from the centre of the patella to the tibial tuberosity (Schuithies *et al.*, 1995). The line of action of the quadriceps muscle can be assumed to be the line of the Q-angle drawn from the midpoint of the patella to the ASIS. According to a study done by Horton and Hall (1989) on young American adults, the mean Q-angles for men and women were 11.2˚ ± 3.0˚ and 15.8˚ ± 4.5˚ respectively.

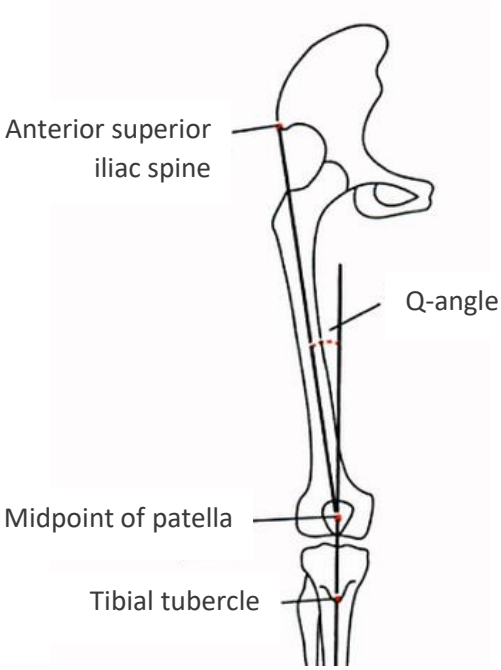

Figure 9: Q Angle (Van de Weghe, 2013)

2.2. Knee Biomechanics

Due to the conflicting needs of mobility and stability, the functions that characterize knee biomechanics are complex. The knee joint is relatively robust against external stresses, while it still offers a wide range of motion. This is accomplished with the help of passive and active stabilizers such as muscles and ligaments as previously discussed.

2.2.1. Knee Joint Degrees of Freedom

The knee joint allows six degrees of freedom (DOF), three in translation and three in rotation. From Figure 10, the translational DOF are medial-lateral (ML), anterior-posterior (AP) and superior-inferior (SI) translation. The rotational degrees of freedom are flexion-extension (FE), internal-external (IE) and varus-valgus (abduction-adduction) (VV) rotation.

The three translational degrees of freedom are restricted by the muscles, ligaments and the fibrous capsule, which is the envelope enclosing the knee joint (Affatato, 2014). The four main ligaments (ACL, PCL, LCL and MCL) are also largely responsible for rotational constraints.

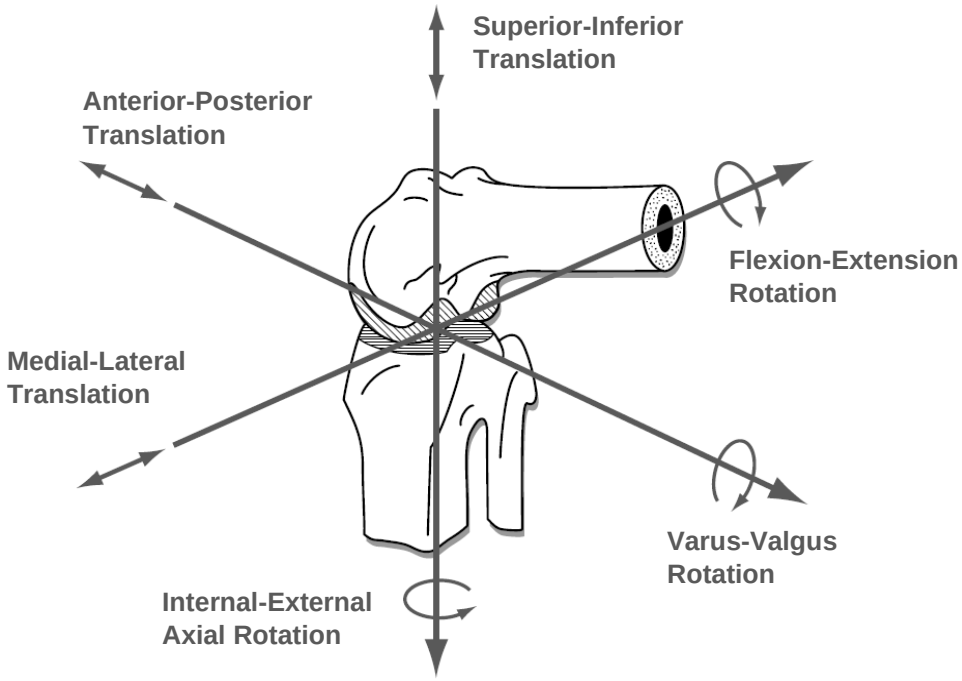

Figure 10: Six Degrees of Freedom of the Knee Joint (Komdeur, Pollo and Jackson, 2002)

2.2.2. Knee Kinematics

Knee motion occurs in all three anatomic planes with the rotation in the sagittal plane having the greatest range of motion as it includes flexion and extension. Extension is the motion which straightens the leg and flexion the movement where the calf moves towards the posterior thigh.

According to Freeman and Pinskerova (2003), most knee activities fall between 0° and 120° of flexion and extension. The moment arms in the knee are insufficient to flex it beyond 120° without the addition of an external force, such as body weight. The flexion-extension ranges vary between 0° and 67° during walking (Kettelkamp *et al.*, 1970) and between 0° and 90° for sitting and stair climbing (Nordin and Frankel, 2001).

Knee flexion and extension occurs through the flexion axis, also called the cylindrical or transverse axis, which passes through the posterior condyles of the femur. The cylindrical profile surrounding this axis, seen in Figure 11, was first observed by the Weber brothers (Weber and Weber, 1992) and later confirmed by Pinskerova, Iwaki and Freeman (2001).

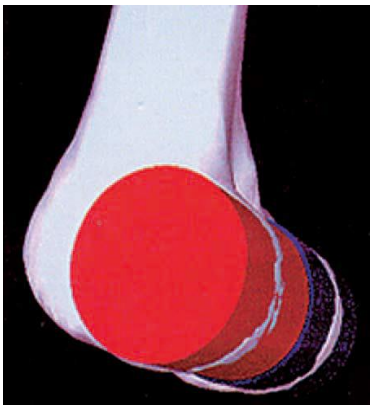

Figure 11: Cylindrical Profile of Femoral Condyles (Bellemans, Ries and Victor, 2005)

Even though the knee is a pivot hinge joint, the centre of its rotation is not fixed during flexion-extension. The working of the cruciate ligaments causes a semi-circular translation of the femur (O'Connor and Zavatsky, 1990). Figure 12 shows femoral rollback, a combined movement of femoral rolling and sliding over the tibia. The contact points, indicated by the red triangles, and the femur's centre of rotation move posteriorly as the knee flexes (Hirschmann and Becker, 2015).

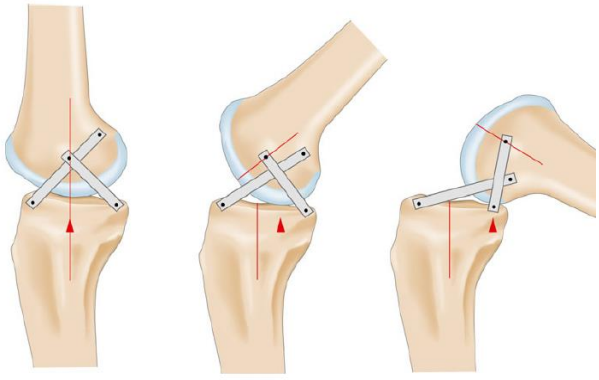

Figure 12: Knee Rollback. The triangles show how the contact points move posteriorly with flexion (Hirschmann and Becker, 2015)

The screw-home mechanism is essential for knee stability when extended (for example when standing upright). It is a phenomenon observed usually between full extension at 0° and 20° of knee flexion where there is rotation between the tibia and femur. The tibia rotates internally during the swing phase (early stages of flexion) and externally during the stance phase (last stages of extension) (Kim *et al.*, 2015). During the external rotation, the collateral and cruciate ligaments are taut, which locks the knee and results in maximum tibia stability with respect to

the femur (Brantigan and Voshell, 1941). The position of the patella is largely influenced by the screw-home movement (Zhang *et al.*, 2016).

The patella increases the efficiency of the quadriceps during knee motion as it acts as a fulcrum when it displaces the quadricep's line of action anteriorly. This increases the patella tendon moment arm (PTMA), illustrated in Figure 13. The patella is free to pivot around the femoral trochlea during motion which causes the patellofemoral contact point to move proximally and distally of the patella centre (Luyckx *et al.*, 2009). With an extended knee, the contact point lies distally, resulting in the quadriceps tendon moment arm being greater than that of the patella tendon moment arm (Yamaguchi and Zajac, 1989). This difference reduces as the contact point moves proximally during flexion. Consequently, less quadriceps force is necessary during early flexion as compared to deep flexion (Luyckx *et al.*, 2009).

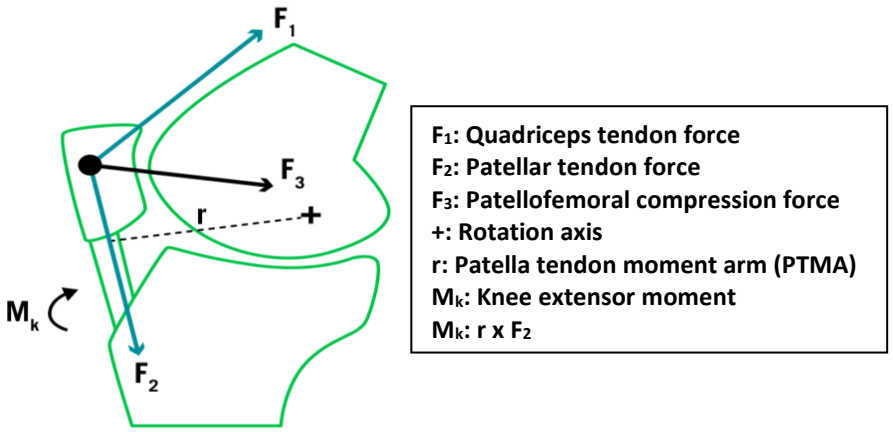

Figure 13: Patella Tendon Moment Arm (Visentini and Clarsen, 2016)

2.3. Total Knee Arthroplasty

Total knee arthroplasty involves the replacement of all articulating surfaces in the tibiofemoral joint, including the patella's face if necessary. The aim of TKA is to reduce knee pain at the articulating surfaces that is caused by osteoarthritis and other pathologies (Shenoy, Pastides and Nathwani, 2013). Apart from the significant rise in TKA procedures predicted (Feng *et al.*, 2018), human life expectancy and medical expectations are also rising which leads to an increased desire for knee replacements to restore the joint as close as possible to its healthy and natural state for a longer period of time.

2.3.1. Prostheses Designs

The first known attempt to treat knee osteoarthritis was in the mid-19th century where it involved the interposition of soft tissue at the articulating surfaces of the tibia and femur (Amendola *et al.*, 2012). However, the modern concept of TKA is based on a series of lectures given by Thermestocles Gluck in 1880 where he described joint replacements by components made of ivory (Amendola *et al.*, 2012).

It was only in the 1950s and 1960s that modern TKA took shape after the first surface replacement of the tibia was developed by McKeever (Mckeever, 1960). It was also during this time that two main joint replacement theories were developed, namely constrained/hinged prostheses and condylar replacements (Amendola *et al.*, 2012). Hinged prostheses are used when soft tissue support in a knee is insufficient for motion. This is usually only considered with very serious injuries or revision surgeries.

The focus of this study will be on total condylar replacements which consists of two separate condylar surfaces for the femur and tibia with a polyethylene bearing between them which provides a smooth articulating surface (Amendola *et al.*, 2012). Tibial and femoral components are mostly made out of biocompatible materials such as cobalt-chromium (CoCr) or Titanium (Ti) alloys with polyethylene bearings (Kaivosoja *et al.*, 2012). Polyethylene is also used to resurface the patella (Manner, 2016).

Figure 14, Table 1 and Table 2 describe different components of the most common total knee implants.

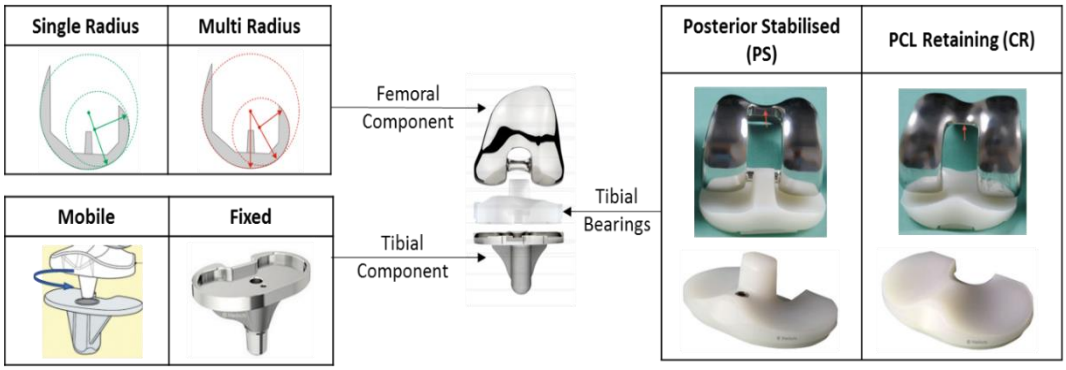

Figure 14: Knee Prostheses Designs
(Adapted from: *Types of Total Knee Implants*, no date; *Medacta: Three-compartment tibial bearing / fixed or mobile-bearing*, no date; Shenoy, Pastides and Nathwani, 2013; Hirschmann and Becker, 2015)

Table 1: Modern TKA Prostheses Designs: Femoral Component

		Description / Design	Advantages	Disadvantages
Femoral Component	**Multi-Radius**	The design is based on the natural anatomy of the femoral condyles. The femoral component has a large anterior radius which gradually reduces posteriorly to form a J-shaped curvature (Stoddard *et al.*, 2012).	Closer representation of anatomical shape and originally designed for the elderly (Stoddard *et al.*, 2012).	Higher force needed for knee extension compared to single-radius (Ostermeier and Stukenborg-Colsman, 2011). It has been reported to cause mid-range instability (Ostermeier and Stukenborg-Colsman, 2011), but Stoddard *et al.*, (2012) dismissed this claim.
	Single-Radius	This design is based on modern knee kinematic theories with the femoral component having one condylar radius in the flexion arc (Coles, 2015).	Better stability in coronal plane (Ezechieli *et al.*, 2012). Improved anterior knee function and improved flexion with better proprioception, while it ensures consistent tension in the collateral ligaments during flexion (Stoddard *et al.*, 2012). Faster recovery after TKA with better extensor mechanism performance (Gómez-Barrena *et al.*, 2010).	

Table 2: Modern TKA Prostheses Designs: Tibial Component

		Description / Design	Advantages	Disadvantages
Tibial Component	**Mobile Bearing**	The polyethylene bearing can rotate or translate with respect to the tibial baseplate. It is generally for younger and more active patients that want a minimally constraint knee (Karadsheh, 2019).	It has an increased contact area which should theoretically cause less wear on the polyethylene bearing (Karadsheh, 2019).	Could cause bearing spin-out as a result of the loose bearing or unnatural tibial rotations (Karadsheh, 2019).
	Fixed Bearing	The polyethylene bearing insert is locked unto the tibial baseplate.	No micromotion as it is fixed (Coles, 2015).	Could potentially wear quicker. Far less tibial rotation (Stiehl, 2009).
Tibial Bearing Constraints	**Cruciate Retaining (PCL Retaining)**	Minimally constrained prosthesis which retains the PCL. Used on patients with minimum bone loss and soft tissue looseness (Karadsheh, 2019).	Compared to the posterior stabilising implant, less femoral bone stock needs to be removed. PCL retention helps with improved proprioception. (Karadsheh, 2019)	With the traditional insert, the condition of the PCL is very important as it can cause accelerated wear on the insert when too tight, and flexion instability when too loose (Karadsheh, 2019).
	Posterior Stabilising	This design sacrifices the ACL and PCL but gives a relatively well constrained prosthesis. The femoral component contains a cam which presses against a post on the tibial insert (tibial post) to prevent the bones from sliding off each other (Karadsheh, 2019). The cam and post compensate for the missing ACL and PCL. The PS design is further explained in Figure 15.	Sufficiently constrained without compromising on range of motion (Karadsheh, 2019).	Tibial post-cam dislocations (cam jump) may occur (Karadsheh, 2019). Wear on the polyethylene tibial post.

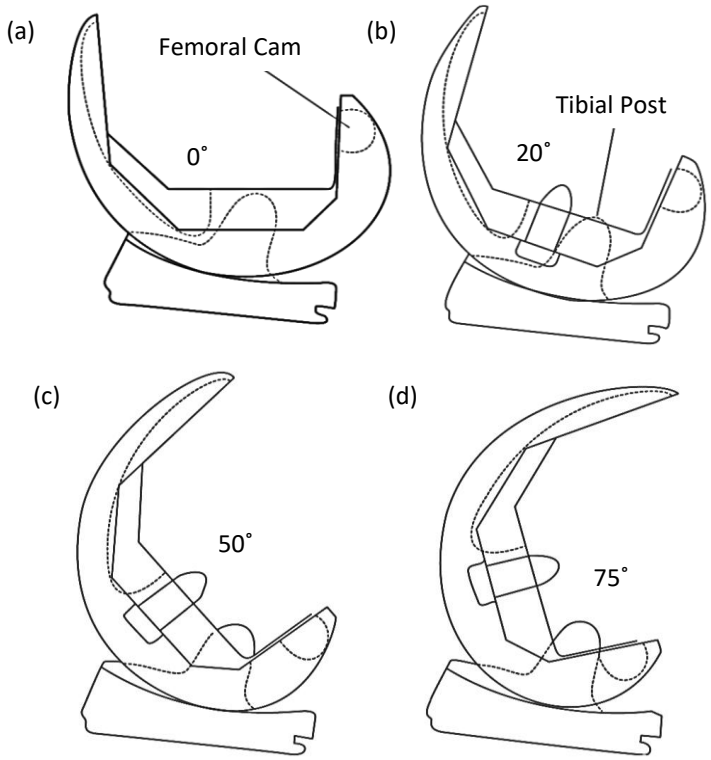

Figure 15: Posterior Stabilised Design (Keller and Amis, 2015). A vertical post at the centre of the tibial component and a crossbar (cam) between the posterior condyles of the femoral component mimics the function of the PCL. The components can move freely during extension (a). During flexion (b, c) the soft tissue surrounding the knee determine how the components interact. Anterior femoral gliding stops when the cam and post engages at deep flexion (d).

2.3.2. Alignment Axes

During TKA, it is crucial to restore knee alignment. Due to the complexity of the knee joint, this is not an easy task. To describe alignment in the lower extremity, certain axes must first be defined.

Mechanical Axes

In the ideal leg (neither varus nor valgus), the mechanical axis is defined as the straight line drawn from the femoral head to the centre of the ankle joint, which is on average approximately 3° valgus compared to the vertical axis, as seen in Figure 16 (Cherian *et al.*, 2014). However, the mechanical axes of the femur and tibia are usually not referred to as one long axis. The femoral mechanical axis runs from the femoral head to the intercondylar notch of the distal femur. The tibial mechanical axis is defined as the axis connecting the centre of the proximal tibia with the centre of the ankle. These two axes should be parallel.

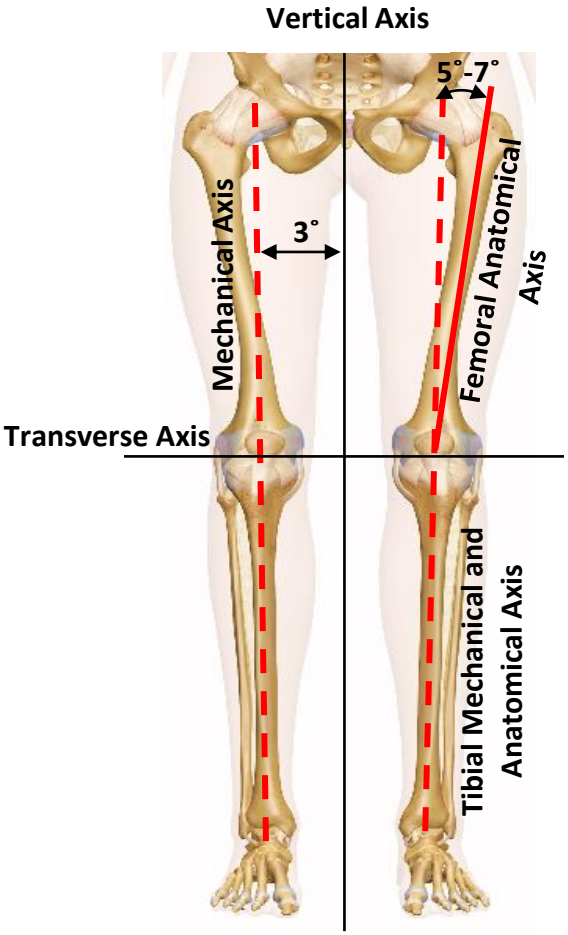

Figure 16: Axes of the Lower Extremity (Adapted from: Barclay, 2019)

Anatomic Axes

The femur and tibia each have a distinct anatomical axis. The tibial anatomical axis usually corresponds with the tibial mechanical axis. The femur's anatomical axis is usually 5° - 7° more valgus than its mechanical axis (Cherian *et al.*, 2014). The anatomical axes of the femur and the tibia bisect the bones through their intramedullary canals (Cherian *et al.*, 2014).

Kinematic Axis

There are three functional kinematic axes about which the knee rotates and flexes (Schiraldi *et al.*, 2016). These axes are intended to describe the dynamic motions of the knee. Figure 17 shows the three axes. The green line indicates the femoral transverse axis about which the tibia flexes and extends (Parisi, Jennings and

Dennis, 2018). This axis passes through the centre of a cylindrical profile fitted to the femoral condyles, as seen in Figure 11.

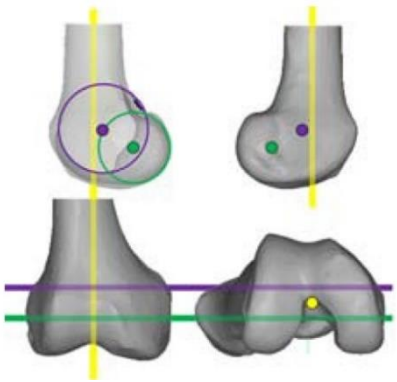

Figure 17: Kinematic Axes of the Knee (Parisi, Jennings and Dennis, 2018)

The second transverse axis, indicated by the magenta line, is parallel and proximal to the first one and indicates the axis about which the patella flexes (Parisi, Jennings and Dennis, 2018).

The longitudinal axis, indicated by the yellow line, is perpendicular to the two transverse axes and is the axis about which the internal-external tibial rotation occurs, relative to the femur (Cherian *et al.*, 2014).

2.3.3. Surgical Techniques / TFJ and PFJ Alignment

Although it is difficult to quantify patient satisfaction after TKA, historical data suggest that 11% to 19% of primary TKA patients are not satisfied after surgical intervention (Bourne *et al.,* 2010). This can be attributed among other things to surgical human error, instrumentation accuracy or incorrect knee alignment (Ferrara *et al.*, 2015).

Malalignment of implants causes discomfort in patients and is a contributing factor to premature implant wear (Ritter *et al.*, 2011). Different alignment theories (mechanical alignment, anatomic alignment and kinematic alignment) and instrumentation techniques (cutting guides, patient specific instrumentation and computer navigation) have been introduced to try and increase TKA success rate and decrease the revisions required. However, there is still no concrete evidence that one specific method is superior in TKA (Howell *et al.*, 2013; Gromov *et al.*, 2014).

Neutral mechanical alignment is currently the gold standard for TKA and was first described by Insall *et al.* (1985). It involves a femoral and tibial resection that is made perpendicular to their respective mechanical axes (Cherian *et al.*, 2014).

Insall noted that although this method ensures an even load distribution between compartments with the knee extended (stance phase), some uneven loading will inevitably occur during gait due to a ground reaction force which is directed laterally (Insall *et al.*, 1985). Insall also suggested to place the femoral component at a 3° external rotation (about the posterior condylar axis, the axis running across the tips of the posterior condyles of the femur) which will help to balance the flexion-extension gap (Insall *et al.*, 1985).

In a study investigating the importance of mechanical alignment, Fang, Ritter and Davis (2009) concluded that the knee's alignment should be restored after TKA to a tibiofemoral angle (angle between femur and tibial anatomical axes) of 2°-7° valgus for optimal performance and neutral alignment. This orientation was confirmed by Ritter *et al.* (2011) for least failure rates.

2.3.4. Tibial Slope

The tibial posterior slope is the angle at which the tibial component is placed in the sagittal plane. It has been shown that increasing it could have a positive or negative impact on the functioning and kinematics of the knee (Okamoto *et al.*, 2015). However, the optimal tibial slope is still controversial.

An increase in the posterior slope can reduce the required quadriceps force (Ostermeier *et al.*, 2006) and improve knee flexion (Bellemans *et al.*, 2005; Shi *et al.*, 2013). Shi *et al.* (2013) found that for each added degree of tibial slope in a posterior stabilised (PS) knee, the flexion range was increased by 1.8˚. However, an increased tibial slope was also shown to cause an anterior translation of the tibia relative to the femur (Giffin *et al.*, 2004) and increases wear on the insert (Wasielewski *et al.*, 1994). An optimal tibial slope of 0° to 7° was suggested by Gromov *et al.* (2014). Smith and Nephew suggests a total tibial slope of 7˚ for their Genesis II posterior stabilised replacement.

2.4. Dynamic Knee Simulator Machines

A simulating machine allows one to dynamically simulate the loads and movement of a knee specimen without restricting the joint. This can help to gain a better understanding of knee biomechanics.

2.4.1. Oxford Knee Rig

The Oxford Knee Rig (OKR) was first developed in 1978 by O'Connor and colleagues to do physiological tests on knee specimens and study different knee arthroplasties (O'Connor, Bourne and Goodfellow, 1978). The machine is used to simulate a flexed knee stance similar to riding a bicycle, climbing stairs or rising from a chair (Zavatsky, 1997).

The original Oxford Knee Rig can be seen in Figure 18. The two main assemblies of the rig are the hip and ankle assemblies. The hip remains vertically above the ankle which causes unrealistic extension moments and leads to high quadriceps forces during extension of the knee. During normal gait and stair climbing, people automatically move their bodies in such a way to reduce the joint reaction force by manipulating the body weight moment arm, which in turn reduces the required quadriceps force (Mason *et al.*, 2008).

Three sets of rotary bearings at the ankle allows the tibia to move spherically about its centre. It is thus capable of all three rotational degrees of freedom, namely flexion-extension, varus-valgus and internal-external tibial rotation. The hip assembly can flex and extend and vertically move up and down.

The combination of the mechanical hip and ankle joints provides the six degrees of freedom required to mimic the physical knee joint. This was mathematically proven by Zavatsky (1997) with the help of screw theory and evaluating the range of motion during movement of the physiological joint.

Body weight can be simulated by vertically applying weight to the hip assembly. To prevent the system from collapsing with the applied weight, tension should be applied to the quadriceps tendon. Varying this tension will cause the specimen to flex or extend. The flexion angle is thus controlled with all the other DOF left free to be dictated by the anatomy and geometry of the joint.

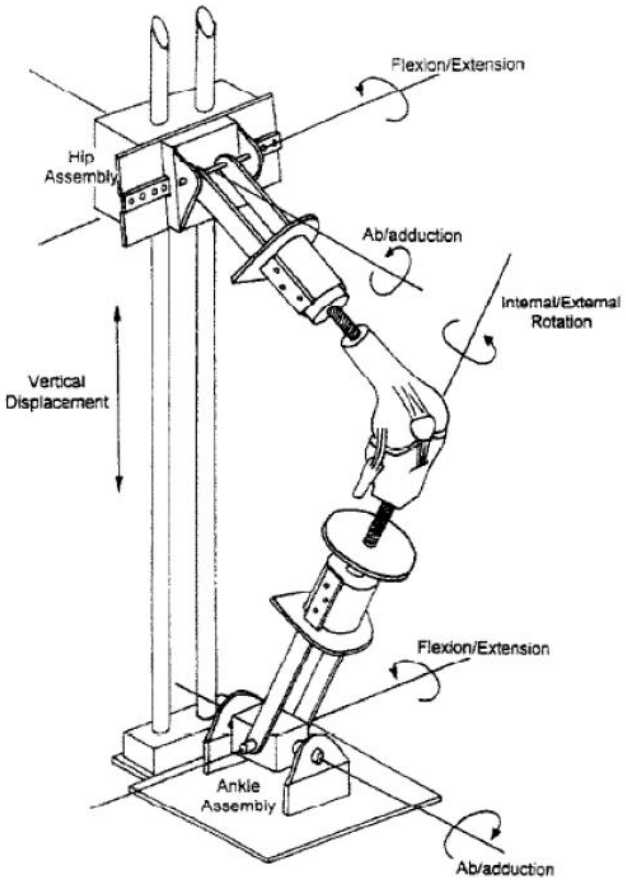

Figure 18: Original Oxford Knee Rig (Zavatsky, 1997)

2.4.2. Control Mechanisms and Loading Conditions

For a knee sample to be flexed inside a simulator, forces must be applied that simulate muscle movement. Muscles are usually tensioned with a linear actuator, whether it is electromechanical (Forlani, 2015), hydraulic (Maletsky and Hillberry, 2005) or pneumatic (Rusly, 2015). Some simulators even use a motor and pulley system (Anglin *et al.*, 2008), but it is easy to lose physiological functioning if careful attention is not given to pulley locations.

As researchers experiment with various objectives, one of the major differences in designs is the application of the quadriceps force and where the actuators that induce this force, are located. The quadriceps actuators are either placed on the femur, the pelvis or on grounded locations that are external to the specimen.

Hast and Piazza (2018) investigated the influence of the position of the quadriceps actuator for knee kinetics and kinematics using a computational model. They found that when the actuator was grounded, the quadriceps force was substantially less than expected and did not monotonically increase with flexion

as observed with the actuator fixed to the femur or pelvis. The latter corresponds with the physiological system. They concluded their study by stating that the actuator location does not significantly affect knee kinematics, but that the actuator should either be attached to the femur or pelvis to get realistic results of quadriceps forces and articulating contact forces within the knee.

The two main control types found in literature are load control and position control. They are either applied individually, or simultaneously as with the Purdue Knee Simulator (Maletsky and Hillberry, 2005) and would often be accompanied by PID-control (Guess and Maletsky, 2005; Baldwin *et al.*, 2012). Long (2011) evaluated the influence of flexion speed and found that it had no significant influence on the quadriceps force at speeds of 3°, 6° and 12°/sec for a hinged replacement.

Specialized cameras, or motion trackers, are used to track knee movement. A motion analysis system, such as the Optotrak (Anglin *et al.*, 2008; Baldwin *et al.*, 2012) or electromagnetic position sensors (Churchill *et al.*, 1998; Mizuno *et al.*, 2001) can be used to collect positional data of the femur, tibia and patella from which relative motion can be computed.

2.4.3. Knee Rig Evolutions

Many iterations of the original knee rig have emerged which simulate the real physiological system better and produce higher flexion angles. The biggest difference among knee simulators is how the driving mechanisms are implemented. They determine how the system is controlled, the loading capabilities, speed and range of motion. Table 3 and Figure 19 shows a few design varieties, as discussed below.

Patients often experience patellofemoral complications after total knee arthroplasty. Steinbrück *et al.* (2013) investigated the pressure distribution of the patella, as well as quadriceps loads and femorotibial rotations before and after TKA by testing cadaveric specimens on the Munich Knee Rig. A constant ground reaction force of 50 N was maintained for all the tests with a flexion velocity of 3˚/s. Angle sensors were placed at the hip and ankle assemblies to measure the flexion angle and femorotibial rotation at the knee. An actuator was attached to the quadriceps and hamstring muscles each to simulate squat motion.

Wünschel *et al.* (2013) did a study with the Tuebingen Knee Simulator to investigate the biomechanical differences after cruciate retaining and posterior stabilised TKA. The simulator has a linear actuator that can apply a variable weight to the hip joint. Additionally, the quadriceps are simulated with three different servo motors with two more servos to simulate the semimembranosus and biceps femoris. All these actuators allow the machine to accurately simulate the

physiological system as it can have different loadings along different lines of action.

Long *et al.* (2013) did a biomechanical evaluation of hinged prostheses by comparing quadriceps forces and patellar tendon moment arms from five different designs. His results showed differences in prostheses performances and can be used as a starting point to improve hinged prostheses designs. The simulator is a simple Oxford Knee Rig representation with one actuator to induce quadriceps loading. The displacement of the hip assembly was measured with a pull-cable transducer.

An Oxford-type weight-bearing knee rig was used by Van Haver *et al.* (2013) to do tests on cadaveric knees. The quadriceps were controlled under simulated body weight to induce flexion and extension. The focus of their study was to investigate the influence of knee surgery on patellofemoral kinetics. Internal-external rotation was possible for both the femur and tibia and the ankle assembly was allowed to slide anterior-posterior and medial-lateral directions. One quadriceps loading actuator was vertically mounted above the hip assembly to the rig. A pulley system was then used to transfer the induced loading to a cadaver's quadriceps.

Table 3: OKR Evolutions

Authors	FE Range	Degrees of Freedom		Number of Actuators	Maximum Quadriceps Load
		Hip Assy.	Ankle Assy.		
Steinbrück *et al.* (2013)	20° - 120°	FE, vertical translation	FE, IE, VV	2	700 N
Wünschel *et al.* (2013)	20° - 110°	FE, vertical translation	FE, IE, VV	6	700 N
Long *et al.* (2013)	20° - 90°	FE, vertical translation	FE, IE, VV	1	1200 N
Van Haver *et al.* (2013)	20° - 60°	FE, IE and vertical translation	FE, IE, VV	1	2700 N

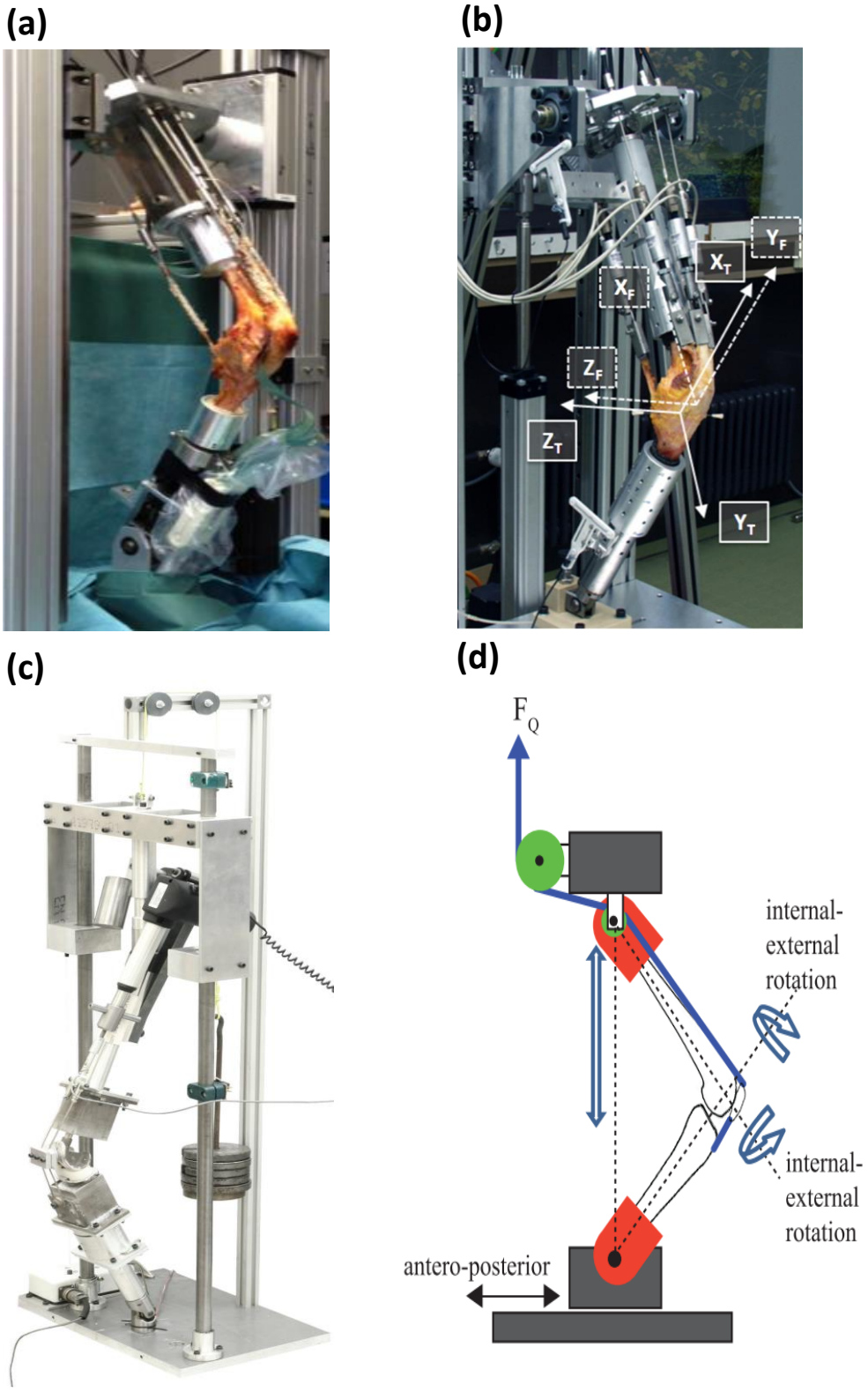

Figure 19: Different OKR Designs. (a) Steinbrück *et al*. (2013); (b) *Wünschel et al*. (2013); (c) Long *et al*. (2013); (d) Van Haver *et al*. (2013)

Chapter 3

3. Simulator Redesign

3.1. Introduction

The first iteration of a Stellenbosch University squat simulator was based on the original Oxford Knee Rig, as discussed in Section 2.4.1. The aim was to develop a simulator that can accurately represent a natural squat. However, the simulator did not function as intended and certain components had to be eliminated and redesigned before it was functional. In the end, only the ankle assembly was kept untouched and could directly be applied to the new simulator.

3.2. Design Requirements and Specifications

The summarised design requirements for the linear actuator, the hip assembly and the squat simulator in general are:

- Linear actuator:
  - Tension force > 2660 N
  - Stroke > 81 mm
- Hip assembly:
  - Left and right legs
  - 7° $\leq$ q-angle $\leq$ 20° (Horton and Hall, 1989)
  - Flexion-extension, proximal-distal translation
  - Withstand shear forces
- Squat simulating machine in general
  - Allow six DOF in knee joint
  - Reproduce knee loading patterns

3.2.1. Body Weight

If it is assumed that the simulated squat motion is that of a person standing on both his legs, the simulated body weight (BW) on the hip assembly should be taken as half the BW as only one leg can be tested at a time. However, this BW is only the percentage of weight above a person's hips. De Leva (1996) presented a paper where the human body was divided into segments with a mass percentage allocated to each segment, as shown in Table 4.

Table 4: De Leva (1996) Body Segment Mass %

	MASS %	
	FEMALE	**MALE**
HEAD	6.68	6.94
TRUNK	42.57	43.46
UPPER ARM	2.55	2.71
FOREARM	1.38	1.62
HAND	0.56	0.61
TOTAL*	58.23	60.28

* The total % takes double body parts into consideration.

The design will be based on a 70 kg male, which results in 21 kg of BW to be applied on the hip assembly.

3.2.2. Linear Actuator Force

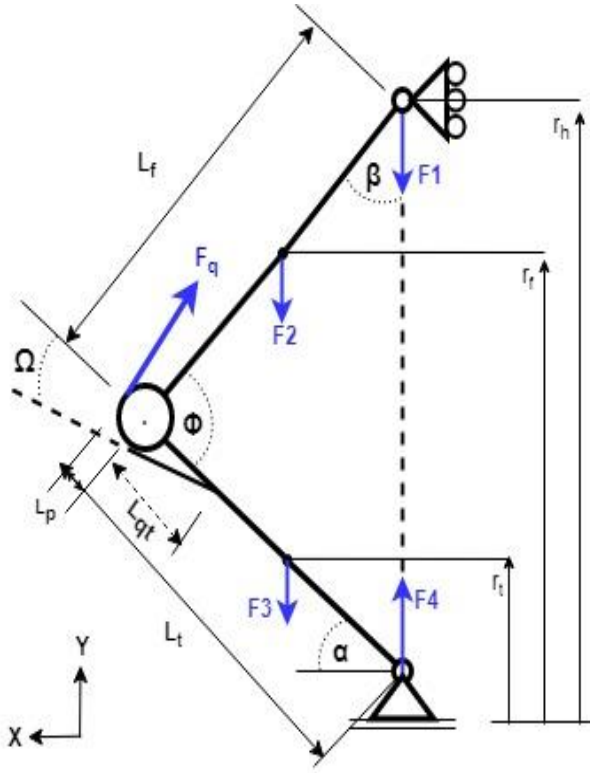

F_1	Gravitational force on the hip due to BW
F_2	Gravitational force on the femur
F_3	Gravitational force on the tibia
F_4	Ground reaction force at the ankle
L_f	Femur length
L_t	Tibia length
L_p	Patella moment arm
L_{qt}	Patella tendon length along tibia
r_h	Hip height
r_f	Femur height
r_t	Tibia height
β	Angle between femur and vertical
α	Angle between tibia and horizontal
Φ	Flexion angle
Ω	Angle between patella tendon and tibia

Figure 20: FBD of Squat Simulator

A linear actuator was used to induce the quadriceps force. To determine the force specification, a free body diagram (FBD) of the squatting machine was drawn, as seen in Figure 20. To calculate unknown forces, we are assuming that: (a) the motion occurs in the sagittal plane only, and is thus two-dimensional, (b) component accelerations are negligible except for gravitational acceleration, (c) a hinge joint connects the femur and tibia, (d) the friction at the linear bearings are small enough to be assumed negligible, (e) the moment of inertia of the femur and tibia is negligible, (f) all components are considered as rigid bodies.

In order to calculate the quadriceps force, F_q, a force balance in the y-direction was done with g = 9.81 m/s^2. F_4 is the ground reaction force experienced at the ankle assembly and was calculated as follows:

$$F_1 = m_{BW} \cdot g \tag{3.1}$$

$$F_2 = m_f \cdot g \tag{3.2}$$

$$F_3 = m_t \cdot g \tag{3.3}$$

$$F_4 = F_1 + F_2 + F_3 \tag{3.4}$$

The femur and tibia masses, m_f and m_t respectively, were based on the thigh and shank masses for a 70 kg male. Based on the finding of de Leva (1996), the masses were 9.91 kg and 3.03 kg for the thigh and shank respectively. With a lot of flesh removed when a cadaver leg is tested in a simulating machine, the thigh and shank masses were halved. The femur and tibia lengths for a male were based on a study done by Dayal, Steyn and Kuykendall (2008) and was consequently chosen as 460 mm and 375 mm respectively. The patella width, L_P, and the tendon length, L_{qt}, were both taken as 52 mm. These values fall within the ranges documented by Norman *et al.* (1983), it gives a normal Insall-Salvatti ratio and are accurate measurements for the specimen used in this study.

With all these values known, the quadriceps force can by calculated by doing a moment balance of the tibia around the hinge joint, taking anti-clockwise as positive.

$$\Omega = \tan^{-1}\left(L_p / L_{qt}\right) \tag{3.5}$$

$$(F_4 \cdot \cos\alpha \cdot L_t) - (F_3 \cdot \cos\alpha \cdot L_t/2) - (F_q \cdot L_{qt} \cdot \sin\Omega) = 0 \tag{3.6}$$

$$\therefore F_q = \frac{F_4 - {F_3}/{2}}{L_{qt} \sin\Omega} \cdot L_t \cos\alpha \tag{3.7}$$

Most knee activities fall between 0° and 120° flexion. However, at full extension of the knee inside a squat simulator, the knee joint will either lock with the BW fully supported by the femur and tibia or hyper extend which will cause soft tissue damage. This is the reason why a lot of existing simulators have an initial flexion angle of 15° or more (Ramappa *et al.*, 2006; Victor, Labey, *et al.*, 2010; Steinbrück *et al.*, 2013). A flexion range of 10° - 90° was used for this study.

A graph of the calculated quadriceps force is shown in Figure 21. An estimated maximum force of 2 443 N was obtained at maximum flexion.

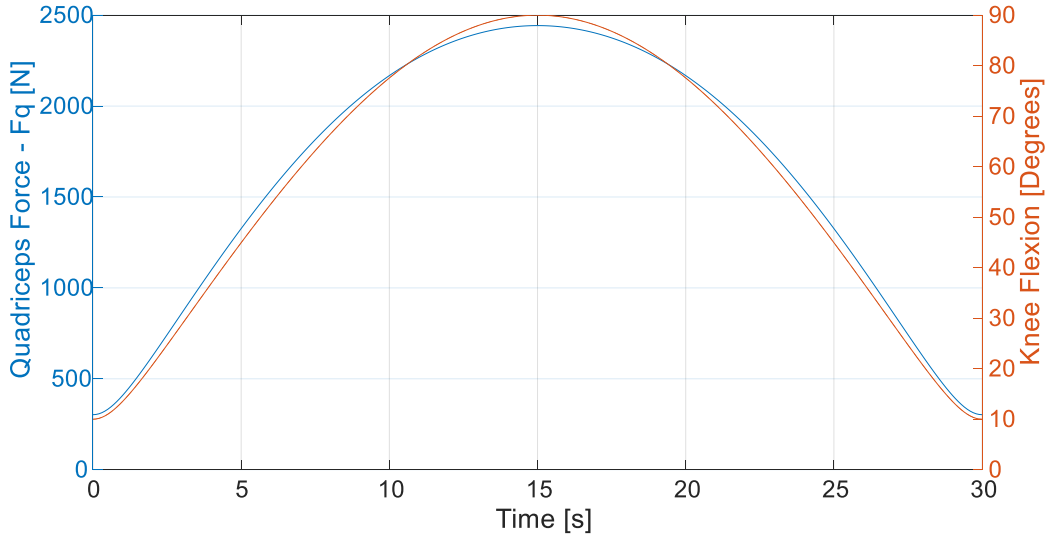

Figure 21: Calculated Quadriceps Force

3.2.3. Linear Actuator Stroke

Reproducing gait or the natural motion during a squat is a complicated task. The OKR allows a simplified, yet unnatural, representation of a squat by vertically aligning the hip and ankle assemblies with the use of only one actuator attached to the quadriceps muscles, as was the case for this study.

Figure 22 helps to better explain the calculation of the required actuator stroke length. To get the required stroke for the flexion range, the difference between the distance from point P to point B at 10° and 90° should be calculated. Point P can be assumed to move on the dashed arc as $\overline{PA}$ will stay constant.

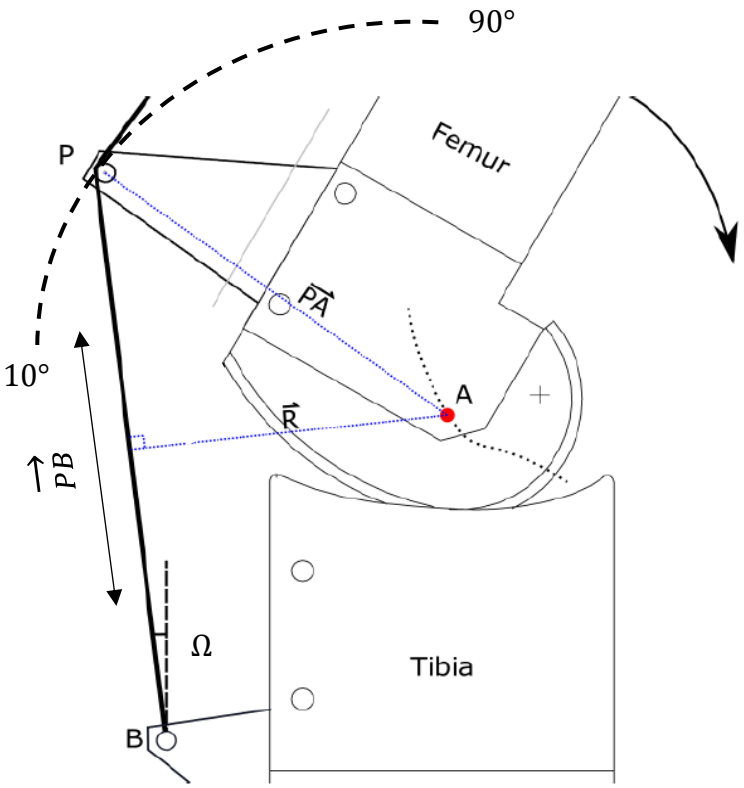

Figure 22: Knee Joint Sketch (Adapted from: Russell *et al.*, 2018)

If we assume that the quadriceps run parallel to the femur, the change in length of $\overline{PB}$ will be the same as the distance point P moves along the arc. With the help of Figure 23 and the notations used in Figure 20, the actuator stroke can be calculated as follows:

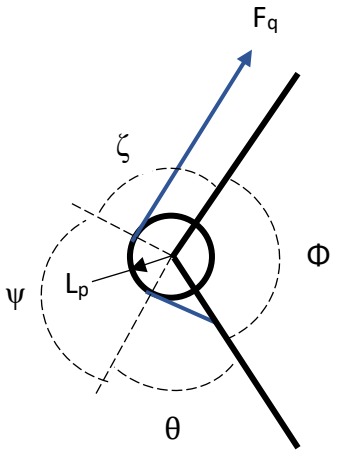

Figure 23: FBD to Calculate Actuator Stroke

$$\theta = \sin^{-1}(\sin \Omega / L_p \cdot L_{qt} \cdot \cos \Omega) \quad (3.8)$$

We know that the arc length can be calculated if we have the circle radius and the covered angle in radians with the formula (s = r ψ).

$$\psi = 360° - (\theta + \phi + \zeta) \quad (3.9)$$

$$s = L_p (\psi \cdot \pi / 180) \quad (3.10)$$

The difference between *s* at 10° and 90° gives an estimated required stroke length of 81 mm.

3.3. Original Squat Simulator

3.3.1. Overview

The original squat simulator can be seen in Figure 24. It consisted of a hip and ankle assembly that combined for seven degrees of freedom at the knee joint. Pneumatic actuators were used to simulate a squat motion by putting tension on the quadriceps and hamstrings while controlling the flexion angle with a distance sensor.

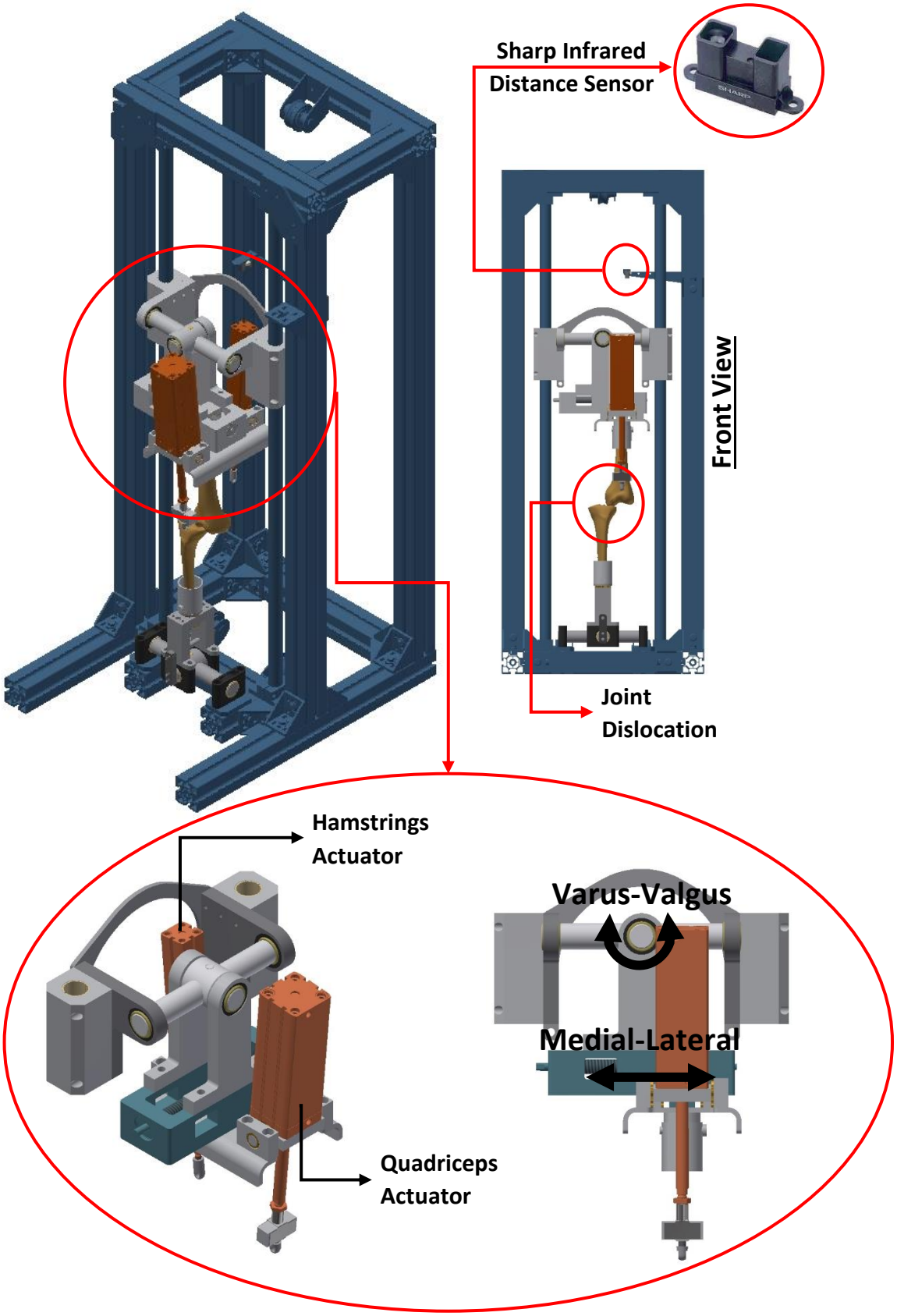

Figure 24: Original Squat Simulator

3.3.2. Hip and Ankle Assemblies

The two pneumatic actuators intended to simulate the quadriceps and hamstring muscles were aligned with the anatomical axis of the femur. The femur could be medially or laterally adjusted to mimic the anatomical offset from the mechanical axis. This, however, adjusted the Q-angle with the femur and did not change the relative distance between the actuator and the femur. Instead, the femur would be medially or laterally dislocated from the tibia at the knee joint.

The hip and ankle assemblies both had a varus-valgus degree of freedom in order to more accurately mimic the physiological range of motion. However, the varus-valgus DOF on the hip assembly increased the risk of instability during a squat motion and it was redundant as only six degrees of freedom at the knee is required.

The original ankle assembly could be used unchanged on the new design. It allows for internal-external rotation of the tibia, flexion-extension and varus-valgus rotations. Together with the hip assembly, these rotational degrees of freedom also result in translational degrees of freedom at the knee joint to complete the full six DOF.

3.3.3. Linear Actuator

Pneumatic actuators and dry bearings were initially implemented to reduce ferromagnetic components. This was necessary if an electromagnetic motion tracking system was to be used.

Due to the nature of an unnatural squat (hip and ankle assemblies vertically aligned), larger forces are required to pull a knee out of deep flexion. Reduced quadriceps load is required to continue extending the knee once it has exited deep flexion. However, during the return stroke the front chamber of the pneumatic cylinder is pressurised. This pressure acts against the piston of the cylinder, applying tension to the quadriceps. The pressure continues to build up until the flexion threshold is overcome. Failure to depressurise it fast enough could cause the actuator to fully retract at high speed and beyond the ability of a pneumatic control system to reduce cylinder pressure fast enough, causing forceful hyperextension of the knee joint.

3.3.4. Control and Motion Tracking

The control variable of the squat simulator is the position of the hip assembly. An Infrared position sensor was used to measure the distance that the hip assembly travelled. However, it was found that the infrared sensor reading was subject to excessive noise.

An electromagnetic motion tracking system, the FASTRAK (Polhemus, Colchester, Vermont), was to be used to track the femur, tibia and patella during a squat motion. An optical motion tracker has since become available, which relaxed some of the original design constraints as ferrous material could now be used. Linear ball bearings could thus replace the dry bearings for smoother motion and other actuator options could be investigated.

3.4. Redesigned Squat Simulator

The redesigned squat simulator can be seen in Figure 25. It makes use of the same working principles as the original design. However, a simplified hip assembly and improved control was designed and implemented.

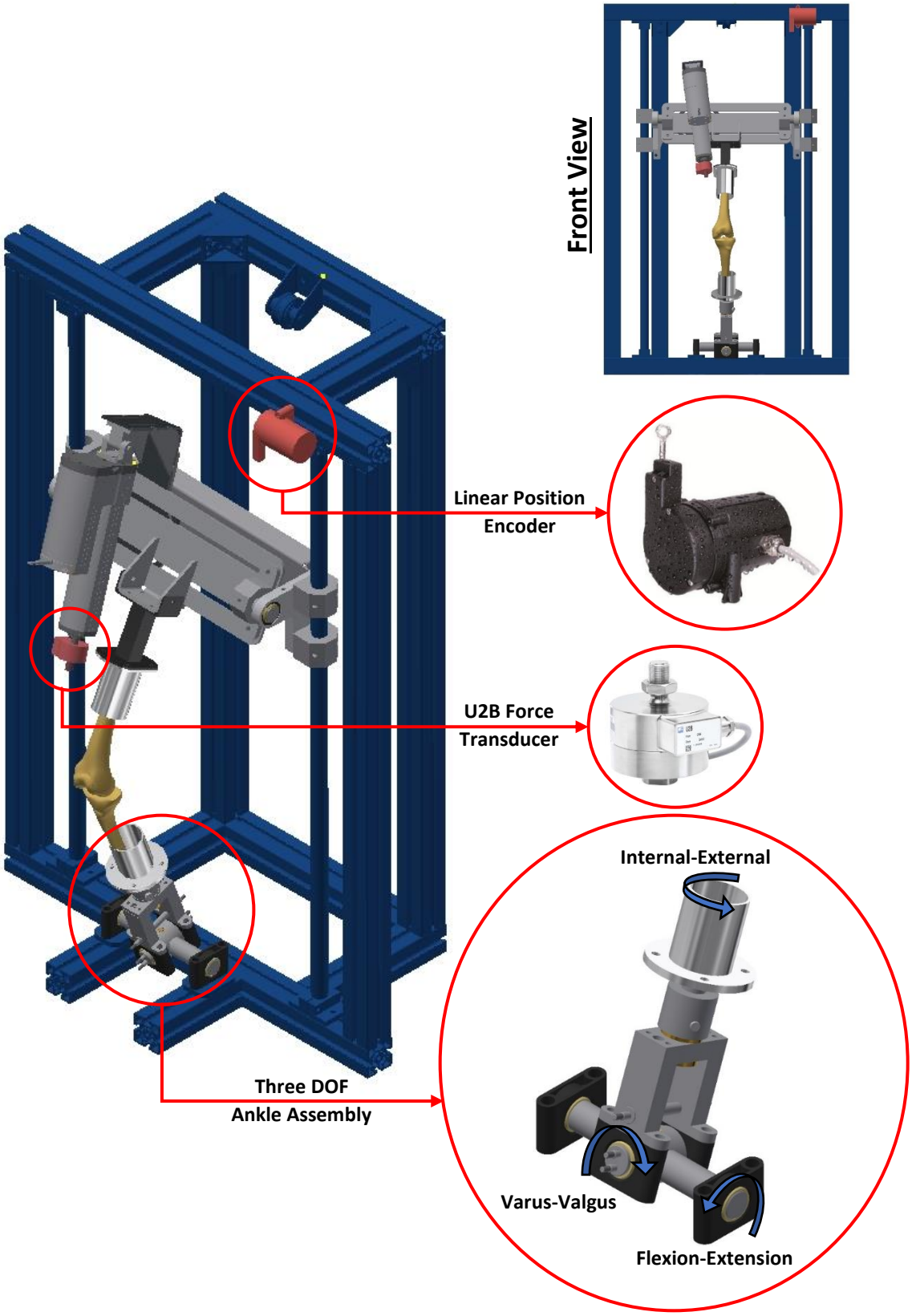

Figure 25: Redesigned Squat Simulator

3.4.1. Hip Assembly

The hip assembly plays an important role in the functioning of a squat simulator. As previously discussed, Hast and Piazza (2018) did a study to see how the position of the quadriceps actuator influences knee loading during a simulated squat. Using this information, it was decided that the quadriceps actuator should be placed on the femur or pelvis to get the most accurate results for the parameters to be investigated in this study.

The addition of hamstrings load does affect the biomechanics of a knee joint inside a squat simulator, as extensively studied before (Macwilliams *et al.*, 1999; Victor, Labey, *et al.*, 2010; Coles, Gheduzzi and Miles, 2014; Rusly *et al.*, 2016). For simplicity in this study, a hamstrings actuator was omitted to first get a functional simulator with only the basic components. Many simulators in literature also omit a hamstrings load (Ramappa *et al.*, 2006; Luyckx *et al.*, 2009; Long *et al.*, 2013; Van Haver *et al.*, 2013).

Considering the design requirements and weighing up the mentioned advantages and disadvantages, an electromechanical linear actuator from RK Rose and Krieger (Minden, Germany) was chosen to simulate quadriceps motion. This actuator makes use of a lead screw which eliminates the type of overshoot encountered with a pneumatic actuator as its motion will be relatively constant. The force is proportional to the torque of the motor and varies to the demand of the load. The selected actuator has a maximum speed of 6 mm/s and stays relatively constant over its load-speed curve. Important specifications are shown in Table 5, all satisfying the design requirements discussed in Section 3.2.

Table 5: Linear Actuator Characteristics and Specifications

RK ROSE AND KRIEGER – LZ 60P, EXTERNAL CONTROL	
SPECIFICATIONS:	
Voltage	24 V
Power input (max.)	180 W
Push/pull force (max.)	4 000 N
Stroke	150 mm
Speed (max)	6 mm/s
Weight	3.8 kg
Duty cycle (at maximum load)	15%

The hip and ankle assemblies should not constrain the knee in a way that restricts the natural six degrees of freedom in a knee joint. The complete hip assembly can be seen in Figure 26. The slots on the hip-plate allow the actuator bracket to be moved to accommodate a left or right leg, as well as Q-angle adjustments.

Linear ball bearings on each side of the hip assembly helps it to smoothly translate vertically up and down on the linear rails. This is the proximal-distal translation which facilitates some of the other degrees of freedom. Plastic bushes and two short shafts on each side of the hip plate allows the flexion-extension DOF. The back plate provides structural support and allows extra body weight to be placed on the hip assembly with the help of a pulley system.

The actuator bracket in Figure 27 also has slots to adjust the angle of the actuator relative to the knee joint as the Q-angle changes. The slots at the back are to move the actuator up and down to get a better balance on the hip assembly with the added actuator weight. This bracket was designed to have the actuator as close as possible to the femur without compromising the patella's function. If the actuator is placed too far away, the tension in the quadriceps can pull the patella away from the femur and thus reduce the contact force.

Assuming the actuator force to be 2660 N and the plate's thickness to be 4 mm, the deflection of the actuator bracket without support flanges was calculated as 11.6 mm, as seen in Appendix C. This will cause yielding in the plate according to Tresca's Maximum Shear Stress failure theory. Two different support structures were implemented to prevent this deflection, as seen in Figure 27.

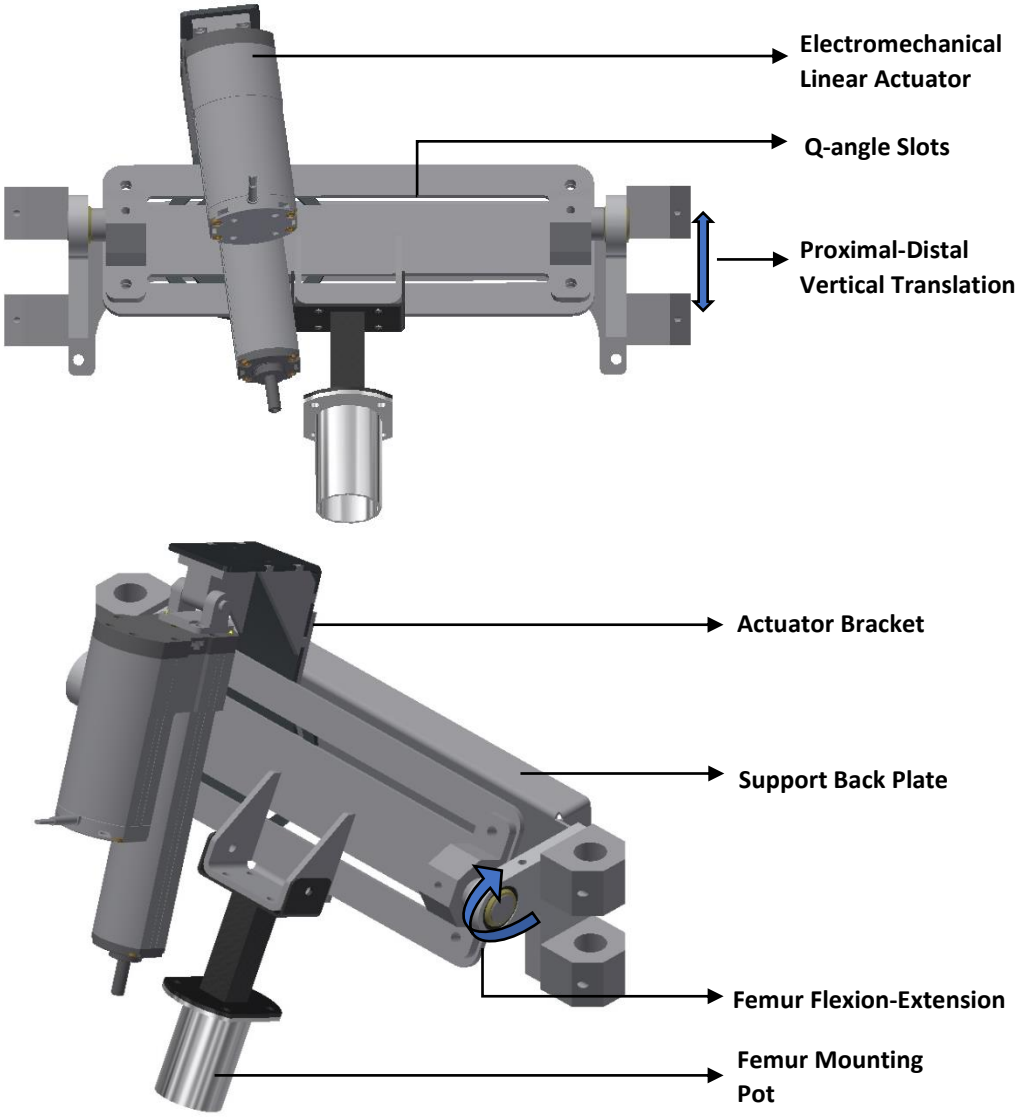

Figure 26: Full Hip Assembly

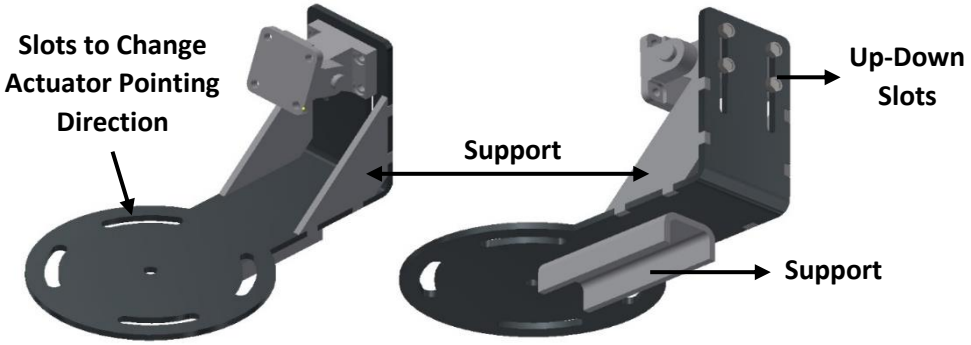

Figure 27: Actuator Bracket with Support

3.4.2. Simulator Control

The controller is responsible for the repeatable functioning of the simulator. The vertical distance that the hip assembly travelled was measured with a UniMeasure JX-EP Series (Corvallis, Oregon) pull-cable position encoder (resolution of 246 counts/inch, or 9.7 counts/mm) and interpreted by an Arduino Mega microcontroller (MCU). The response of the MCU to the measured distance was to either extend the linear actuator for flexion or retract the actuator for extension with bang-bang control between two boundary values. The circuit diagram for the functioning and control of the squat simulator is shown in Figure 28.

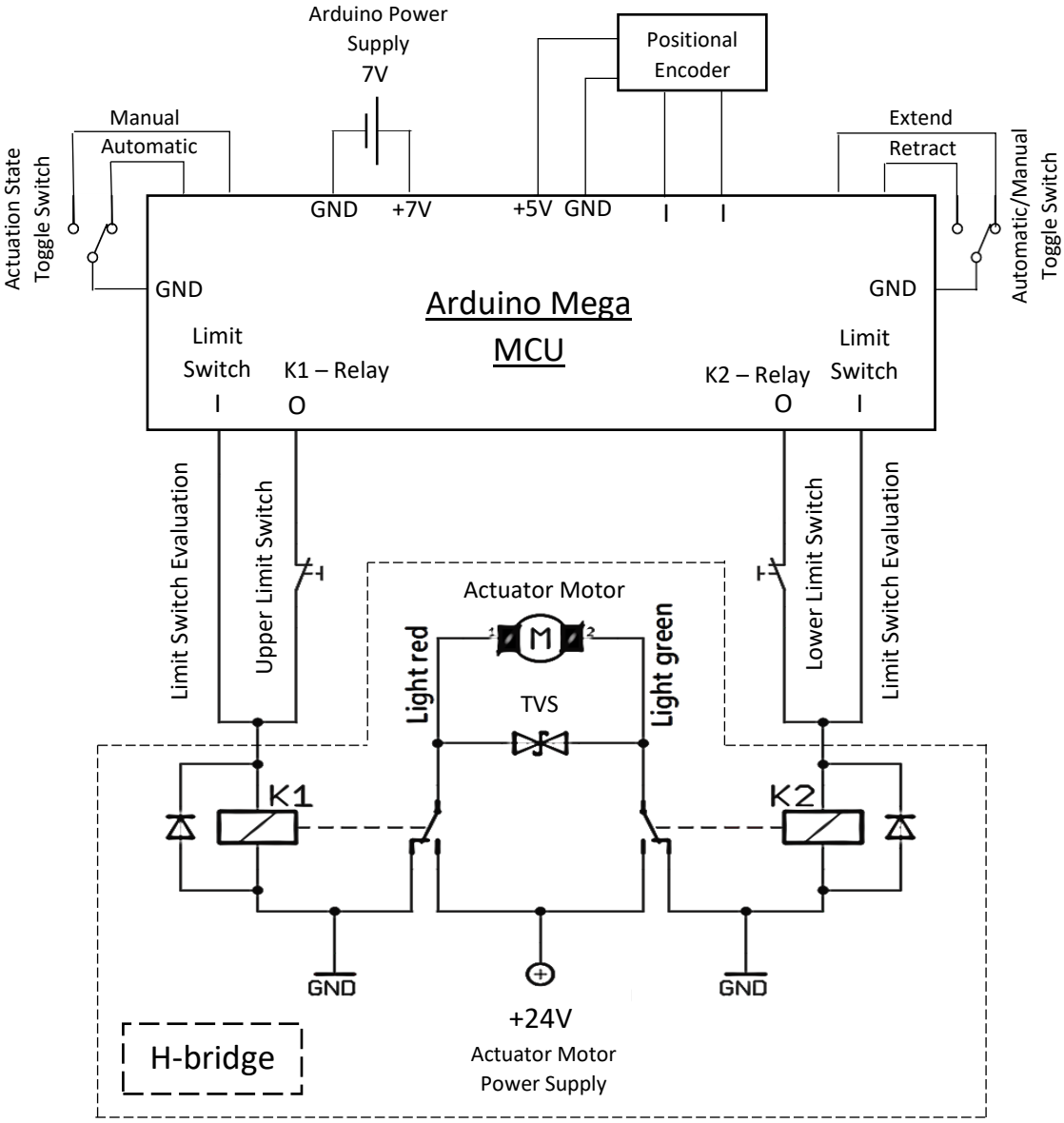

Figure 28: Simulator Controller Circuit Diagram

The H-bridge, indicated by the dashed lines in Figure 28, switches the polarities of the DC motor. There are two relays present in the H-bridge, represented by K1 and K2. Both normally open (NO) contacts of the relays are connected to the 24V voltage source and the normally closed (NC) contacts are connected to ground. When relay K1 is energised, the light red wire of the motor will be connected to the positive 24V source and the light green wire will stay connected to ground through the NC contact of K2. This will cause the motor to turn in one direction. The turning direction is reversed when K2 is energized, and K1 de-energised.

To brake the motor, both K1 and K2 should be de-energised as their NC contacts are both connected to ground. Short circuiting the motor will mechanically brake it and thus prevent any overshoot experienced at the actuator's linear motion. Finally, the transient voltage suppressor diode (TVS) gives protection against rapid voltage spikes.

The actuator can either be manually or automatically retracted and extended. The various modes can be set via the use of two toggle switches, whose applications and operating procedures are described in Appendix B. The UniMeasure pull-cable and the actuator limit switches were attached to interrupt pins on the MCU. The limit switches were safety features to the actuator and the pull-cable provided positional feedback of the hip assembly. All of this allowed the machine to successfully perform a squat with the actuator simulating the quadriceps muscle.

The flow diagram in Figure 29 gives an indication of the required control inputs, the functioning of the toggle switches and a simple summary of how the squat simulator is operated with its controller. The main functions of the controller include energizing and de-energizing relays to extend or retract the actuator, evaluating built-in actuator limit switches, respond to distance measurements of the hip assembly and interpreting toggle switch states.

Knowing the encoder resolution and the lengths of the femur and tibia, the controller could convert the pull-cable encoder counts to millimetres in order to calculate the immediate flexion angle. The controller first had to be calibrated to accurately convert the travelled linear distance of the hip assembly to a flexion angle. A known reference angle and corresponding hip position could be used for this. Bang-bang control was implemented to keep the flexion angle within the specified flexion range.

Starting at the flexion start angle, the controller knows how many pull-cable encoder counts will take the hip assembly to the flexion stop angle. The actuator will thus continuously be extended until the hip assembly reaches its end location. Immediately thereafter the actuator will start to retract until the hip assembly again reaches its starting location.

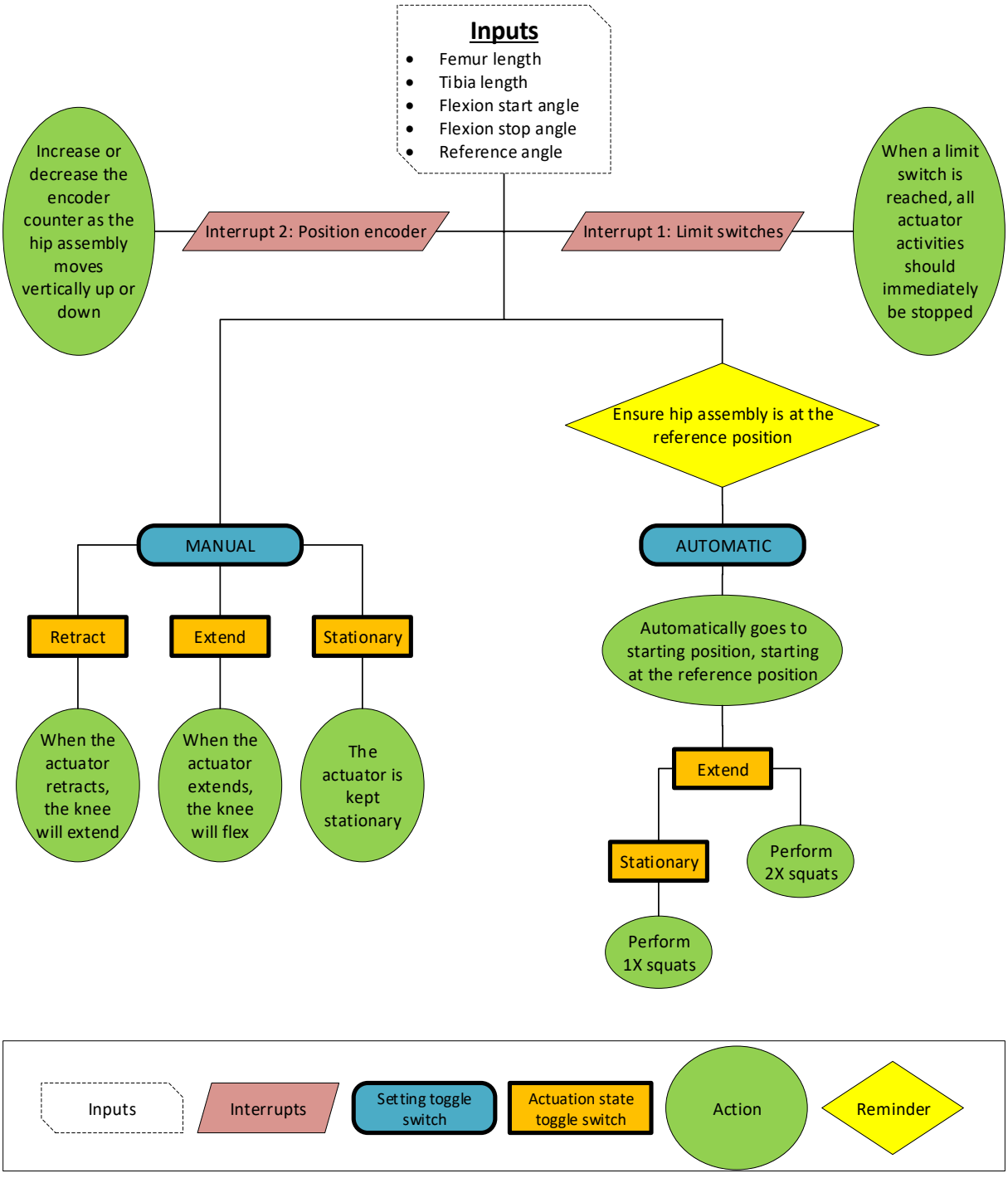

Figure 29: Simulator Operation Flow Diagram

3.5. Conclusion

The original squat simulator was successfully re-designed with a completely new hip assembly and controller. The simulator was proved to be functional and could successfully perform a squat. The complete simulator, with an artificial knee sample, can be seen in Figures 30 and 31.

The body weight pulley system is demonstrated in Figure 32. The weight attached to the rope pulls the hip assembly downwards to simulate body weight.

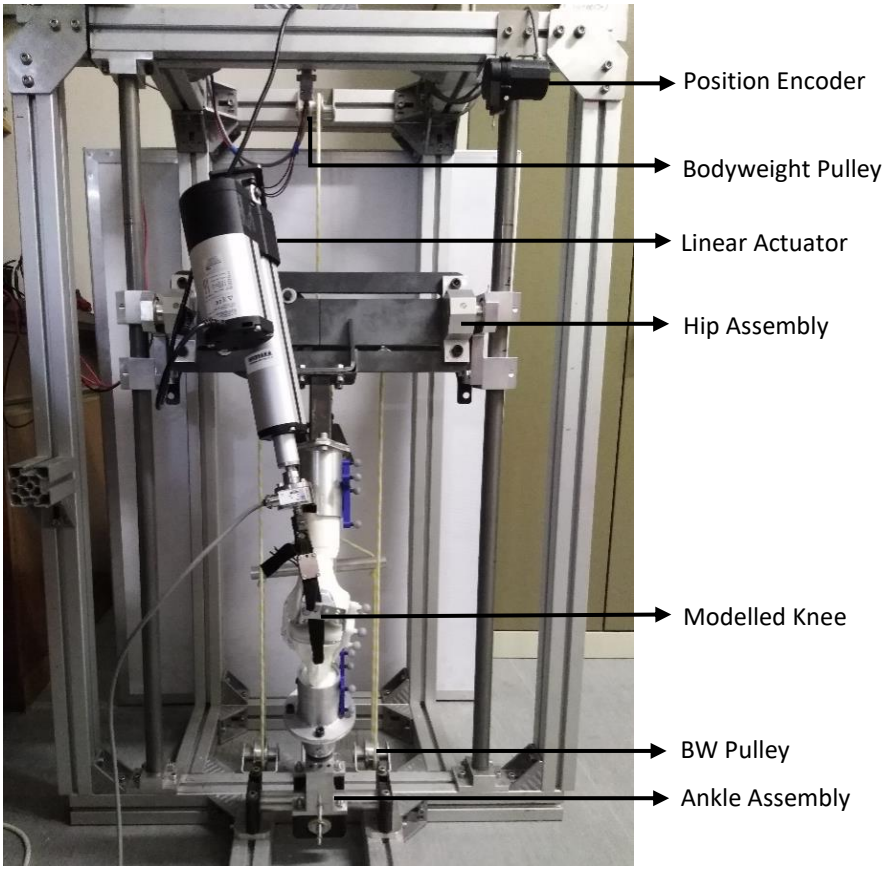

Figure 30: Squat Simulator Front View

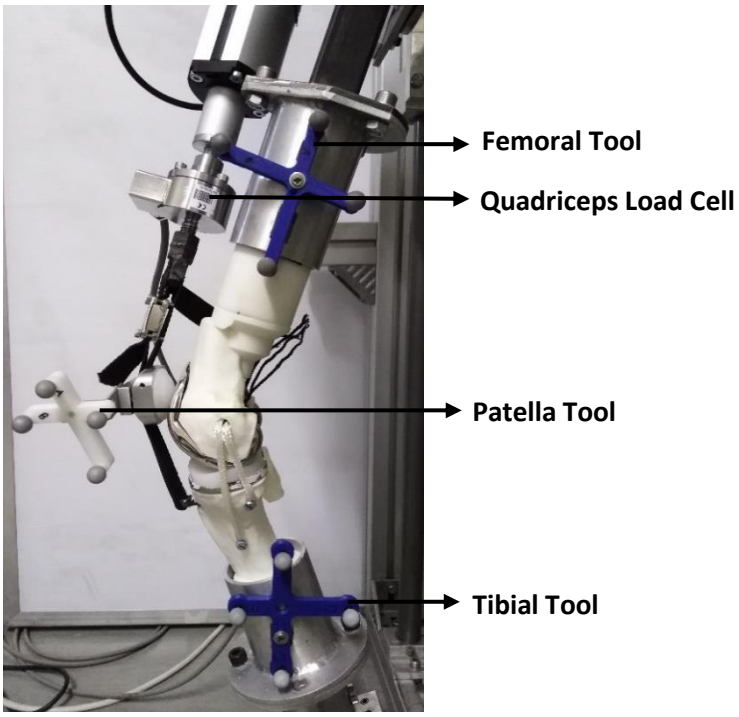

Figure 31: Squat Simulator Side View

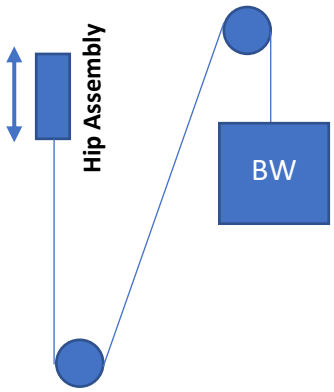

Figure 32: Body Weight Pulley System

Chapter 4

4. Evaluation of the Squat Simulator

4.1. Introduction

To evaluate the squat simulator described in Chapter 3, a physiologically realistic knee sample was required on which an implant could be fixed. The six degrees of freedom present in a knee joint should all be measurable in the simulator, and present in the knee sample to be tested. These degrees of freedom can be described when coordinate systems are established on the femur and tibia. The quadriceps muscle initiates the squat motion and has an influence on the knee kinematics and forces experienced at the articulating surfaces. Realistic quadriceps forces are thus essential to verify the simulating machine.

4.2. Modelling an Artificial Knee

4.2.1. Cadaver Specimen or Artificial Knee

The best representation of a knee would be that of a cadaver as it is a genuine representation of the joint and it has all the naturally present soft tissues and accurate ligament and tendon properties. However, the use of cadaveric specimens require ethical approval, they may suffer from soft tissue deterioration, variability between specimens are highly likely and they require sufficient preparation time (Coles, 2015). This has led to studies using alternative specimens for repeatability and better control over biological variables. Metal fixtures (Guess and Maletsky, 2005; Luyckx *et al.*, 2009; Arnout *et al.*, 2015) or synthetic bones (Coles, Gheduzzi and Miles, 2014) have been used with ropes, synthetic bands and actuators fulfilling the soft tissue functions.

Although variability between specimens is desired for actual research on knees, the consistency of an artificial knee is preferred for the verification of the squat simulator. Making an artificial knee allows highly controlled tests as the same knee joint can be reproduced by following the same processes and re-used without soft tissue deterioration. This makes it possible to isolate certain parameters and observe the exact impact of geometric differences.

To ensure that the artificial knee is still a relatively good natural representation, a 3D computed tomography (CT) scan of a healthy 37-year-old male knee was used to recreate the femur and tibia bones. The femur and tibia were isolated from each other and could thus be handled independently. The scanned files were converted to solids in MeshLab: An Open-Source Mesh Processing Tool.

4.2.2. Digital Prosthesis Cuts

The bone cuts were simulated by performing them on the 3D computer models of the femur and tibia. A posterior stabilised Genesis II Total Knee System from Smith and Nephew was selected to verify the machine as it is a relatively well constrained implant without compromising on joint functionality, as discussed in Section 2.3.1. A size 7 femoral component and size 5 tibial component were used. A well constrained implant was desirable as it eliminated the need for all soft tissue structures to be included on the artificial knee. An HP David 3D Scanner (0.05 mm resolution) was used to get 3D models of these components, as seen in Figure 33. This allowed simulating the placement and bone cuts on the digital 3D models of the femur and tibia for improved repeatability.

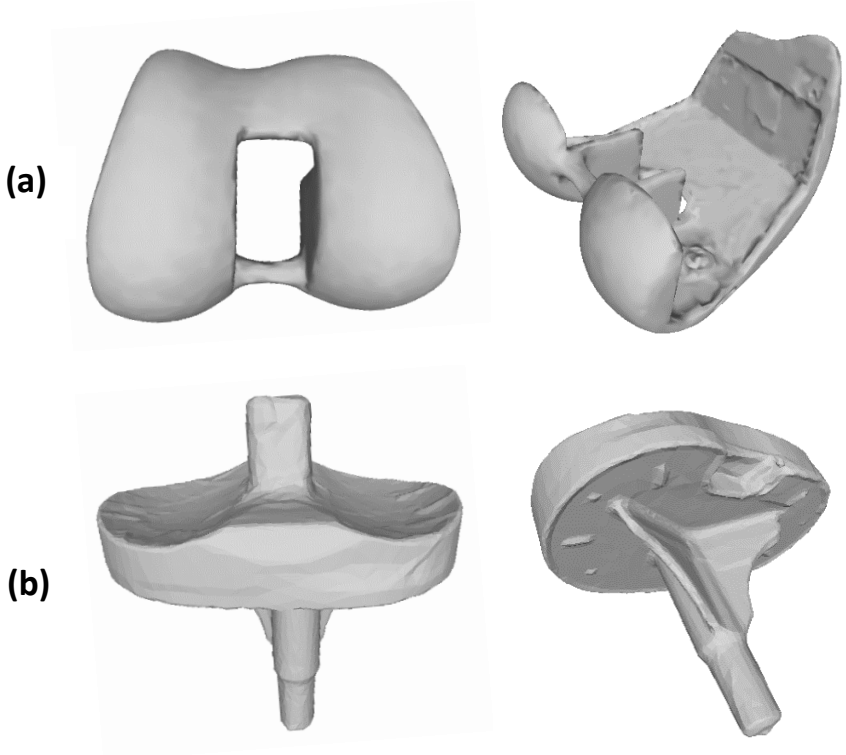

Figure 33: 3D Scan of Femoral (a) and Tibial (b) Implant Components

The bone models only contained the distal femur and proximal tibia which prevented definition of the mechanical and anatomical axes, as defined in Section 2.3.2. These axes function as references for the bone cuts and thus had to be carefully defined on the computer models. Therefore, in order to reproduce these axes from partial knee models, the femoral anatomical axis was defined as starting at the intercondylar notch of the distal femur, running towards the proximal centre of the partial femur bone, as if bisecting it in half. The femoral mechanical axis was defined as 6˚ varus to this axis, as shown in Figure 34. The tibial

mechanical and anatomical axes were defined parallel to the femoral mechanical axis and started at the medial intercondylar eminence of the proximal tibia.

After consulting literature and a leading knee specialist, the bone cuts were performed on the computer models to mechanically align the femur and tibia. An anterior view of the knee joint used in this study is shown in Figure 34. The distal femoral cut was made at a 6° angle from the line connecting the distal femoral condyles, and 9 mm proximal as shown in Figure 35. Additionally, a femoral box was cut out of the centre of the distal femur to accommodate the tibial post.

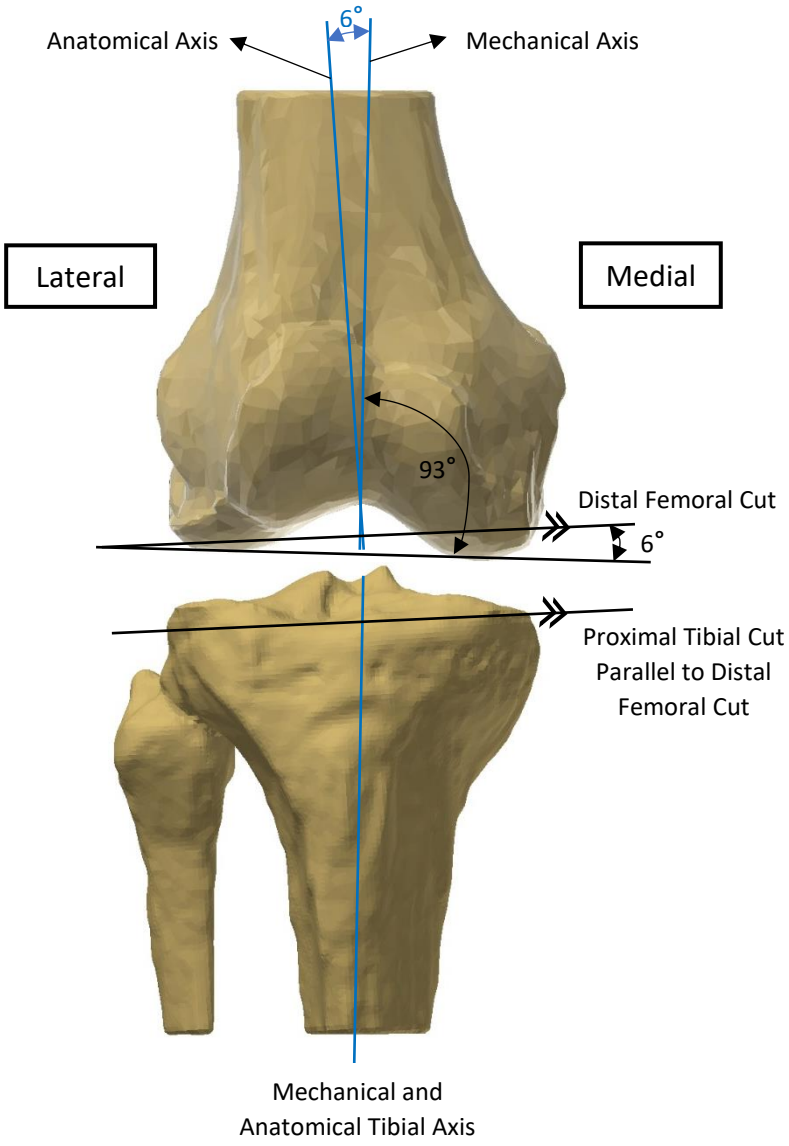

Figure 34: Anterior View of Knee Joint with Axes

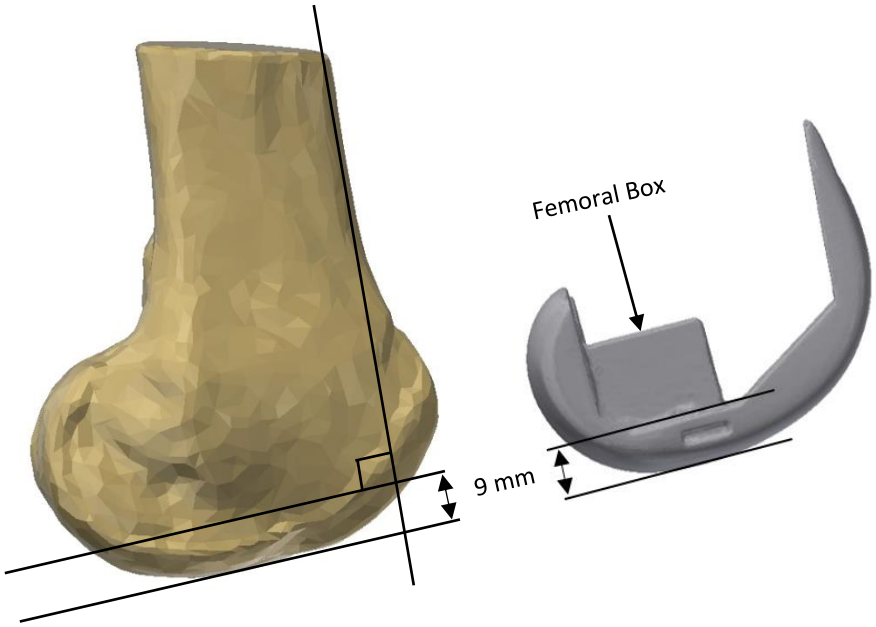

Figure 35: Medial View of Femur and Femoral Implant

The femoral component was externally rotated by 3° from the posterior condylar axis, shown in Figure 36. This rotated line corresponds to a line drawn between the most lateral and medial edges of the femur, called the transepicondylar axis.

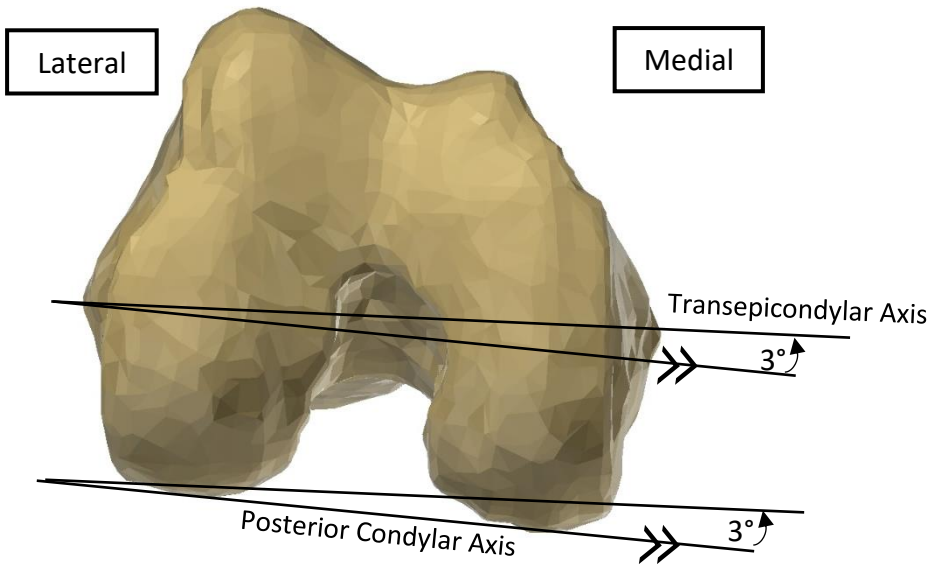

Figure 36: Femoral Component 3° External Rotation

A 0° tibial slope corresponds to the line that runs parallel to the proximal tibial surface, as seen in Figure 37. According to the surgical guidelines for a Genesis II PS implant, the tibial cut should be made at a 3° posterior slope. The PS insert has another 4° slope, which gives a total tibial slope of 7°. The tibial cut was made parallel to the femoral cut at the right depth so that the articulating surfaces of the newly inserted tibial bearing was located where the natural articulating surfaces on the tibial condyles were.

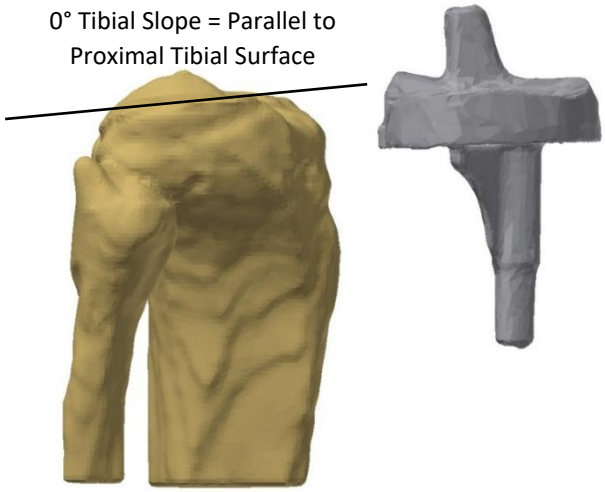

Figure 37: Tibial Slope Benchmark

4.2.3. Moulding and Casting of the Femur and Tibia

Before the femur and tibia bones were 3D printed with their completed bone cuts, the bones were extended at their shaft ends on the computer model. This was to ensure that the femur and tibia lined up with each other after being cemented to their respective mounting pots. Moulds were made from the 3D printed femur and tibia from which stronger bones could be casted for artificial knees.

Mold Star 30 silicon, a Smooth-On product, was used to make the moulds. It has a relatively low viscosity, is mixed 1:1 by volume or weight and vacuum degassing is not required. Fast Cast F180 was originally used to cast the femur and tibia. However, with the tibia experiencing high forces at the quadriceps tendon insert, the tibia would crack after a few squat repetitions. The tibia bone was then casted with another Smooth-On product, Task 9. It is a high-performance casting resin with superior tensile and compression properties which worked well as a tibia bone. The F180 resin was used as potting cement due to its short curing time. A cross-section and a top view of the tibia mould can be seen in Figure 38.

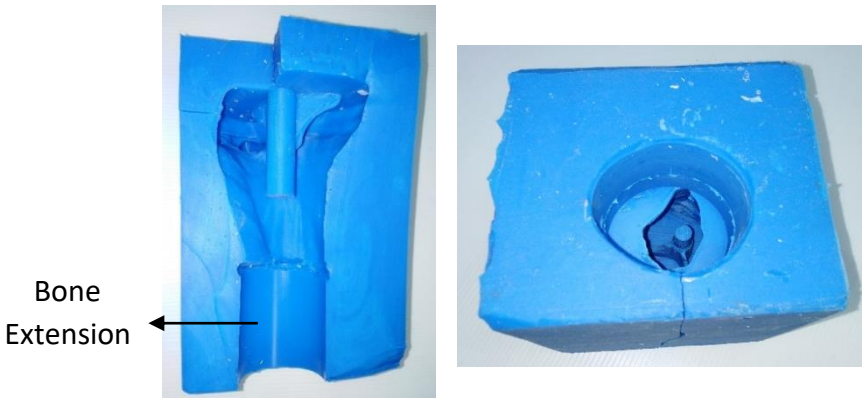

Figure 38: Mold Star 30 Tibial Mould

4.2.4. Assembling the Artificial Knee

The patella and quadriceps tendons were represented by 20 mm wide nylon webbing, as was used and validated by Moran (2005). The webbing was "doubled-up" to make it stronger and ease attaching it to the knee.

Although it was possible to do a full squat without ligaments due to the constrained nature of a posterior stabilised tibial bearing, ligaments were still included for a better natural representation. According to Coles (2015), a 5 mm diameter polyester braided rope offers a good synthetic alternative to the natural ligament. In the study, the rope was compared to porcine ligaments and found to be an accurate representation thereof.

The MCL, LCL and ALL were included on the physically modelled knee. The ligaments were attached with screws to the tibia to form loops as seen in Figure 39 (a). The ligaments could easily be tensioned with the loops at the femur side by using another looped rope to tension the ligaments by pulling it into the femur bone, as illustrated in Figure 39 (b). The black nylon rope looped around the ligament rope and was used to tension the ligaments. To keep the tension in the ligaments when the knee is fully extended, the black rope was clamped in position with screws, as seen Figure 39 (c). The LCL and ALL were represented by one loop and the wide MCL ligament was represented with another, similar to Dauster (2012). The ligament insertion sites were discussed in Section 2.1.4.

A dome-shaped patella button was used for the Genesis II implant, as suggested by Smith and Nephew and shown in Figure 40. The button was fixed to an aluminium piece which represented the rest of the patella. Its total thickness was 24 mm (Moran, 2005). The default patella position was set at an Insall-Salvatti ratio of 1.0. For patella alta and baja, the ratio was 1.23 and 0.77 respectively (Loudon, 2016). The complete knee joint is shown in Figure 41.

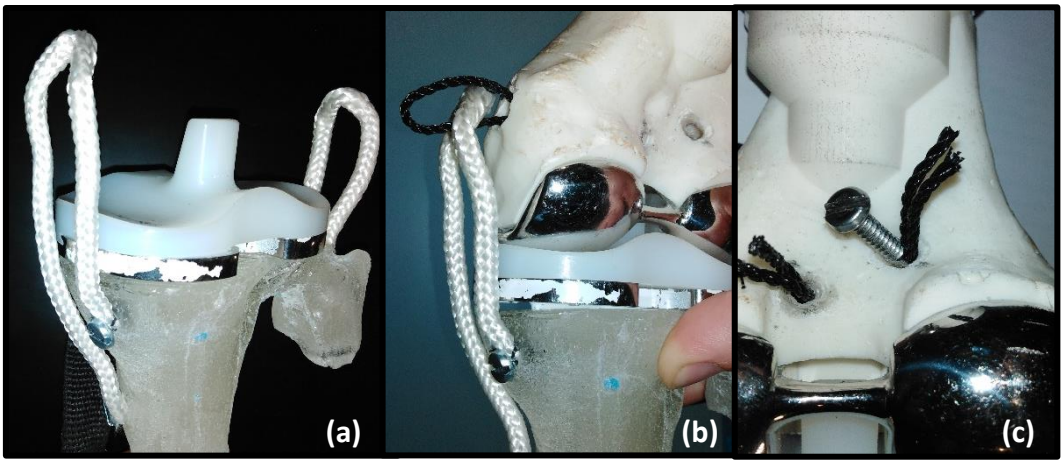

Figure 39: Ligament Tensioning. (a) Ligaments forming loops, attached with screws to the tibia; (b) The looped end of the ligament gets pulled into the femur with another looped nylon rope to tension the ligaments; (c) The clamped nylon rope at the back of the femur.

Figure 40: Modelled Patella with Dome-Shaped Button

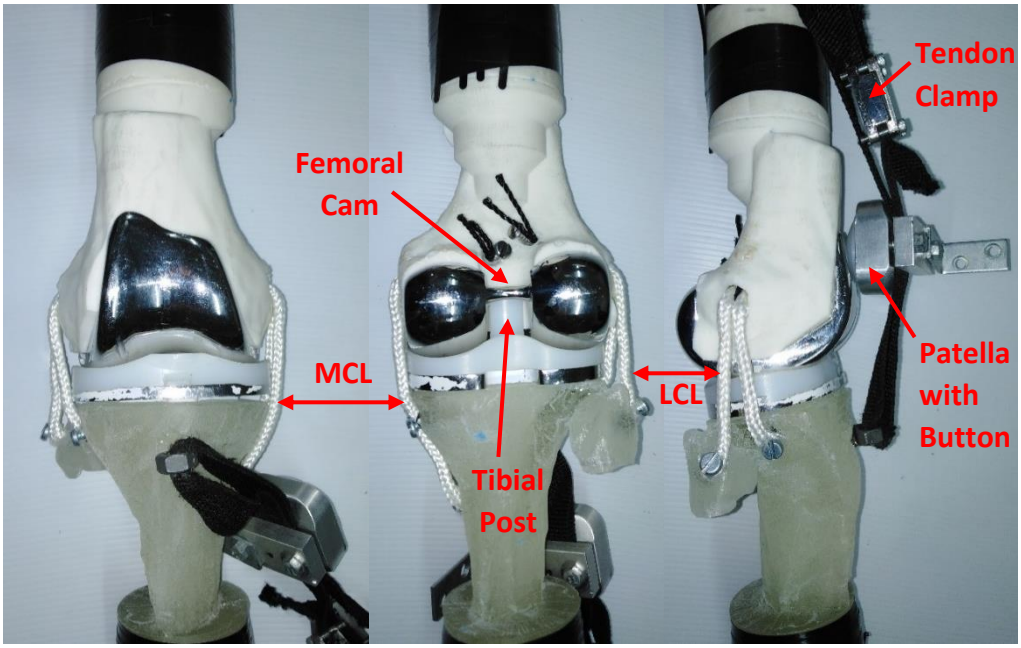

Figure 41: The Complete Artificial Knee Joint

4.2.5. Alignment Rig

Without the ligaments in their natural state that keep a knee joint intact, it is difficult to correctly align the femur and tibia with each other, as well as mechanically align them inside the machine. An alignment rig was made to help with this. The rig, shown in Figure 42, can also be used when potting a cadaver knee. Although a cadaver knee will be correctly aligned at the joint, it should still be mechanically aligned with the hip and ankle assemblies. The alignment rig helped to cement the femur and tibia bones correctly into their respective mounting pots.

Figure 42: Alignment Rig

4.3. Knee Joint Coordinate Systems

Coordinate systems were essential to describe the relative position between two bodies. Each bone in the knee joint (femur, tibia and the patella) was regarded as a rigid body. Bony landmarks were used to establish coordinate systems on the femur and the tibia.

4.3.1. Axes and Coordinate Systems

According to Grood and Suntay (1983), three things had to be specified in order to construct the coordinate systems of the knee: 1) the fixed Cartesian coordinate systems in each bone that is present in the joint; 2) the body fixed axes of the joint

coordinate system; and 3) the location of the translation reference point, chosen as the origin of the Cartesian coordinate system.

The Cartesian coordinate system of each bone was fixed to that bone. Two body fixed axes were defined so that they correspond with two Cartesian axes in the bodies whose relative motion was described. The body fixed axis on the femur, defined as $\mathbf{e_1}$, was the x-axis of the femoral Cartesian system and the axis about which flexion-extension motion was defined. On the tibia, $\mathbf{e_3}$ was defined as the body fixed axis and corresponds to the tibia's z-axis about which internal-external rotation occurs.

The axes $\mathbf{e_1}$ and $\mathbf{e_3}$ form part of the joint coordinate system, with a third axis obtained from their cross product (assuming they are already normalised):

$$\boldsymbol{e_2} = (\boldsymbol{e_3} \times \boldsymbol{e_1}). \tag{4.1}$$

$\mathbf{e_2}$ is called a floating axis, identified by ***F*** in Figure 43, as it is not fixed to the femur or tibia but moves in relation to both.

To summarise, the Cartesian coordinate systems were fixed to their corresponding bones and the joint coordinate system consisted of the body fixed axes and was used to describe the relative motion between the femur and the tibia.

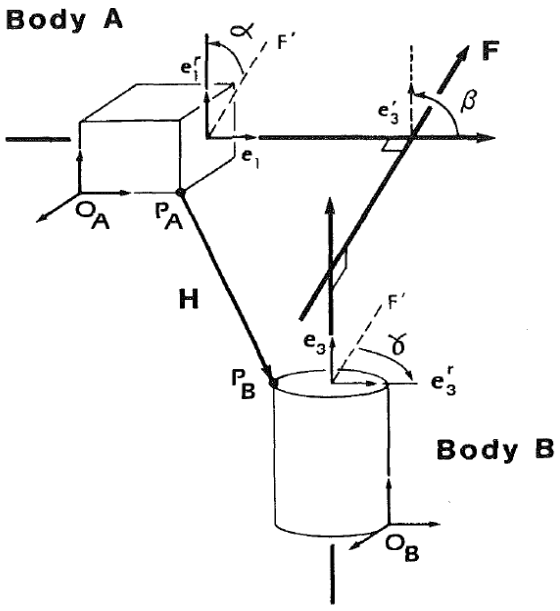

Figure 43: Generalised Joint Coordinate System. The body fixed axes, e_1 and e_2, were embedded in the two bodies whose relative motion was described. The floating axis, e_2 or F, is the common perpendicular to both body fixed axes and was not fixed to either body. (Grood and Suntay, 1983)

4.3.2. Bony Landmarks and Cartesian Coordinate Systems

The Cartesian coordinate systems were defined by identifying bony landmarks with a digitizing probe. The eight landmarks that were digitized are indicated in Figure 44. All six Cartesian axes on the femur and tibia were constructed from these landmarks.

The bony landmarks were (Grood and Suntay, 1983; Benoit *et al.*, 2006):

1. Proximal femur – the centre of the femoral head.
2. Distal femur – most distal point on the femoral intercondylar groove, midway between the medial and lateral condyles; femoral coordinate system origin.
3. Femoral lateral epicondyle – most lateral point of the distal femur.
4. Femoral medial epicondyle – most medial point of the medial femur.
5. Distal tibia – the centre of the ankle.
6. Proximal tibia – midway between the two intercondylar eminences; tibial coordinate system origin.
7. Lateral plateau – the centre of the lateral plateau on the proximal tibia.
8. Medial plateau – the centre of the medial plateau on the proximal tibia.

The axes were established as follows (Grood and Suntay, 1983):

- $\mathbf{Z_F}$ Femoral mechanical axis, a vector joining points 1 and 2, pointing proximally.
- $\mathbf{Y_F}$ The cross product of $\mathbf{Z_F}$ and a vector joining points 3 and 4. It was directed anteriorly from the femoral origin.
- $\mathbf{X_F}$ The cross product of $\mathbf{Z_F}$ and $\mathbf{Y_F}$. It was directed laterally from the femoral origin and was the same as the body fixed axis $\mathbf{e_1}$ and the flexion-extension axis.
- $\mathbf{Z_T}$ Femoral mechanical axis, a vector joining points 5 and 6, pointing proximally. It was the same as the body fixed axis $\mathbf{e_3}$ and the internal-external rotation axis.
- $\mathbf{Y_T}$ The cross product of $\mathbf{Z_T}$ and a vector joining points 7 and 8, directed anteriorly from the tibial origin.
- $\mathbf{X_T}$ The cross product of $\mathbf{Z_T}$ and $\mathbf{Y_T}$, directed laterally from the femoral origin.

The base vectors for the femoral Cartesian coordinate system axes $\mathbf{X_F}$, $\mathbf{Y_F}$, $\mathbf{Z_F}$ were **I**, **J**, **K** respectively. For the tibial axes $\mathbf{X_T}$, $\mathbf{Y_T}$, $\mathbf{Z_T}$ the base vectors were **i**, **j**, **k** respectively. The bone's Cartesian coordinate systems were called their anatomical coordinate systems (ACS) to simplify explaining the translations between coordinate systems.

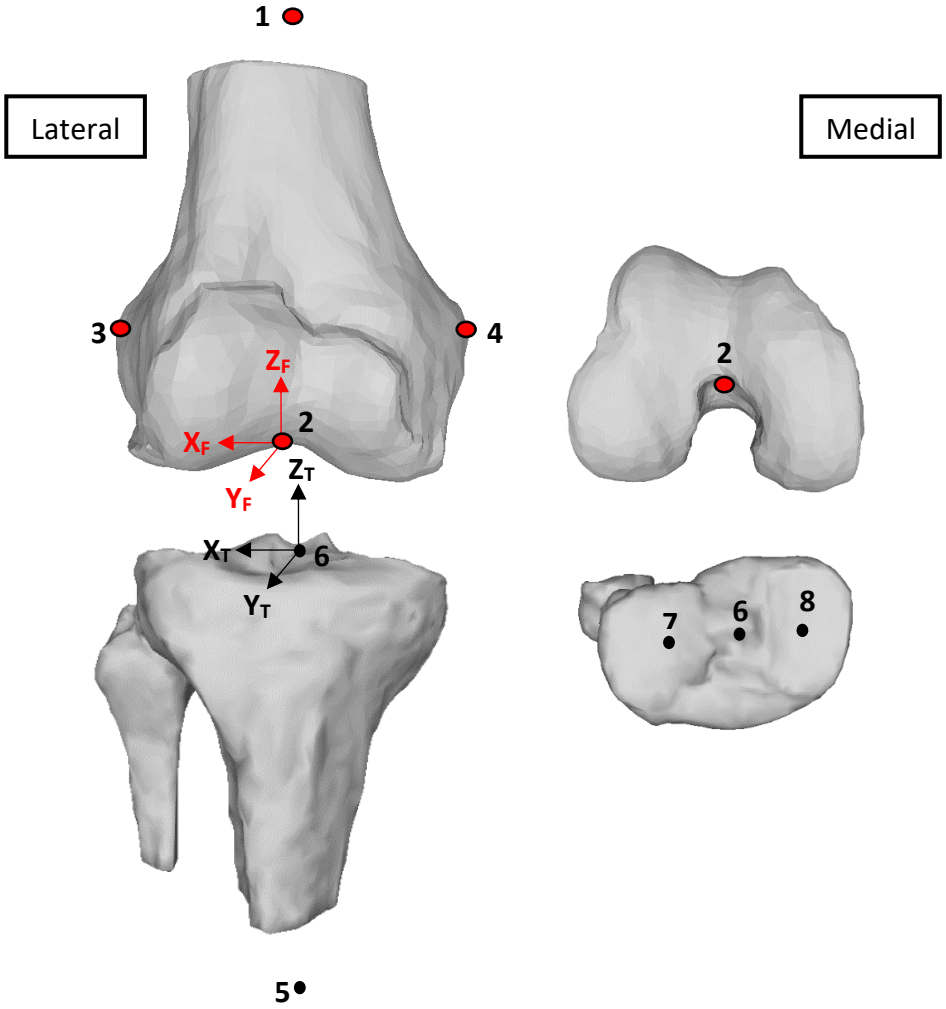

Figure 44: Bony Landmarks for a Right Knee

4.3.3. Rotations and Translations

The relative motion between the femur and tibia, combining to form six degrees of freedom, can be fully described with the axes mentioned in the previous section. The rotations and their directions, as shown by Grood and Suntay (1983) in Figure 45 (a), were described with the joint coordinate system axes ($\mathbf{e_1}$, $\mathbf{e_2}$, $\mathbf{e_3}$) and the Cartesian coordinate systems base vectors. The rotations were as follows:

$$\cos\alpha = \mathbf{J}\cdot\mathbf{e_2} \qquad \text{Positive } \alpha = \text{flexion} \qquad (4.2)$$

$$\sin\gamma = -\mathbf{e_2}\cdot\mathbf{i} \qquad \text{Positive } \gamma = \text{external rotation; right knee} \qquad (4.3)$$

$$\sin\gamma = \mathbf{e_2} \cdot \mathbf{i} \qquad \text{Positive } \gamma = \text{external rotation; left knee} \qquad (4.4)$$

$$\cos\beta = \mathbf{I} \cdot \mathbf{k} \qquad \begin{matrix}\text{Adduction} = \beta - {}^{\pi}/_{2}\text{; right knee} \\ \text{Adduction} = {}^{\pi}/_{2} - \beta\text{; left knee}\end{matrix} \qquad (4.5)$$

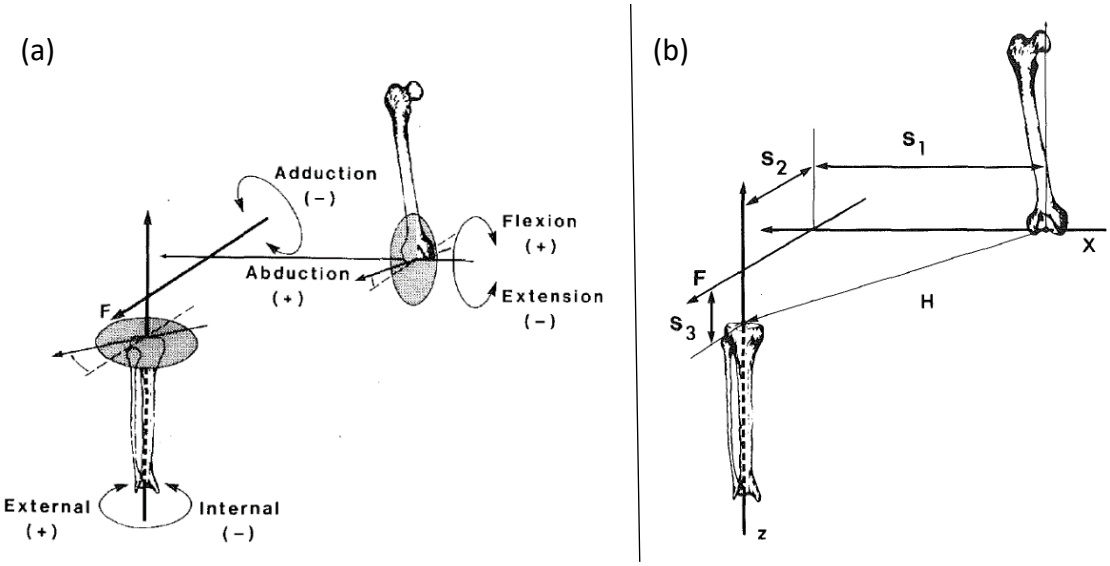

Figure 45: a) Knee Rotations about the Joint Coordinate Axes; b) Translation between the Femur and Tibia (Grood and Suntay, 1983)

Flexion-extension occurred about the femoral body fixed axis, internal-external tibial rotation about the tibial body fixed axis and varus-valgus (abduction-adduction) rotation about the floating axis.

The translation between the femur and the tibia, as described by Grood and Suntay (1983) and denoted by the vector running from the femoral origin to the tibial origin, **H**, is illustrated in Figure 45 (b). This vector can be constructed with the joint coordinate system base vectors and the three joint translations: S_1, S_2 and S_3.

$$\mathbf{H} = S_1\boldsymbol{e_1} + S_2\boldsymbol{e_2} + S_3\boldsymbol{e_3} \qquad (4.6)$$

S_1 is the distance from the femoral origin along $\mathbf{e_2}$ to where it crosses with $\mathbf{e_1}$; S_2 is the distance between $\mathbf{e_1}$ and $\mathbf{e_3}$ along the floating axis, $\mathbf{e_2}$; S_3 is the distance from the tibial origin along $\mathbf{e_3}$ to where it intersects with $\mathbf{e_2}$.

The clinical translations (t_1, t_2, t_3) are medial-lateral tibial shift, anterior-posterior tibial drawer, and joint distraction-compression, respectively. Lateral shift, anterior drawer and joint distraction were taken as positive translations. These

translations can be defined as the projections of **H**, the translation vector, along each of the joint coordinate system base vectors as:

$$t_1 = \mathbf{H} \cdot \boldsymbol{e_1} \tag{4.7}$$

$$t_2 = \mathbf{H} \cdot \boldsymbol{e_2} \tag{4.8}$$

$$t_3 = -\mathbf{H} \cdot \boldsymbol{e_3} \tag{4.9}$$

The base vectors ($\mathbf{e_1}$, $\mathbf{e_2}$, $\mathbf{e_3}$) are non-orthogonal and therefore:

$$\mathbf{H} \neq t_1\boldsymbol{e}_1 + t_2\boldsymbol{e}_2 + t_3\boldsymbol{e}_3. \tag{4.10}$$

The clinical translations for a right knee could now be expressed for all joint positions in terms of the three joint translations as:

$$t_1 = S_1 + S_3 \cos\beta \tag{4.11}$$

$$t_2 = S_2 \tag{4.12}$$

$$t_3 = -S_3 - S_1 \cos\beta. \tag{4.13}$$

4.4. Coordinate Transformations

To successfully track the motion of the knee joint, tracking tools were placed on each moving bone in the knee joint (the femur, tibia and the patella). The bony landmarks identified in Section 4.3.2 could then be described in terms of the tracking tool fixed to the bone on which the landmarks were identified with a digitizing probe.

As the bones were assumed to be rigid bodies, the relative orientation and translation of the bone's coordinate system to that of the tracking tool would stay constant. For example, in Figure 46, the orientation and position of the femoral ACS relative to tool A would stay constant regardless of the position of the knee. The exact orientation and position of the femoral and tibial ACS at any given time were thus known while the tools were tracked. This was important as these ACS were used to describe the relative motion of the rigid bodies.

To simplify calculations, the femoral tracking tool was set as the reference/world coordinate system. The tibial and patellar tools were thus all tracked relative to the femoral tool. Positional information of each tool was given in normal *x*, *y*, *z* notation and the orientation was given in quaternion format.

Quaternions are a mathematical abstraction used to represent rotations in 3D space and are usually expressed as a scalar and a 3-element vector:

$$\mathbf{q} = (s, \mathbf{V}) = q_0 + q_1\,\mathbf{i} + q_2\,\mathbf{j} + q_3\,\mathbf{k} \tag{4.14}$$

with **i, j, k** the base vectors of some reference system (Beaty, 2011).

In kinematics, the scalar is related to a right-hand rule rotation angle about the direction specified by the vector part. In this application, quaternions were used to describe orientations, without the risk of gimbal lock as experienced with Euler angles.

Quaternion orientations were converted to direction cosine matrices (DCM). These transformation matrices could be used to transform vectors from one coordinate reference frame to another. Using the notation from (4.14), a DCM can be constructed from a quaternion as follows (Beaty, 2011):

$$\mathbf{R} = \begin{bmatrix} 1 - 2({q_2}^2 + {q_3}^2) & 2(q_0\, q_3 + q_1\, q_2) & 2(q_1\, q_3 - q_0\, q_2) \\ 2(q_1\, q_2 - q_0\, q_3) & 1 - 2({q_1}^2 + {q_3}^2) & 2(q_0\, q_1 + q_2\, q_3) \\ 2(q_0\, q_2 + q_1\, q_3) & 2(q_2\, q_3 - q_0\, q_1) & 1 - 2({q_1}^2 + {q_2}^2) \end{bmatrix}. \quad (4.15)$$

Coordinates of a vector, $\boldsymbol{v}$, can be transformed from one coordinate system to another with a quaternion, $\boldsymbol{q}$, or the DCM matrix, $\mathbf{R}$, such that (Beaty, 2011):

$$\boldsymbol{v}' = \boldsymbol{q}^*\, \boldsymbol{v}\, \boldsymbol{q} = \mathbf{R}^{-1}\, \boldsymbol{v} \quad (4.16)$$

Where:

- $\boldsymbol{v}$: vector in original coordinate system (when it is multiplied with a quaternion, it should be written as a quaternion with a zero scalar part - $\boldsymbol{v} = [\mathbf{0}\ \boldsymbol{v}]$)
- $\boldsymbol{v}'$: vector in new coordinate system
- $\boldsymbol{q}^*$: conjugate of quaternion, $\boldsymbol{q}$
- $\mathbf{R}^{-1}$: inverse of DCM matrix, $\mathbf{R}$.

To establish the axes of the bony Cartesian coordinate systems with the digitized landmarks, the direction of the desired axis vector should be known. A vector between points A and B, directed from B towards A, is:

$$\mathbf{V_{BA}} = A - B. \quad (4.17)$$

As all digitized landmarks were taken with the femoral tool as reference, the resulting axes vectors were also with regards to this reference tool. Equation (4.16) was used to transform the vector to the relevant tracking tool's coordinate system that is fixed to the bone on which the landmarks were digitized. These transformed vectors were used to get the constant transformation matrix from the tracking tool coordinate system to the ACS of the relevant bones.

In Figure 46 the rotations are indicated in red and two relevant vectors are indicated in blue. If $\mathbf{X_T}$, $\mathbf{Y_T}$ and $\mathbf{Z_T}$ are axis row vectors of the tibial ACS with regards to the tibial tool, the transformation matrix $\mathbf{R_T\_t2a}$ is as follows:

$$\mathbf{R_T\_t2a} = [\mathbf{X_T};\ \mathbf{Y_T};\ \mathbf{Z_T}]. \tag{4.19}$$

Furthermore, it is important to note that when rotation matrices are multiplied, it should be reversed from the order of rotations. For example:

$$\mathbf{R_T\_w2t} = \mathbf{R_T\_t2a}^{-1} \times \mathbf{R\_F_a2T_a} \times \mathbf{R_F\_t2a}. \tag{4.18}$$

In Figure 46, the vector **V_F_a2T_a** is equal to vector **H** introduced in equation (4.6) as the vector from the femoral ACS origin to the tibial ACS origin. Vector **V_F_a2P_a** is the vector that runs from the femoral ACS origin to the patellar ACS origin.

All these calculations were computed and processed in MatLab software (The MathWorks, Inc., Natick, USA). The complete code can be seen in Appendix F.

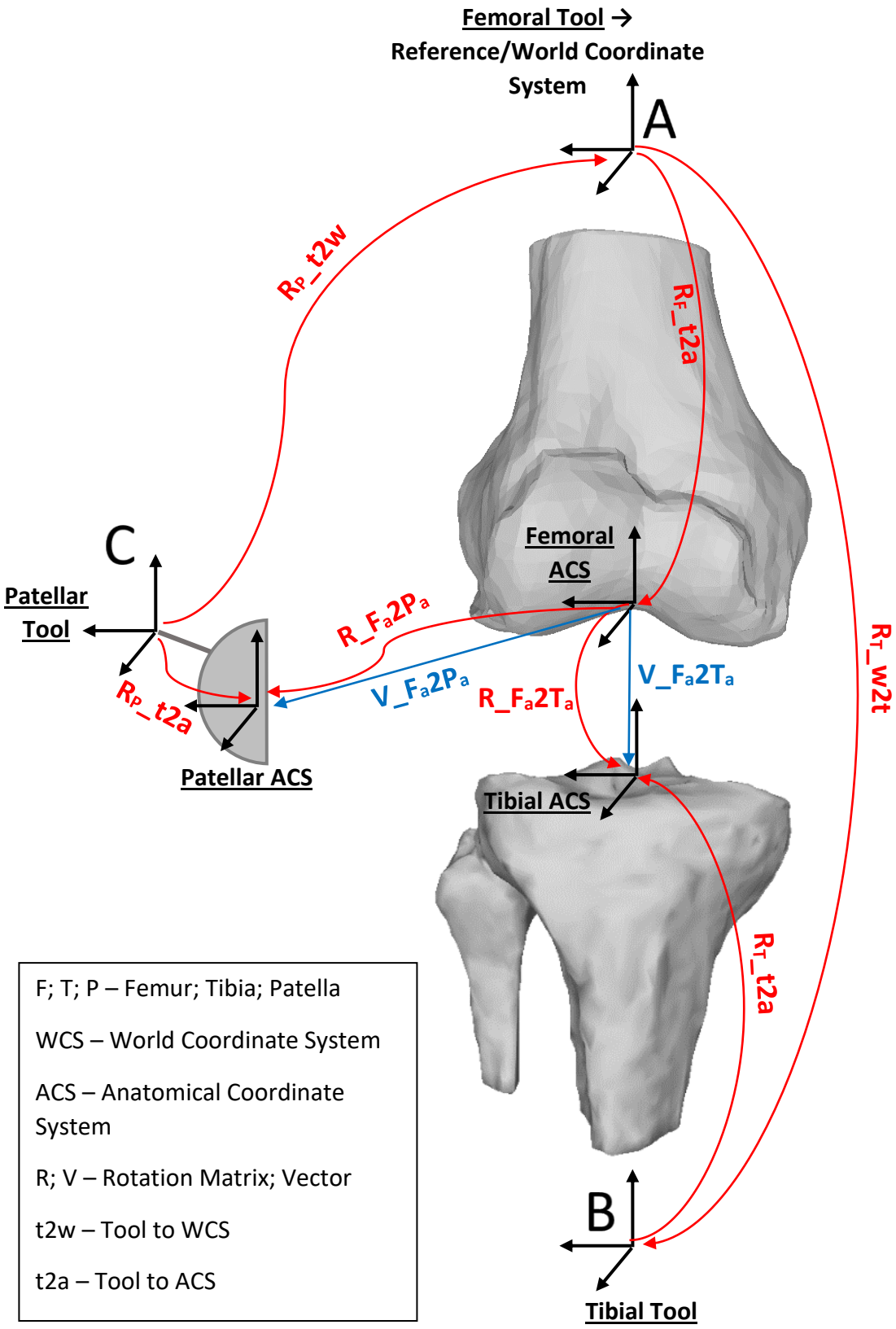

Figure 46: Knee Joint Rotations

4.5. Motion and Force Tracking

A Polaris Vicra (Northern Digital, Waterloo, Canada) position sensor was used to track the 3D position of the femur, tibia and patella at a volumetric accuracy of 0.25 mm RMS. Passive tracking tools with reflective spheres, as seen in Figure 47, were attached to each bone in the knee and bony landmarks, essential to describe relative knee motion, were identified with a digitizing probe or pointer tool.

The position sensor measured the position of the tools and calculated its transformations (position and orientation). Transformations are given by default with regards to the world coordinate system, located at the position sensor. However, for this study the femoral tool was allocated as the reference tool/coordinate system. The position transformations were given as normal X-Y-Z values, with the orientation transformations given in quaternion format.

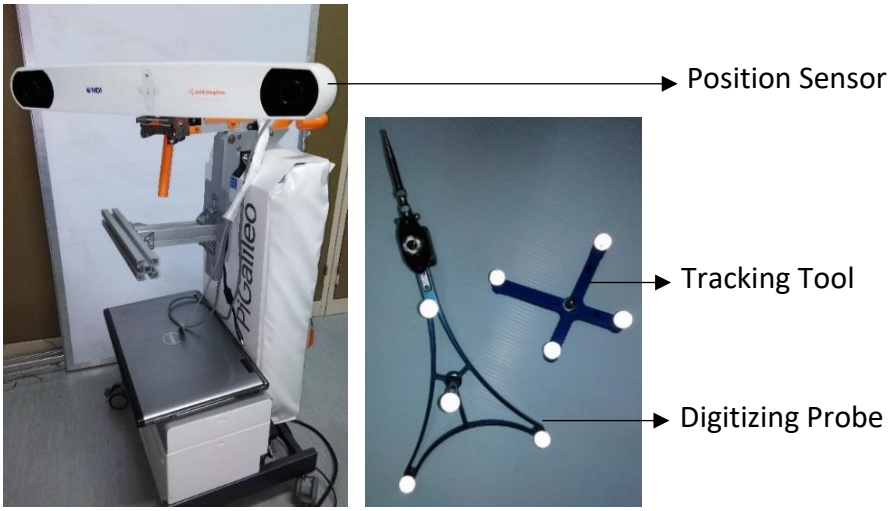

Figure 47: NDI Polaris Vicra Position Sensor with Tool and Probe

A Lorenz Messtechnik GmbH (Alfdorf, Germany) LCV-USB2 amplifier was used with a 5 kN HBM (Darmstadt, Germany) U2B force transducer to measure the quadriceps force. The force transducer was calibrated with software supplied by Lorenz and a professionally calibrated MTS tensile machine.

Autohotkey software was used to synchronize the Polaris Vicra position sensor and Lorenz amplifier at 20 samples per second. Two separate recordings could thus be made simultaneously. The Autohotkey code can be seen in Appendix A.

4.6. Summarised Test Method

The test methods are summarised to conclude the methods discussed in this chapter.

A squat simulator, based on the Oxford Knee Rig and described in Chapter 3, was used to perform squats on artificial knees. The squat simulator consisted of a hip and ankle assembly that allowed the six degrees of freedom present in a knee joint. Squat motions were performed by inducing tension on the quadriceps with an electromechanical linear actuator while receiving feedback data of the hip assembly's position. A full squat cycle consisted of a flexion phase ranging from 13˚ to 90˚ flexion, followed by the extension phase ranging from 90˚ back to its starting position at 13˚ (13˚ - 90˚ - 13˚). This range is a good representation of sitting and stair climbing (Nordin and Frankel, 2001).

All test subjects were right knees from a 70 kg male, with a set Q-angle of 14˚. The full femur and tibia lengths were set as 460 mm and 375 mm, respectively. The artificial knee specimens were discussed in Section 4.2.4. The collateral ligaments were represented with 5 mm thick polyester braided rope (Coles, 2015). For the purpose of this study, all the tests were carried out using a Genesis II posterior stabilised prosthesis. A size 7 femoral component and size 5 tibial component was mounted to the bones after the necessary cuts were performed to mechanically align the femur and tibia, as described in Section 4.2.2. The effective tibial slope was 7˚ and a dome-shaped patella button was used, with a total patella thickness of 24 mm. The default patella position was set at an Insall-Salvatti ratio of 1.0. For patella alta and baja, the ratio was 1.23 and 0.77 respectively.

The Polaris Vicra optical tracking sensor was first used to digitize the bony landmarks required to establish the knee joint coordinate systems, as described in Section 4.3. With a tracking tool fixed to the femur, tibia and the patella, the knee motion could be tracked with the Polaris Vicra. The processes described in Section 4.4 were used to process the tracking data to get the relative motion between the rigid bodies inside the knee joint.

A complete testing procedure can be found in Appendix B. It describes how the software should be used, how the landmarks introduced in Section 4.3.2 should be digitized and what aspects should be focussed on while performing the tests to ensure better repeatability.

4.7. Repeatability of the Squat Simulator

The repeatability of the squat simulating machine was evaluated to ensure that kinematic tests performed with the simulator were not inconsistently influenced by the machine itself when all variables and test conditions were kept constant.

To test repeatability, the mean kinematic curves were calculated for each set of repeated tests under the same test conditions (five squat repetitions per knee). The residual error was then calculated between the mean values and each trial curve, with the standard deviations (SD) of the errors recorded as measures of variability. Using the largest variability values, the coefficients of repeatability (CR) were calculated as double the standard deviation of the residuals (Bland and Altman, 1986). This gives an approximate 95% confidence interval of the kinematic parameters around their mean curves.

The repeatability of the following parameters was evaluated: flexion-extension, internal-external tibial rotation, varus-valgus rotation, medial-lateral translation, anterior-posterior, superior-inferior and quadriceps force (QF). The results are summarised in Table 6.

Table 6: Repeatability of the Squat Simulator Across Different Trials

	KNEE 1	KNEE 2	KNEE 3	KNEE 4	KNEE 5	WORST CR
FE (˚)						
Mean	48.6	48.8	49	48.9	48.8	
2 SD	1.28*	0.87	0.53	0.38	0.42	1.28
IE (˚)						
Mean	-2.76	-2.2	-2.14	-2.38	-2.38	
2 SD	0.063	0.12*	0.09	0.107	0.104	0.12
VV (˚)						
Mean	1.61	1.67	1.72	1.74	1.77	
2 SD	0.015	0.025*	0.017	0.019	0.017	0.025
ML (mm)						
Mean	-0.66	-0.72	-0.73	-0.73	-0.69	
2 SD	0.046	0.051*	0.04	0.035	0.042	0.051
AP (mm)						
Mean	-4.5	-4.76	-4.93	-5.02	-5.09	
2 SD	0.29	0.25	0.175	0.14	0.29*	0.29
SI (mm)						
Mean	19.72	19.66	19.63	19.62	19.62	
2 SD	0.17*	0.1	0.073	0.045	0.059	0.17
QF (N)						
Mean	691	695	702	711	708	
2 SD	47.8	47	66.5*	38.2	44.7	66.5

* The worst coefficient of repeatability

Looking at the worst CR, 95% of the measurements are expected to fall within the following ranges about a mean curve of a specific set of tests:

- Flexion-extension: 1.28˚
- Tibial internal-external rotation: 0.12˚
- Varus-valgus rotation: 0.025˚
- Medial-lateral tibial shift: 0.051 mm
- Anterior-posterior tibial translation: 0.29 mm
- Superior-inferior translation: 0.17 mm
- Quadriceps force: 66.5 N

These variability ranges are small compared to the total ranges of motion and force data. It thus suggests that a set of squat tests, with any specific knee specimen used in this study, will give similar results within the ranges listed above.

4.8. Results

All the results in this section were obtained from the average of five different knees with ligaments, doing five squat tests each, with a Genesis II PS prosthesis.

4.8.1. Quadriceps Force

The quadriceps force in Newtons is presented in Figure 48 against the squat cycle on the left and against the flexion angle in degrees on the right. The maximum average quadriceps force over all the tests was 2185 ± 19 N and occurred at a 57% completed squat cycle.

The rate of extension was faster than the flexion rate with initial high quadriceps forces required to start the extension phase. A force increase of almost 600 N was required to go from flexion to extension at a constant 90˚ flexion.

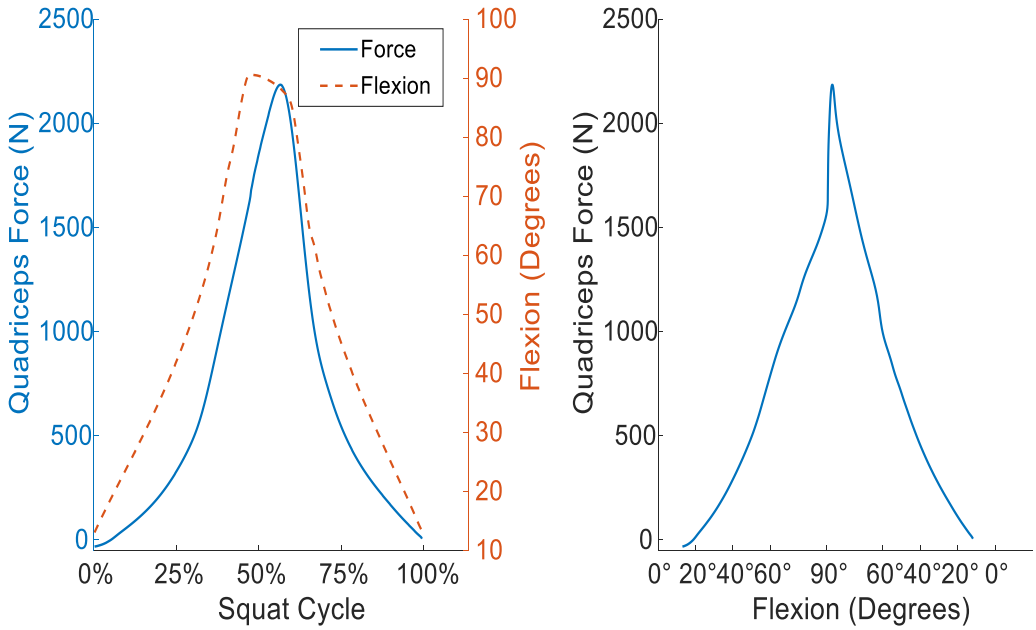

Figure 48: Left: Quadriceps Force vs Squat Cycle. Right: Quadriceps Force vs Flexion

4.8.2. Rotational DOF

The average rotational motions are shown in Figure 49 with the rotations in degrees on the vertical axis vs the squat cycle on the horizontal axis. The flexion phase started at 13˚ and ended at 90˚ with the extension phase returning it to 13˚ flexion. The tibia slightly rotated internally (0.55˚) during the flexion phase and externally (1.35˚) during extension. The maximum difference in tibial varus-valgus rotation was limited to 0.5˚. There was a slight valgus rotation as flexion approaches 90˚ but returned to varus rotation as the quadriceps force increased to start the extension phase. The rest of the extension phase experienced valgus rotation. The average flexion speed achieved was 7˚/sec which is comparable to Long (2011).

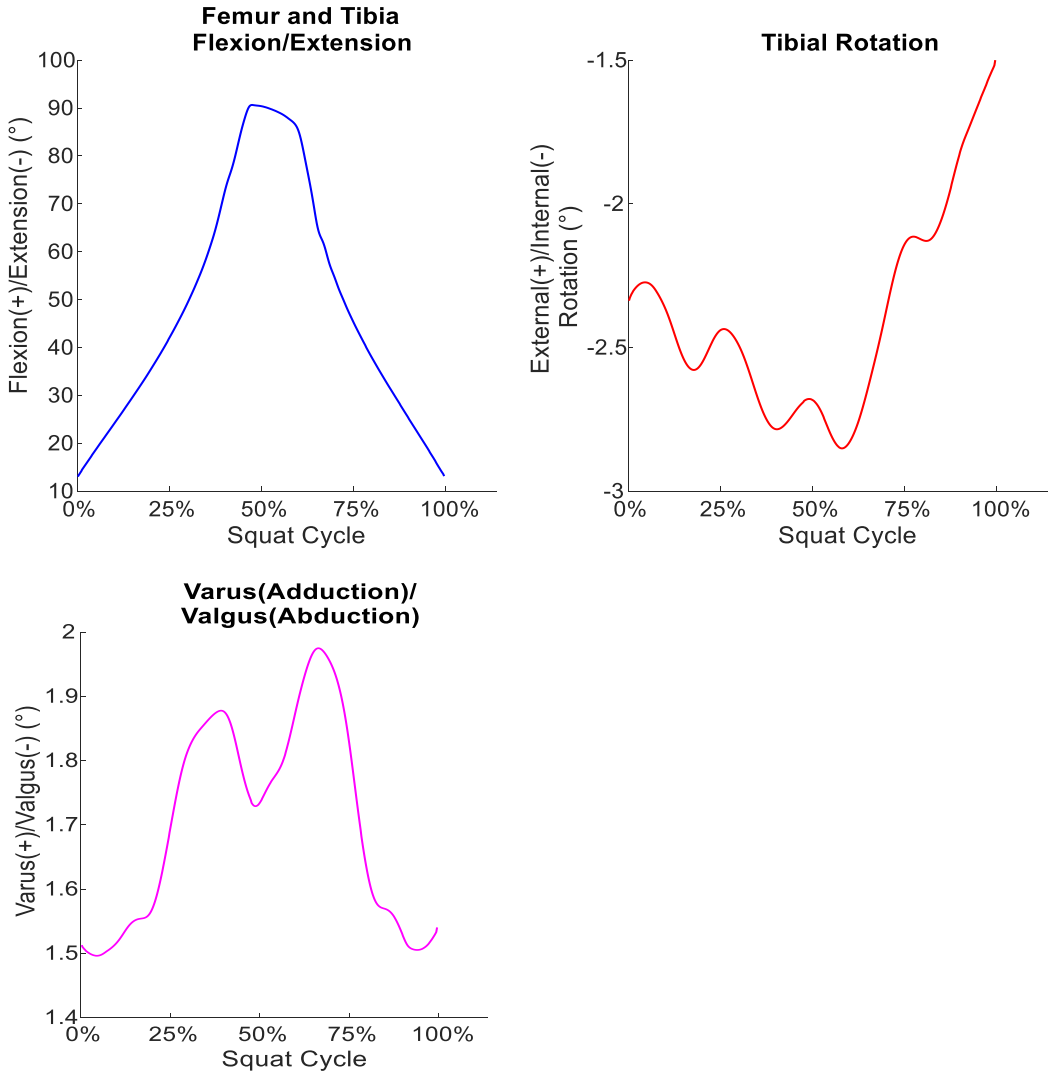

Figure 49: Rotational Degrees of Freedom

4.8.3. Translational DOF

The average translational motions are shown in Figure 50 with the translations in millimetres on the vertical axis vs the squat cycle on the horizontal axis. The tibia experienced a lateral movement during the flexion phase and medial movement during extension. The femur moved anteriorly during flexion, giving the illusion that the tibia moved posteriorly. All translational degrees of freedoms were relatively symmetric for the flexion and extension phases. As the knee reached deep flexion, the height of the femoral origin above the tibial transverse plane (compression translation) was at its lowest.

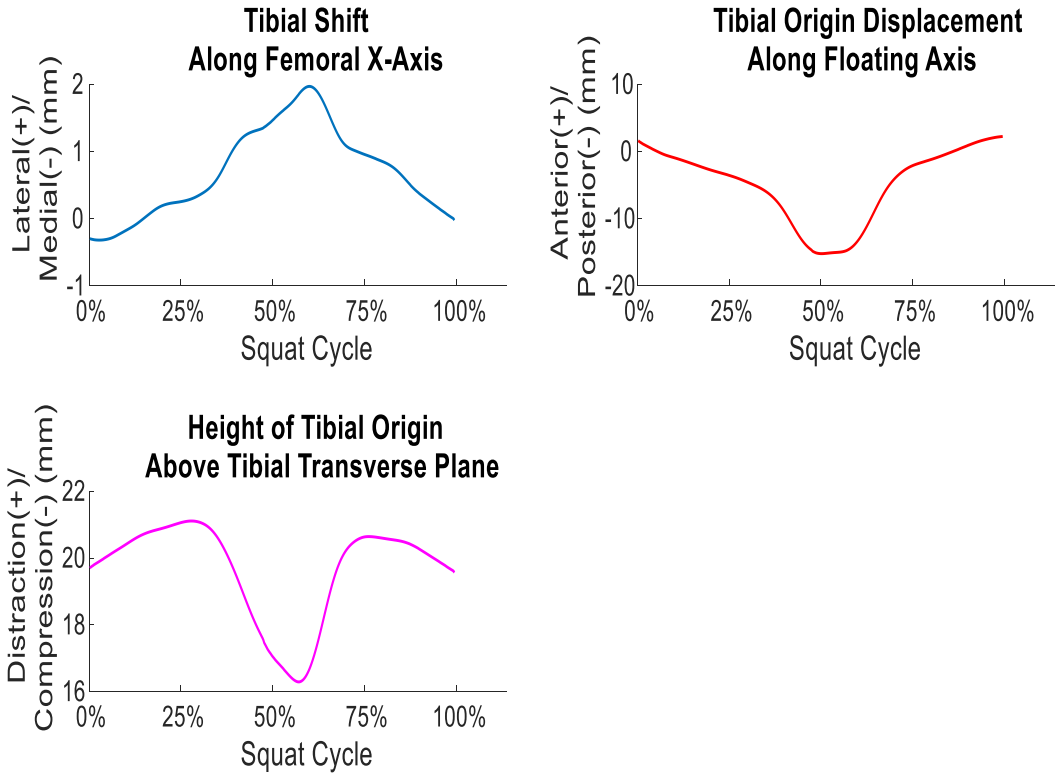

Figure 50: Translational Degrees of Freedom

4.8.4. Patella Alta/Baja Influence on Quadriceps Force

The vertical position of the patella was increased and decreased during tests for Insall-Salvatti ratios of 1.23 and 0.77 respectively to evaluate the influence of the patellar position on the quadriceps force. Figure 51 shows the quadriceps force in Newtons vs the patella flexion cycle.

Patella baja resulted in an average quadriceps force increase of 540 N and patella alta in an average force decrease of 400 N compared to the normal patella position for the same flexion range. The patella baja curve is different than the normal and alta curves due to the earlier lateral movement of the patella.

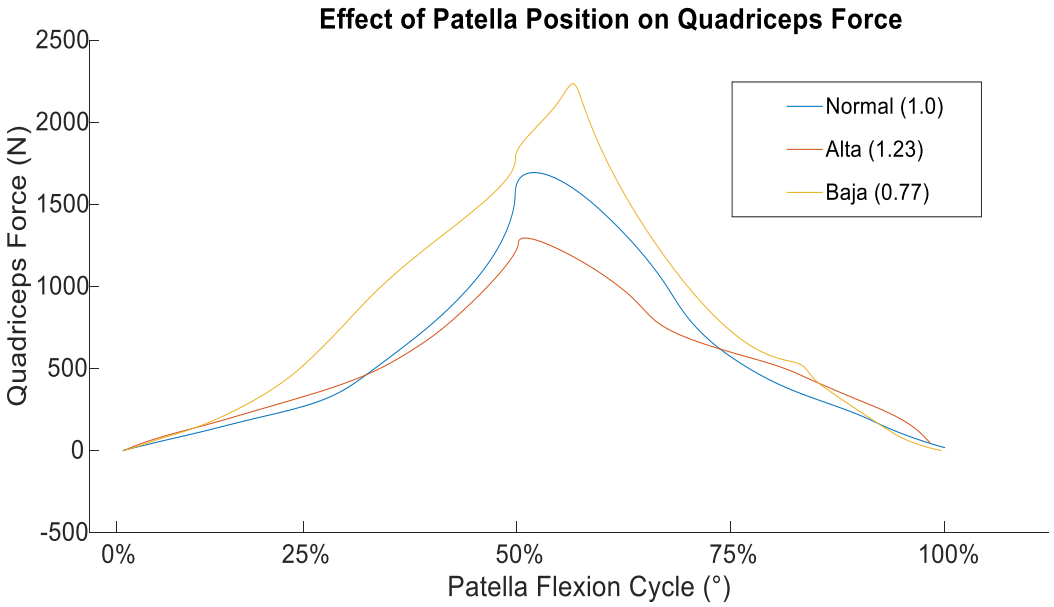

Figure 51: The Influence of Patella Position on Quadriceps Force

4.9. Discussion

4.9.1. General Overview

Cadaveric specimens provide the most accurate representation of the natural knee but are highly variable between specimens and cannot be tested for extended periods of time. Artificial knees provided consistency and repeatability and made it easy to isolate certain parameters. The limited number of tests per knee and the limited flexion range were due to the amount of knee failures experienced during preliminary testing. Failed samples can be viewed in Appendix D.

Due to the high variability in the physiological structure of knees between different natural specimens, different surgical techniques and the variety of knee implants, literature findings are often not consistent (Victor, Labey, *et al.,* 2010). To keep the test variables to a minimum, the aim was to perform all the tests with the same casted femur and tibia by only adjusting ligament tensioning between knee samples. This goal was achieved when a new material was used to cast the tibia, as explained in Section 4.2.3.

4.9.2. Quadriceps Force

From Figure 48, the considerable jump in quadriceps forces of 600 N on average to start the extension phase is a phenomena also documented by Steinbrück *et al.* (2013). This can possibly be attributed to the larger normal forces between the linear bearings and sliding rail at the hip assembly as well as the positioning of the

patella, as further discussed in Section 4.9.5. The general trend of a decreasing patella tendon moment arm with increasing flexion (Long *et al.*, 2013) also contributed to the gradual quadriceps force increase during the flexion phase.

The maximum average force of 2 185 ± 19 N was realistic when compared to similar knee simulator studies in literature (2 400 N - Hast, 2011; 2 700 N - Van Haver *et al.*, 2013; 1 400 N - Baldwin *et al.*, 2012). It also confirmed the FBD from Section 3.2.2 to be an accurate mathematical representation of the squat simulator where the calculated quadriceps force was 2 443 N.

The addition of hamstring muscles would have further increased the quadriceps force (Macwilliams *et al.*, 1999; Rusly *et al.*, 2016).

4.9.3. Rotational DOF

The flexion-extension DOF was indirectly controlled by the simulator to go from 13˚ to 90˚ and again returning to 13˚. The relatively slow turnaround at 90˚ compared to the rest of the flexion-extension phase was due to the high forces required to start the extension phase, as seen in Figure 48.

The rate of flexion was faster the greater the flexion angle becomes. A fast extension occurred between 85˚ and 65˚ likely due to the high elastic potential energy built-up in the quadriceps tendon while attempting to breach the critical flexion point discussed in Section 3.3.3.

The fit of the tibial post inside the femoral box restricted the internal-external rotation (Keller and Amis, 2015) and was possibly one of the causes for the limited maximum change in tibial rotation of 1.35˚ compared to the natural knee (Victor *et al.* (2009) observed a change in tibial rotation of up to 2˚ at 90˚ flexion for a cadaver knee specimen). The reason for the oscillating pattern during the flexion phase is speculated to be due to the friction on the tibial bearing.

Internal rotation during flexion is supported by literature for PS implants (Cates *et al.*, 2008; Victor, Mueller, *et al.*, 2010), with maximum internal rotation occurring at maximum quadriceps force. The external rotation during the extension phase could possibly be attributed to the increased quadriceps force compared to the flexion phase and the Q-angle which caused a lateral quadriceps force vector that will externally rotate the tibia.

The internal-external rotations were in accordance with the screw-home mechanism described in Section 2.2.2. Although the patterns were not similar, a comparable small range of rotation was also measured by Wünschel *et al.* (2013) for a Genesis II PS implant.

The small range of varus-valgus rotation can possibly be attributed to the constrained femur in the varus-valgus direction and how well the tibial post fitted into the box cut out for it in the femur. The reason for the slight drop in rotation and then an increase again at 50% squat cycle is unknown and not confirmed by literature.

4.9.4. Translational DOF

The medial-lateral tibial translation occurs along the femoral x-axis and is called tibial shift. The maximum lateral tibial shift was in the vicinity of maximum quadriceps force. A correlation between lateral tibial movement during flexion and a varus rotation was assumed. However, a direct correlation between the varus-valgus rotational graph and medial-lateral translational graph could not be established. This can possibly be due to the constrained nature of the PS implant.

The range of anterior-posterior tibial translation along the floating axis was similar to that of Wünschel *et al.* (2013) for a Genesis II PS implant. Without contact force measurements on the tibial post, it is difficult to determine exactly when the post and cam engage with each other. However, Wünschel *et al.* (2013) reported that they engaged at 80˚ flexion and that a markedly more posterior movement can be observed. Arnout *et al.* (2015) and Fitzpatrick *et al.* (2013) did similar studies on the Genesis II PS implant and reported a 71˚ and 50˚ flexion at post-cam engagement respectively. All these studies had the hamstrings included and the tests were done on physical simulators similar to this study, except for Fitzpatrick *et al.* who did it on a computerised squat simulator. This emphasizes the differences in measured results for the same implant, but slightly different loading patterns and specimens.

A rapid change in posterior movement can be observed at 60˚ for the measured data and a complete stop of movement at 90˚ until the start of the extension phase. This could possibly be the working of the post-cam. The addition of hamstring muscles would enhance posterior translation of the tibia and earlier post-cam engagement would have been experienced (Macwilliams *et al.*, 1999).

The tibial slope has an influence on the anterior translation of the tibia (Giffin *et al.*, 2004). Reducing the slope will also reduce anterior translation. Wünschel *et al.* (2013) also concluded that the cam and post on a PS implant may have little influence on anterior-posterior femoral rollback.

The distraction-compression translation is not often reported in literature. However, the readings do support the presence of a degree of freedom along the tibial mechanical axis. The femoral and tibial component sizes were not exact fits for the femur and tibia bones used in this study. However, they were available for use and did not violate surgical recommendations. A consequence thereof,

however, is that the bony landmarks on the femur used to define the flexion-extension axis, were possibly not at the centre of the cylindrical profile, shown in Figure 11, for the slightly smaller femoral condyles. This will have an influence on the distraction-compression profile during knee rollback, but the extent thereof is difficult to tell.

4.9.5. The Effect of Patella Alta/Baja

The effect of patella alta/baja could visually and experimentally be observed. Less force is required during early flexion as compared to deep flexion due to the quadriceps tendon moment arm being greater than the patella tendon moment arm. Deeper flexion could be achieved with patella alta and 400 N less quadriceps forces were needed to perform a squat in the same flexion range compared to a patella placed at the normal Insall-Salvatti ratio of 1.0. This is because the patella stays longer in the trochlear groove as it slides over the anterior surface of the femur and results in a bigger patella tendon moment arm for a longer period.

As the flexion gets deeper, the patella moves more distally towards the intercondylar notch of the femur. When the patella reaches this position, a lot of quadriceps force is required to pull the knee out of deep flexion due to the small patella tendon moment arm, as apparent from Figure 52. This distal position is naturally reached faster with patella baja, as confirmed by the 540 N quadriceps force increase at the same flexion angle compared to the normal patella position.

It is favourable to have a reduced quadriceps force during daily activities, which can be achieved with patella alta (Lenhart *et al.*, 2017). However, patella alta also causes higher contact forces between the patella and femur (Luyckx *et al.*, 2009). Thus, if the aim is to evaluate kinematics at an increased flexion range inside the squat simulator without fearing knee failure, the patella can be moved higher (patella alta) on the artificial knee. This, however, should be avoided when contact and soft tissue forces are evaluated.

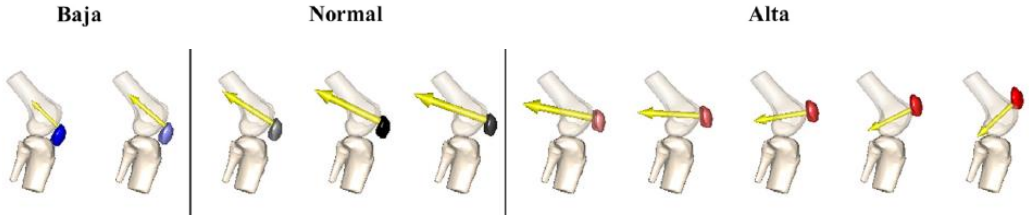

Figure 52: The Interaction Between the Patella Position and Knee Flexion. The yellow arrow indicates the direction and magnitude of the patella contact force. (Adapted from: Lenhart *et al*. (2017))

4.10. Conclusion

This study showed that the squat simulator was able to produce repeatable results and could realistically model knee motion and quadriceps loading. It can thus be concluded that the simulator successfully performed its tasks and that it is fit for further research in prosthesis design and knee biomechanics.

Chapter 5

5. Knee Implant with and without Ligaments

5.1. Introduction

The constrained nature of a PS prosthesis allows a squat to be performed without ligaments. With the collateral ligaments usually kept intact after a PS TKA, the influence of these ligaments on knee kinematics were investigated. The hypothesis is that the addition of collateral ligaments on a knee with a PS implant influences the kinematics during a squat motion.

5.2. Test Methods

The same test data obtained in Chapter 4 could be used to investigate the hypothesis. However, additional squat data from knees without ligaments had to be obtained. Knowing that the simulator produces repeatable results when all parameters are kept constant, as proved in Section 4.7, five squats were done with a knee without ligaments. The average of these tests was compared with the average data obtained from the knees with ligaments. All knee sample parameters were the same as described in Section 4.6, except for the removed collateral ligaments.

To evaluate the influence of collateral ligaments on the kinematics of a PS knee, analysis of variance (ANOVA) was conducted. For statistical significance, alpha was selected as 0.05. The average kinematic data of the specimens with ligaments was compared with the average kinematic data of the specimens without ligaments.

For the ANOVA evaluation, an *F*-critical value (constant across evaluating parameters) was calculated against which an *F*-value (unique for each parameter) was compared. If the *F*-value is bigger than the critical value, the null hypothesis can be rejected.

5.3. Results

Analysis of variance was performed to investigate the statistically significant differences between the two groups (with ligaments vs without ligaments). With alpha taken as 0.05, the *F*-critical value is 3.85. Table 7 shows the calculated *F*-values used to determine statistical significance. Internal-external rotation and varus-valgus rotation were the only two parameters found to have statistical significance, as indicated with an asterix (*).

Table 7: ANOVA F-Values

PARAMETER	*F*-VALUE
FLEXION-EXTENSION	0.0044
INTERNAL-EXTERNAL ROTATION	94.82*
VARUS-VALGUS ROTATION	405.26*
MEDIAL-LATERAL TIBIAL SHIFT	1.16
ANTERIOR-POSTERIOR TIBIAL DRAWER	0.448
SUPERIOR-INFERIOR TRANSLATION	0.199
QUADRICEPS FORCE	0.44

* Statistically Significant Parameters

5.4. Discussion

As the flexion-extension DOF was used as the control input, there should be no variation between the two groups, as confirmed by the ANOVA. It is expected that the translational DOF will not be much influenced by the addition of collateral ligaments as the translations are mostly governed by the tibial post which is unaltered between the two groups. No significant difference was found in the quadriceps load between the two groups.

Anatomically, the collateral ligaments restrict varus-valgus rotations and thus justifies the statistical significance for this parameter. Without the ligaments, the varus-valgus rotation can possibly cause the femoral condyles to lift from the tibial component. The reason for no statistical significance in the medial-lateral tibial shift in conjunction with the varus-valgus rotation can possibly be due to the constrained nature of a PS implant in this translational direction.

The cruciate ligaments, absent in a PS replacement, is naturally more responsible for constraining internal-external rotation than the collateral ligaments. However, the collateral ligaments also have an influence on tibial rotation (Chahla *et al.*, 2016). Additionally, with a PS implant replacing the cruciate ligaments, the implant itself does not provide rotational stability and confirms the rotational differences experienced as confirmed by the ANOVA.

5.5. Conclusion

With a PS implant already so constrained, the influence of the collateral ligaments was expected to be minimum, as confirmed by the ANOVA findings. However, the hypothesis can still be accepted as two of the rotational degrees of freedom showed statistical differences.

Chapter 6

Conclusions

6.1. Summary

A squat simulator was used to reproduce knee loading and evaluate in vitro performance of the joint with a posterior stabilised prosthesis. The interaction between different anatomic components was evaluated and can help to gain a better understanding of knee kinematics.

The main design aspects that were focussed on included the hip assembly, the control of the machine and an artificial knee with a well constrained prosthesis fixed to it. A hip assembly was successfully implemented. It made use of an electromechanical linear actuator, allowed Q-angle adjustments and, together with the ankle assembly, allowed six DOF in a knee joint. The simulator was successfully controlled and the system was repeatable. An artificial knee was constructed and used to verify the machine by evaluating the degrees of freedom present inside the joint and measuring the quadriceps forces during a simple squat motion.

Bone cuts were performed on a computer after which the bones were casted for construction of the artificial knee. A position sensor was used to track the motion of a knee while performing a squat inside the simulator. Position and orientation data were successfully used to establish coordinate systems on the femur and tibia to describe their relative motion. The posterior stabilised knee replacement used in the study was constrained enough to allow squat motion with and without added joint ligaments. The kinematical results of the two groups were compared in search of any statistically significant differences. It was proved that the machine can consistently give the same results when all parameters are kept constant.

The results showed that the squat simulator allows the six degrees of freedom present in the knee joint and that realistic quadriceps forces are present during a simple squat motion. Due to the high variability in knee specimens and many variables that all influences joint kinematics, it was difficult to find accurate results in literature against which findings could be compared. However, all results fell within realistic ranges and similarities were found in previous studies to verify the squat simulator.

6.2. Limitations

There were several limitations in this dissertation. Although common among many knee simulators in literature, the squat simulator did not accurately represent in vivo movement as the hip and ankle assemblies stay vertically aligned throughout a squat motion. This resulted in unrealistic extension moments which may not be

experienced during a natural squat. The flexion was controlled by a single actuator attached to the quadriceps.

The geometries of only one knee sample were used, with only the proximal part of the tibia and distal part of the femur received from a CT scan. The shortened bones made it difficult to define the mechanical and anatomical axes, which are critical references for the bone cuts. These axes were carefully defined with the limited geometries, but full femur and tibia models would have simplified the identification thereof, without uncertainty.

Polyester braided rope was used to represent the collateral ligaments. The validation thereof as an accurate representation of ligaments was based on one study only (Coles, 2015). The ligament tensions were not based on any numerical value which made it difficult to repeat the process of tensioning new ligaments.

Only one type and size of prosthesis was used for all the tests (Genesis II PS prosthesis from Smith and Nephew). The biomechanical results could thus possibly be as a result of the simulator design and not so much the knee prosthesis as there was no alternative to compare it to. However, most biomechanical patterns did match other literature and previous physiological observations.

The flexion range and limited test repetitions were a result of artificial knee failures experienced during preliminary tests. The high quadriceps forces resulted in cracks forming at the patella tendon insertion points during deep flexion.

6.3. Future Work Recommendations

The squat simulator could be further verified by testing an artificial knee with a different prosthesis. The testing and validation of cadaver specimens can follow. Hamstrings loading can be included on the simulator and more actuators can be added with the aim of reproducing gait inside the simulator. When more validation studies are completed, a computational model can be made of the complete setup with the aim to reproduce the results. A functional computational model will allow researchers to investigate many parameters with a single test run.

Clinically the aim would be to scan a patient's knee and project the exact geometries and defects of that specific knee to a 3D computer model. The performance of that knee joint can then be evaluated inside the computer simulation. Performing a virtual knee replacement on the scanned joint will allow the direct performance comparison after TKA with the simulated results obtained for the natural joint. The performance of customised knee replacement could be evaluated in this way on a specific patient's knee joint before the actual physical replacement is performed. Given the prevalence of knee replacements and the

amount of replacement failures, the advance of customised replacements is critical to improve the success rate of TKA.

References

Affatato, S. (2014) *Biomechanics of the knee*, *Surgical Techniques in Total Knee Arthroplasty (TKA) and Alternative Procedures*. Woodhead Publishing Limited. doi: 10.1533/9781782420385.1.17.

Ali, S. A., Helmer, R. and Terk, M. R. (2009) 'Patella alta: Lack of correlation between patellotrochlear cartilage congruence and commonly used patellar height ratios', *American Journal of Roentgenology*, 193(5), pp. 1361–1366. doi: 10.2214/AJR.09.2729.

Amendola, L. *et al.* (2012) 'History of Condylar Total Knee Arthroplasty', (January). doi: 10.5772/28203.

Anderson, D. M. (2012) *Mosby's Medical Dictionary*. Elsevier.

Anglin, C. *et al.* (2008) 'Intraoperative vs. weightbearing patellar kinematics in total knee arthroplasty: A cadaveric study', *Clinical Biomechanics*, 23(1), pp. 60–70. doi: 10.1016/j.clinbiomech.2007.08.005.

Anjum, Z. and Abbas, S. (2015) 'Osteoarthritis, classification, prevalence and risk factors', *Journal of Natural Sciences*, 3.

Arnout, N. *et al.* (2015) 'Post-cam mechanics and tibiofemoral kinematics: a dynamic in vitro analysis of eight posterior-stabilized total knee designs', *Knee Surgery, Sports Traumatology, Arthroscopy*, 23(11), pp. 3343–3353. doi: 10.1007/s00167-014-3167-2.

Baldwin, M. A. *et al.* (2012) 'Dynamic finite element knee simulation for evaluation of knee replacement mechanics', *Journal of Biomechanics*. Elsevier, 45(3), pp. 474–483. doi: 10.1016/j.jbiomech.2011.11.052.

Barclay, T. (2019) *Bones of the Leg and Foot*. Available at: https://www.innerbody.com/anatomy/skeletal/leg-foot.

Beaty, J. R. (2011) *Introduction to the Theory and Application of Quaternions - Part 1 of 2*.

Bellemans, J. *et al.* (2005) 'The influence of tibial slope on maximal flexion after total knee arthroplasty', *Knee Surgery, Sports Traumatology, Arthroscopy*, 13(3), pp. 193–196. doi: 10.1007/s00167-004-0557-x.

Bellemans, J., Ries, M. D. and Victor, J. (2005) *Total Knee Arthroplasty: A Guide to Get Better Performance*. Springer Berlin Heidelberg.

Benoit, D. L. *et al.* (2006) 'Effect of skin movement artifact on knee kinematics during gait and cutting motions measured in vivo', *Gait and Posture*, 24(2), pp. 152–164. doi: 10.1016/j.gaitpost.2005.04.012.

Bland, J. M. and Altman, D. G. (1986) 'Statistical methods for assessing agreement

between two methods of clinical measurement', *The Lancet*, (February), pp. 307–310.

Bourne, R. B. *et al.* (2010) 'Patient satisfaction after total knee arthroplasty: Who is satisfied and who is not?', *Clinical Orthopaedics and Related Research*, 468(1), pp. 57–63. doi: 10.1007/s11999-009-1119-9.

Brantigan, O. C. and Voshell, A. F. (1941) 'The machanics of the ligaments and menisci of the knee joint', *The Journal of Bone and Joint Surgery*, American v, pp. 44–66.

Carter, C. (2015) *Quizlet: Lower Extremity*. Available at: https://quizlet.com/98047380/biomech-2-lower-extremity-knee-ankle-and-foot-flash-cards/.

Cates, H. E. *et al.* (2008) 'In Vivo Comparison of Knee Kinematics for Subjects Having Either a Posterior Stabilized or Cruciate Retaining High-Flexion Total Knee Arthroplasty', *Journal of Arthroplasty*, 23(7), pp. 1057–1067. doi: 10.1016/j.arth.2007.09.019.

Chahla, J. *et al.* (2016) 'Posterolateral Corner of the Knee: Current Concepts', *The Archives of Bone and Joint Surgery*, 4(2), pp. 97–103.

Cherian, J. J. *et al.* (2014) 'Mechanical, anatomical, and kinematic axis in TKA: Concepts and practical applications', *Current Reviews in Musculoskeletal Medicine*, 7(2), pp. 89–95. doi: 10.1007/s12178-014-9218-y.

Churchill, D. L. *et al.* (1998) 'The Transepicondylar Axis Approximates the Optimal Flexion Axis of the Knee', *Clinical Orthopaedics and Related Research*, 356, pp. 111–118. doi: 10.1097/00003086-199811000-00016.

Claes, S. *et al.* (2013) 'Anatomy of the anterolateral ligament of the knee', *Journal of Anatomy*, 223(4), pp. 321–328. doi: 10.1111/joa.12087.

Coles, L. G. (2015) *Functional Kinematic Study of Knee Replacement - The Effect of Implant Design and Alignment on the Patellofemoral Joint*. University of Bath.

Coles, L. G., Gheduzzi, S. and Miles, A. W. (2014) 'In vitro method for assessing the biomechanics of the patellofemoral joint following total knee arthroplasty', 228(12), pp. 1217–1226. doi: 10.1177/0954411914560835.

Dauster, A. J. (2012) 'Development of University of Toledo Knee Simulator: First Generation', p. 301.

Dayal, M. R., Steyn, M. and Kuykendall, K. L. (2008) 'Stature estimation from bones of South African whites', *South African Journal of Science*, 104(March/April), pp. 24–26.

Ezechieli, M. *et al.* (2012) 'The influence of a single-radius-design on the knee

stability', *Technology and health care: official journal of the European Society for Engineering and Medicin*, 20(6).

Fang, D. M., Ritter, M. A. and Davis, K. E. (2009) 'Coronal Alignment in Total Knee Arthroplasty. Just How Important is it?', *Journal of Arthroplasty*. Elsevier B.V., 24(6 SUPPL.), pp. 39–43. doi: 10.1016/j.arth.2009.04.034.

Feng, J. E. *et al.* (2018) 'Total knee arthroplasty: Improving outcomes with a multidisciplinary approach', *Journal of Multidisciplinary Healthcare*, 11, pp. 63–73. doi: 10.2147/JMDH.S140550.

Ferrara, F. *et al.* (2015) 'Implant Positioning in TKA: Comparison Between Conventional and Patient-Specific Instrumentation', *Orthopedics*, 38(4), pp. e271–e280. doi: 10.3928/01477447-20150402-54.

Fitzpatrick, C. K. *et al.* (2013) 'Mechanics of Post-Cam Engagement during Simulated Dynamic Activity', (September), pp. 1438–1446. doi: 10.1002/jor.22366.

Forlani, M. (2015) *A NEW TEST RIG FOR IN-VITRO EVALUATION OF THE KNEE JOINT BEHAVIOUR*.

Freeman, M. A. R. and Pinskerova, V. (2003) 'The movement of the knee studied by magnetic resonance imaging', *Clinical Orthopaedics and Related Research*, (410), pp. 35–43. doi: 10.1097/01.blo.0000063598.67412.0d.

Giffin, J. R. *et al.* (2004) 'EFFECTS OF INCREASING TIBIAL SLOPE ON THE BIOMECHANICS OF THE KNEE', *American Journal of Sports Medicine*, 32(2), pp. 376–82.

Gilroy, A. M., MacPherson, B. R. and Ross, L. M. (2012) *Atlas of Anatomy*. 2nd Editio. Thieme.

Gómez-Barrena, E. *et al.* (2010) 'Functional performance with a single-radius femoral design total knee arthroplasty', *Clinical Orthopaedics and Related Research*, 468(5), pp. 1214–1220. doi: 10.1007/s11999-009-1190-2.

Gromov, K. *et al.* (2014) 'What is the optimal alignment of the tibial and femoral components in knee arthroplasty? An overview of the literature', *Acta Orthopaedica*, 85(5), pp. 480–487. doi: 10.3109/17453674.2014.940573.

Grood, E. S. and Suntay, W. J. (1983) 'A Joint Coordinate System for the Clinical Description of Three-Dimensional Motions: Application to the Knee', *Journal of Biomechanical Engineering*, 105(2), p. 136. doi: 10.1115/1.3138397.

Guess, T. M. and Maletsky, L. P. (2005) 'Computational Modeling of a Dynamic Knee Simulator for Reproduction of Knee Loading', *Journal of Biomechanical Engineering*, 127(7), p. 1216. doi: 10.1115/1.2073676.

Hamstring Muscle Injuries - OrthoInfo (2015). Available at: https://orthoinfo.aaos.org/en/diseases--conditions/hamstring-muscle-injuries/ (Accessed: 8 May 2018).

Hast, M. (2011) *ASSESSMENT OF TOTAL KNEE REPLACEMENT PERFORMANCE USING MUSCLE-DRIVEN DYNAMIC SIMULATIONS*. The Pennsylvania State University.

Hast, M. W. and Piazza, S. J. (2018) 'Position of the quadriceps actuator influences knee loads during simulated squat testing', *Journal of Biomechanics*. Elsevier Ltd, 73, pp. 227–232. doi: 10.1016/j.jbiomech.2018.03.024.

Van Haver, A. *et al.* (2013) 'Pilot validation study on a quasi-static weight-bearing knee rig', *Proceedings of the Institution of Mechanical Engineers, Part H: Journal of Engineering in Medicine*, 227(3), pp. 229–233. doi: 10.1177/0954411912472595.

Hirschmann, M. and Becker, R. (2015) *The unhappy total knee replacement: a comprehensive review and management guide*.

Horton, M. G. and Hall, T. L. (1989) 'Quadriceps Femoris Muscle Angle : Normal Values and Relationships with Gender and Selected Skeletal Measures', 69(11), pp. 897–901.

Howell, S. M. *et al.* (2013) 'Does a kinematically aligned total knee arthroplasty restore function without failure regardless of alignment category? Knee', *Clinical Orthopaedics and Related Research*, 471(3), pp. 1000–1007. doi: 10.1007/s11999-012-2613-z.

Huberti, H. and Hayes, W. (1984) 'Patellofemoral contact pressures. The influence of q-angle and tendofemoral contact.', *J Bone Surg Am*, 66(5).

Insall, J. N. *et al.* (1985) 'Total knee arthroplasty', *Clinical Orthopaedics and Related Research*, (192). doi: 10.1016/B978-0-443-10233-2.50030-4.

Insall, J. and Salvati, E. (1971) 'Patella position in the normal knee joint.', *Radiology*, 101(1), pp. 101–104. doi: 10.1148/101.1.101.

Kaivosoja, E. *et al.* (2012) 'Materials used for hip and knee implants', *Wear of Orthopaedic Implants and Artificial Joints*, (March 2018), pp. 178–218. doi: 10.1016/B978-0-85709-128-4.50007-8.

Karadsheh, M. (2019) *TKA Prosthesis Design*. Available at: https://www.orthobullets.com/recon/5019/tka-prosthesis-design.

Keller, R. T. and Amis, A. A. (2015) 'Anatomy and Biomechanics of the Natural Knee and After TKR', in *The Unhappy Total Knee Replacement*, pp. 3–15.

Kettelkamp, D. *et al.* (1970) 'An electrogoniometric study of knee motion in normal

gait', *Journal of Bone and Joint Surgery*, 52(4), pp. 775–790.

Kim, H. Y. *et al.* (2015) 'Screw-home movement of the tibiofemoral joint during normal gait: Three-dimensional analysis', *CiOS Clinics in Orthopedic Surgery*, 7(3), pp. 303–309. doi: 10.4055/cios.2015.7.3.303.

Komdeur, P., Pollo, F. E. and Jackson, R. W. (2002) 'Dynamic Knee Motion in Anterior Cruciate Impairment: A Report and Case Study', *Baylor University Medical Center Proceedings*, 15(3), pp. 257–259. doi: 10.1080/08998280.2002.11927850.

LaPrade, R. F. *et al.* (2007) 'The anatomy of the medial part of the knee', *Journal of Bone and Joint Surgery - Series A*, 89(9), pp. 2000–2010. doi: 10.2106/JBJS.F.01176.

Lenhart, R. L. *et al.* (2017) 'Influence of patellar position on the knee extensor mechanism in normal and crouched walking', *Journal of Biomechanics*. Elsevier, 51, pp. 1–7. doi: 10.1016/j.jbiomech.2016.11.052.

de Leva, P. (1996) 'Adjustments to Zatsiorsky-Seluyanov's Segment Inertia Parameters', *Journal of Biomechanics*, 29(9), pp. 1223–1230. doi: 10.1002/ima.22019.

Long, R. (2011) *The Bimechanics of Hinged Total Knee Replacements: An In Vitro Comparative Evaluation of Five Prostheses*. University of Bath.

Long, R. *et al.* (2013) 'A biomechanical evaluation of hinged total knee replacement prostheses', *Proceedings of the Institution of Mechanical Engineers, Part H: Journal of Engineering in Medicine*, 227(8), pp. 875–883. doi: 10.1177/0954411913488506.

Loudon, J. K. (2016) 'BIOMECHANICS AND PATHOMECHANICS OF THE PATELLOFEMORAL JOINT', *Journal of Toxicologic Pathology*, 11(6), p. 820.

Luyckx, T. *et al.* (2009) 'Is there a biomechanical explanation for anterior knee pain in patients with patella alta?', *The Journal of Bone and Joint Surgery. British volume*, 91–B(3), pp. 344–350. doi: 10.1302/0301-620x.91b3.21592.

Macwilliams, B. A. *et al.* (1999) 'Hamstrings concontraction reduces internal rotation, anterior translation, and anterior cruciate ligament load in weight bearing flexion'.

Maletsky, L. P. and Hillberry, B. M. (2005) 'Simulating Dynamic Activities Using a Five-Axis Knee Simulator', *Journal of Biomechanical Engineering*, 127(1), p. 123. doi: 10.1115/1.1846070.

Manner, P. W. (2016) *OrthoInfo - Knee Replacement Implants*. Available at: https://orthoinfo.aaos.org/en/treatment/knee-replacement-implants/ (Accessed: 19 June 2018).

Mason, J. J. *et al.* (2008) 'Patellofemoral joint forces', *Journal of Biomechanics*, 41(11), pp. 2337–2348. doi: 10.1016/j.jbiomech.2008.04.039.

Mckeever, D. C. (1960) 'Tibial Plateau Prosthesis', *Clinical Orthopaedics and Related Research*, 192, pp. 3–12. doi: 10.1097/01.blo.0000187336.17627.ea.

Medacta: Three-compartment tibial bearing / fixed or mobile-bearing (no date). Available at: http://www.medicalexpo.com/prod/medacta/product-94141-606551.html#product-item_744536 (Accessed: 18 May 2019).

Mizuno, Y. *et al.* (2001) 'Q-angle influences tibiofemoral and patellofemoral kinematics', *Journal of Orthopaedic Research*, 19(5), pp. 834–840. doi: 10.1016/S0736-0266(01)00008-0.

Moran, M. F. (2005) *COMPUTATIONAL AND EXPERIMENTAL ASSESSMENT OF TOTAL KNEE REPLACEMENT MOTION*.

Nakamura, S. *et al.* (2017) 'Superior-inferior position of patellar component affects patellofemoral kinematics and contact forces in computer simulation', *Clinical Biomechanics*. Elsevier Ltd, 45, pp. 19–24. doi: 10.1016/j.clinbiomech.2017.04.005.

Neumann, D. (2015) *Rheumatology - The Knee*. Available at: https://clinicalgate.com/knee-5/.

Nordin, M. and Frankel, V. (2001) *Biomechanics of the knee*. 3rd edn. New York: Lippincott Williams and Wilkins.

Norman, O. *et al.* (1983) 'The Vertical Position of the Patella', 6470. doi: 10.3109/17453678308992932.

O'Connor, J. J., Bourne, R. and Goodfellow, J. W. (1978) 'A functional analysis of various knee arthroplasties.', *Trans. Orthop. Res. Soc.*, 24.

O'Connor, J. and Zavatsky, A. (1990) 'Kinematics and mechanics of the cruciate ligaments of the knee', *Biomechanics of Diarthrodial*, 2, pp. 197–241.

O'Rahilly, R. *et al.* (2008) *Basic Human Anatomy - A Regional Study of Human Structure*. Available at: https://www.dartmouth.edu/~humananatomy/index.html.

Okamoto, S. *et al.* (2015) 'Effect of Tibial Posterior Slope on Knee Kinematics, Quadriceps Force, and Patellofemoral Contact Force After Posterior-Stabilized Total Knee Arthroplasty', *Journal of Arthroplasty*. Elsevier B.V., 30(8), pp. 1439–1443. doi: 10.1016/j.arth.2015.02.042.

Ostermeier, S. *et al.* (2006) 'In vitro investigation of the influence of tibial slope on quadriceps extension force after total knee arthroplasty', *Knee Surgery, Sports Traumatology, Arthroscopy*, 14(10), pp. 934–939. doi: 10.1007/s00167-006-0078-

x.

Ostermeier, S. and Stukenborg-Colsman, C. (2011) 'Quadriceps force after TKA with femoral single radius', *Acta Orthopaedica*, 82(3), pp. 339–343. doi: 10.3109/17453674.2011.574564.

Palastanga, N. and Soames, R. (2012) *Anatomy and Human Movement - Structure and Function*. 6th edn. London: Elsevier.

Parisi, T. J., Jennings, J. M. and Dennis, D. A. (2018) 'Coronal Alignment in TKA: Traditional Principles Versus New Concepts', *Reconstructive Review*, 8(2). doi: 10.15438/rr.8.2.213.

Pasta, G. *et al.* (2010) 'Sonography of the quadriceps muscle', *Journal of Ultrasound*, 13(2), pp. 76–84.

Peterson, C. (1994) 'Posterior Cruciate Ligament Injury'. Available at: http://emedicine.medscape.com/article/90514-overview#a0106.

Pinskerova, V., Iwaki, H. and Freeman, M. A. (2001) 'Tibial Femoral Movement. 1: The shape and relative movements of the femur and tibia in the unloaded cadaver knee.', *J Bone Joint Surg*, 82.

Platzer, W., Kahle, W. and Leonhardt, H. (1986) *Color Atlas/Text of Human Anatomy, Vol.1 - Locomotor System*. 3rd edn. Thieme. Available at: https://universalflowuniversity.com/Books/Medicine/Anatomy/Color Atlas and Textbook of Human Anatomy ,Volume I Locomotor System - Werner Platzer, Werner Kahle, M. Frotscher.pdf (Accessed: 15 April 2018).

Ramappa, A. J. *et al.* (2006) 'The effects of medialization and anteromedialization of the tibial tubercle on patellofemoral mechanics and kinematics', *American Journal of Sports Medicine*, 34(5), pp. 749–756. doi: 10.1177/0363546505283460.

Ritter, M. A. *et al.* (2011) 'The effect of alignment and BMI on failure of total knee replacement', *Journal of Bone and Joint Surgery - Series A*, 93(17), pp. 1588–1596. doi: 10.2106/JBJS.J.00772.

Rusly, R. (2015) 'CONTRA-COMPARTMENTAL JOINT MECHANICS IN UNICONDYLAR KNEE ARTHROPLASTY'.

Rusly, R. J. *et al.* (2016) *Influence of Hamstrings Activation on Knee Mechanics Using a Novel Deep Knee Bending Simulator*.

Russell, F. *et al.* (2018) 'A biomimicking design for mechanical knee joints', *Bioinspiration and Biomimetics*. IOP Publishing, 13.

Saxby, D. J. *et al.* (2016) 'Tibiofemoral contact forces during walking, running and sidestepping', *Gait and Posture*. Elsevier B.V., 49, pp. 78–85. doi: 10.1016/j.gaitpost.2016.06.014.

Schiraldi, M. *et al.* (2016) 'Mechanical and kinematic alignment in total knee arthroplasty', *Annals of Translational Medicine*, 4(7), pp. 130–130. doi: 10.21037/atm.2016.03.31.

Schuithies, S. *et al.* (1995) 'Does the Q Angle Reflect the Force on the Patella in the Frontal Plane?', *Physical Therapy*, 75(1).

Shenoy, R., Pastides, P. S. and Nathwani, D. (2013) '(iii) Biomechanics of the knee and TKR', *Orthopaedics and Trauma*. Elsevier Ltd, 27(6), pp. 364–371. doi: 10.1016/j.mporth.2013.10.003.

Shi, X. *et al.* (2013) 'The effect of posterior tibial slope on knee flexion in posterior-stabilized total knee arthroplasty', *Knee Surgery, Sports Traumatology, Arthroscopy*, 21(12), pp. 2696–2703. doi: 10.1007/s00167-012-2058-7.

Solomon, D. *et al.* (2006) 'Does This Patient Have a Torn Meniscus or Ligament of the Knee?', *Annals of Emergency Medicine*, 47(5), pp. 499–501. doi: 10.1016/j.annemergmed.2006.02.004.

Steinbrück, A. *et al.* (2013) 'Patellofemoral contact patterns before and after total knee arthroplasty: An in vitro measurement', *BioMedical Engineering Online*, 12(1), pp. 1–13. doi: 10.1186/1475-925X-12-58.

Stiehl, J. B. (2009) 'Comparison of tibial rotation in fixed and mobile bearing total knee arthroplasty using computer navigation', *International Orthopaedics*, 33(3), pp. 679–685. doi: 10.1007/s00264-008-0562-7.

Stoddard, J. E. *et al.* (2012) 'The kinematics and stability of single-radius versus multi-radius femoral components related to Mid-range instability after TKA', *Journal of Orthopaedic Research*, 31(1), pp. 53–58. doi: 10.1002/jor.22170.

Types of Total Knee Implants (no date) *FARM - Foundation for the Advancement in Research in Medicine*. Available at: https://bonesmart.org/knee/types-of-total-knee-implants/ (Accessed: 18 May 2019).

Victor, J. *et al.* (2009) 'An experimental model for kinematic analysis of the knee', *Journal of Bone and Joint Surgery - Series A*, 91(SUPPL. 6), pp. 150–163. doi: 10.2106/JBJS.I.00498.

Victor, J., Mueller, J. K. P., *et al.* (2010) 'In vivo kinematics after a cruciate-substituting TKA', *Clinical Orthopaedics and Related Research*, 468(3), pp. 807–814. doi: 10.1007/s11999-009-1072-7.

Victor, J., Labey, L., *et al.* (2010) 'The influence of muscle load on tibiofemoral knee kinematics', *Journal of Orthopaedic Research*, 28(4), pp. 419–428. doi: 10.1002/jor.21019.

Visentini, P. and Clarsen, B. (2016) 'Overuse Injuries in Cycling', *Aspetar Sports MEdicine Journal*, 5, pp. 486–492.

Wasielewski, R. C. *et al.* (1994) 'Wear patterns on retreived polyethylene tibial inserts and their relationship to technical considerations during total knee arthroplasty', *Clinical Orthopaedics and Related Research*, (299), pp. 31–43.

Weber, W. and Weber, F. (1992) *Mechanics of the Human Walking Apparaturs.* Springer Berlin Heidelberg.

Van de Weghe, I. (2013) *Q Angle*. Available at: https://www.physio-pedia.com/%27Q%27_Angle.

Wünschel, M. *et al.* (2013) 'Differences in knee joint kinematics and forces after posterior cruciate retaining and stabilized total knee arthroplasty', *Knee*. Elsevier B.V., 20(6), pp. 416–421. doi: 10.1016/j.knee.2013.03.005.

Yamaguchi, G. T. and Zajac, F. E. (1989) 'A planar model of the knee joint to characterize the knee extensor mechanism', *Journal of Biomechanics*, 22(1), pp. 1–10. doi: 10.1016/0021-9290(89)90179-6.

Zavatsky, A. B. (1997) 'A kinematic freedom analysis of a flexed-knee-stance testing rig', *Journal of Biomechanics*, 30(3).

Zhang, L. K. *et al.* (2016) 'Relationship between Patellar Tracking and the "Screw-home" Mechanism of Tibiofemoral Joint', *Orthopaedic Surgery*, 8(4), pp. 490–495. doi: 10.1111/os.12295.

Appendix A Autohotkey Sample Code

Sample code of the Autohotkey programs to simultaneously click on two locations on the computer screen at once in order to synchronize the Polaris Vicra position sensor and the Lorenz load cell.

Coord.ahk

```
CoordMode, Mouse, Screen
SetTimer, Check, 20
return

Check:
MouseGetPos, xx, yy
Tooltip %xx%`, %yy%
return

Esc::ExitApp
```

Click.ahk

```
CoordMode, Mouse, Screen
SetDefaultMouseSpeed, 0  ; Sets default mouse speed to maximum

a::
   MouseGetPos, X, Y   ; Stores current mouse position
   Click 184, 461
   Click 1082, 457
   MouseMove, % X, % Y ; Moves mouse back to original position
Return

Esc::ExitApp
```

Appendix B Squat Simulator Testing Procedure

1. Get the knee to a fully extended position by manually extending the linear actuator.
2. Make sure that the patella is located at the correct fully extended position. Measure the vertical position of the patella, the perpendicular distance from the distal edge of the patellar articular surface to the femoral condylar plane. This should be 40 mm, as determined by Norman et al.
3. Attach marker tools to tibia, femur and patella. Ensure that they are fixed in such a way that they will not move around during tests.
4. Ensure that the position sensor and the force transducer with amplifier are all plugged into the computer. Open their respective software and make sure that the hardware is identified by the software. Set the sample rate to 20 samples per second on both programs and have a 0 seconds time delay for recordings.
5. Ensure that the required markers are all visible to the Polaris Vicra position sensor.
6. The femur tool should be set as the global reference tool.
7. For each new knee sample, a reference position/angle should be determined. The reference angle is an angle within the flexion range and is determined as follows:
    - With the setting switch on automatic, position the hip assembly at any position so that the immediate flexion angle of the knee falls within the desired flexion range.
    - Make a mark with a permanent marker on the vertical shaft to indicate where the hip assembly is located. This will be its reference and starting position before any automatic squat is performed.
    - Take a reading with the motion sensor while the hip assembly is kept stationary at its reference location. The reading should be evaluated to determine the flexion angle of the knee at this position. This is the reference flexion angle.
8. Make sure that the input values for the Arduino code are correct. E inputs include the full femur and tibia lengths, the desired flexion range and the reference angle. Make sure the code is uploaded to the Arduino before an automatic squat can be performed.
9. Get the femur bony landmarks, indicated in the table below, with the digitizing probe. Keep the probe's point at the required landmark, while taking a reading with the Polaris software. It might be necessary to manually adjust the flexion to better digitize some points.

It is only necessary to record the femur tool and probe tool during these recordings.

File Name	Landmark	Location
F_prox	Proximal femur	Center of hip assembly, right above femur attachment bracket.
F_dist	Distal femur	Most distal point at the intercondylar groove. (Femoral reference point.)
F_lat	Lateral femur	Point on most lateral part of the distal femur.
F_med	Medial femur	Point on most medial part of the medial femur.
F_sMCL	Superficial medial-collateral ligament attachment on femur.	Same point as F_med.
F_LCL	Lateral collateral ligament attachment on femur.	Same point as F_lat.

10. Get the tibia bony landmarks, as indicated in the table below, with the probe tool. Do the same as with the femur landmark recordings. The femur, tibia and probe tools should be recorded during these recordings so make sure all of them are visible to the sensor.

File Name	Landmark	Location
T_dist	Distal tibia	Center of ankle assembly – the top of a brass pin located underneath the ankle assembly.
T_prox	Proximal tibia	Just anterior of the post cam on the tibial bearing insert. (Tibial reference point.)
T_lat	Lateral tibia	Center of the lateral tibial plateau, on the poly insert.
T_med	Medial tibia	Center of the medial tibial plateau, on the poly insert.
T_LCL	Lateral-collateral ligament attachment	Top of fibula.
T_ALL	Anterolateral ligament attachment	Dimple just medially of where the fibula attaches.

T_psMCL	Proximal superficial medial-collateral ligament attachment on the tibia.	The more proximal insert point of the MCL, on the medial side of the tibia.
T_dsMCL	Distal superficial medial-collateral ligament attachment on the tibia.	The more distal insert point of the MCL, on the medial side of the tibia.

11. The last bony landmark to obtain, is a posterior point on the patella. The femur, patella and probe tools should be recorded during this recording.

File Name	Landmark	Location
P_post	Point at center of posterior patella.	Marked point on posterior patella. This is the origin of the patella coordinate system.

12. With the control setting still on “manual”, retract or extend the actuator until the linear bearings are at their reference position, as indicated by markers on the linear rail. This position should be pre-determined as described at point 7.
13. With the hip assembly at its reference position and the string of the position encoder hooked to the hip assembly, the setting switch can now be switched to “automatic”. The controller will automatically retract the actuator until it stops at its starting angle, as specified by the flexion range.
14. Adjust the tibia around its own axis so that it directly faces forward. Make a mark on the ankle assembly so that the tibia can be rotated to this exact starting position before every test.
15. With the knee kept stationary in this reference/starting position, take a recording of the femur, tibia and patella tools. Call this file “FT_refPos”.
16. An Autohotkey program was written to do a mouse click on 2 different locations on the screen. This is to start the quadriceps force and motion tracking recordings at the same time. Open both recording programs and make sure their “record” and “stop” buttons are all visible on one screen. Make sure Autohotkey is installed on the computer.
17. Use the Coord.ahk Autohotkey program to determine the screen coordinates of the recording and stop recording buttons on both programs. Write all four coordinates down.
18. To close an Autohotkey program, look for an “H” in ‘n green square in the taskbar. It is usually at the bottom right corner of the computer screen. Right click on it and click on “exit”.

19. Right click on the Click.ahk Autohotkey program and select “edit script”. Under “a::”, fill in the “start recording” button coordinates. Under “s::”, fill in the “stop recording” button coordinates.
20. For one last time, make sure that the femoral, tibial and patellar tools are all visible to the Polaris Vicra position sensor.
21. Tare the force transducer on the Lorenz program so that it is zeroed at the starting position.
22. Now, when ready, press the “a” button on the keyboard and immediately after that flick the actuation state toggle switch to “extend”. The machine should now start to flex with both recordings running.
23. If the actuation toggle switch is kept on “extend”, two squats will be performed in succession. However, if it is switched back to its middle stationary state, only one squat will be performed.
24. When the machine returns to its starting position and stops, press the “s” button on the keyboard. The recordings should now also stop.
25. Exit the Click.ahk script.
26. Save the force and position data with appropriate names.

Appendix C Actuator Bracket Deflection and Yielding

The actuator bracket will experience high tension forces from the actuator itself. When calculating its deflection, it can be assumed to be a cantilever beam, as seen in Figure C.1.

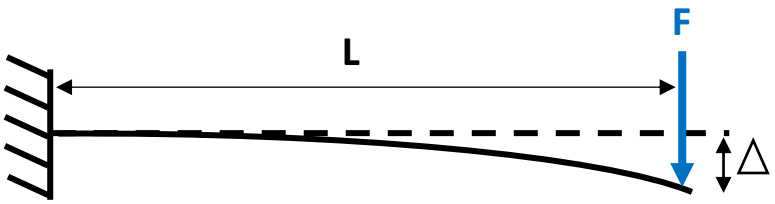

Figure C.1: Cantilevered Beam

The deflection can be calculated as follows:

$$\Delta = \frac{F\,L^3}{3\,E\,I} \qquad \text{C.1}$$

E is the Young's Modulus of the beam's material (mild steel) and I is the plate's moment of inertia, calculated as follows:

$$I = \frac{b\,h^3}{12} \qquad \text{C.2}$$

b is the width (breadth) of the bracket-plate and h is its thickness (height). With F = 2660 N, L = 100 mm, $E_{mild\ steel}$ = 205 GPa, b = 70 mm and h = 4 mm, the deflection is:

$$\Delta = \frac{(2500)\,(0.1)^3}{3\,(205 \times 10^9)\left(\frac{(0.07)(0.004)^3}{12}\right)} = 11.6\ \text{mm}. \qquad \text{C.3}$$

To see whether this will cause permanent deflection (plastic deformation), the maximum shear (τ) and bending (σ) stresses are calculated, assuming the stresses occur along one axis only:

$$\tau = \frac{3\,F}{2\,b\,h} = 14.25\ \text{MPa} \qquad \text{C.4}$$

$$\sigma = \frac{F\,L\,h}{2\,I} = 1425\ \text{MPa}. \qquad \text{C.5}$$

Tresca's Maximum Shear Stress failure theory is used to determine whether the bracket-plate will permanently deform. This theory states that yielding will occur when the maximum shear stress is greater than or equal to half the material's yielding stress, σ_y (250 MPa):

$$\tau_{max} \geq {}^{\sigma_y}/_{2} = 125 \text{ MPa} \quad \text{C.6}$$

The maximum shear stress is as follows:

$$\tau_{max} = \sqrt{\left(\frac{\sigma}{2}\right)^2 + \tau^2} = 712.6 \text{ MPa} > \frac{\sigma_y}{2}. \quad \text{C.7}$$

We can thus conclude that yielding will occur and that the plate should either be made thicker or reinforced with something like a web or flange to prevent it from deflecting this much.

Appendix D Artificial Knee Failures

Inconsistencies in Fast Cast F180 resulted in many failed squat attempts. Up to 15 squats were possible with the original batch before the tibia would fail. However, some newer batches did not last two squats before failure occurred. Cracks usually started at the patella tendon insertion point. Tibias made from a new material, Task 9, completed 35 squats without failure. A few failed samples can be seen in Figure D.1.

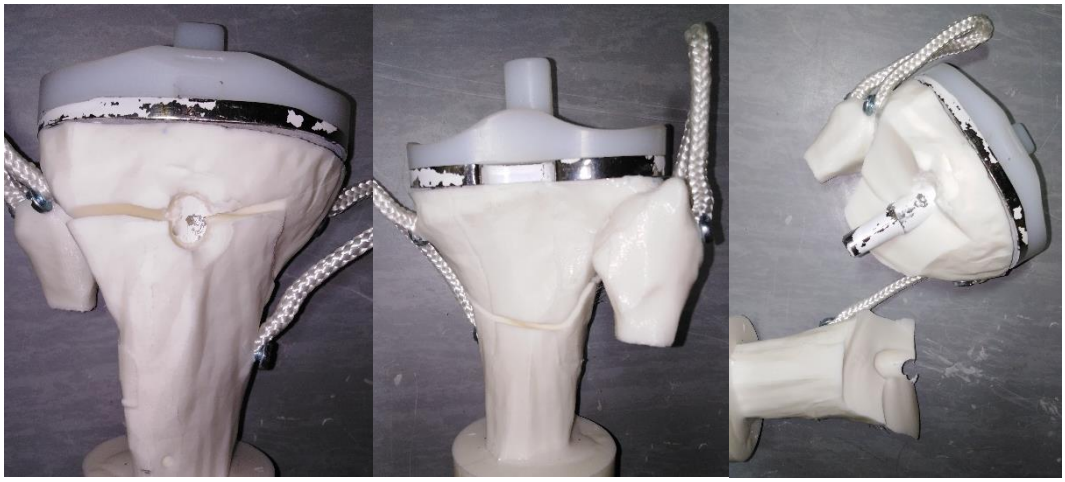

Figure D.1: Knee Failures

Appendix E Functionality Testing

To evaluate the functioning of the squat simulator, tests were done with a constrained knee replacement where the tibial and femoral components are linked together with a hinged mechanism, as seen in Figure E.1. Only the flexion-extension and tibial internal-external rotational degrees of freedom are present with this implant, but it still allows one to test the functioning of the hip and ankle assemblies and the use of the linear actuator before spending too much time on producing an artificial knee.

These tests were not to evaluate the kinematic performance of the implant. It was mainly used to see if the hip assembly could manage the forces present in a squat, whether the electric linear actuator can successfully perform its task and if the control system could successfully manage the simulating machine. The practical functioning of the Q-angle adjustments could also be evaluated. Informed adjustments could be made after the completion of the tests.

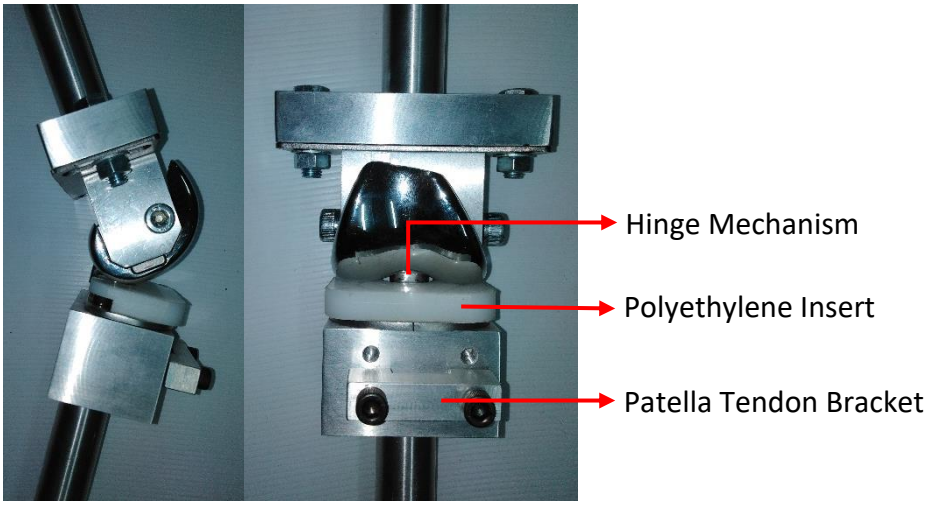

Figure E.1: Hinged Modelled Knee

Appendix F MatLab Calculations

Analise Script:

```
% ***********************************************************
clear all
% The femoral tool is established as the world/reference
coordinate system.

% If my rotation is XYZ, then the multiplication would be RzRyRx
=> Thus,
% order of multiplication is reversed from order of rotation.

% ***********************************************************

% F - Femur
% T - Tibia
% t2w - tool to world => world = femoral tool
% t2a - tool to anatomic coordinate system
% L - Length of array

% +++++++++++++++++++++++++++++++++++++++++++++++++++++++++++++
% Read landmark probe and tool points:
A_data = xlsread('Combined Patella Normal','C2:O17');
% Tibia tool data during motion:
T_data = xlsread('Tibia Tool 339 Normal.xls');
% Patella tool data during motion:
P_data = xlsread('Patella Tool 338 Normal.xls');
% Quadriceps force data during flexion:
Quad_data = xlsread('Quadriceps Force Normal.xls');

quadForce = Quad_data(:,2);
% +++++++++++++++++++++++++++++++++++++++++++++++++++++++++++++

% Building a low pass Butterworth filter:
fc = 2; % Cutoff frequency
fs = 20;    % Sample frequency => 20 Hz
[b a] = butter(2,fc/(fs/2),'low');  % Low pass 2nd order
butterworth filter

% -----------------------------

% Tool 339 attached to tibia
[ RT_t2a, TO_p2t, ZT_p2t ] = func_tibiaProbe(A_data);
% RT_t2a - Rotation matrix of tibial tool to its ACS - Constant
value
%          [XT_p2t(1) XT_p2t(2) XT_p2t(3);
%          YT_p2t(1) YT_p2t(2) YT_p2t(3);
%          ZT_p2t(1) ZT_p2t(2) ZT_p2t(3)]
% TO_p2t - Proximal tibia point (tibia ACS origin), relative to
tibial tool
% ZT_p2t - Tibia ACS z-axis, i.t.o. tibial tool (column vector)
```

```
% % At full extension, assume that the tibial, femoral and
patellar anatomic
% % coordinate systems are parallel. The constant rotation matrix
from the
% % femur tool, also the reference tool, to the femoral ACS:
% RF_t2ai = RT_t2a*RT_ref';    %
!!!!!!!!!!!!!!!!!!!!!!!!!!!!!!!!!!!!!!!!!!!!!!!!!!!!!!!!!!!!!!!
% % !!!!!!!! See if the RF_t2a is necessary or can I use the probe
points as
% % below?

% Tool 449
[ RF_t2a, FO_p2t, F_LCL_p2t, F_MCL_p2t ] = func_femurProbe( A_data
);
% RF_t2a - Rotation matrix of femur tool to femur ACS - Constant
value
% FO_p2t - Distal intracondylar femur notch point (femur ACS
origin),
%           relative to world CS.
% F_LCL_p2t - LCL insertion point on femur, i.t.o. world/femur
tool
% F_MCL_p2t - MCL insertion point on femur, i.t.o. world/femur
tool
XF_p2t = RF_t2a(1,:)';
% XF_p2t - Femur ACS x-axis, i.t.o. femur/world tool

% Tool 338 attached to patella
[ RP_t2a, PO_t2p ] = func_patella(A_data, RF_t2a);
% RP_t2a - Rotation matrix of patellar tool to its ACS - Constant
value
% PO_t2p - Patella ACS origin point, realtive to patella tool
(Constant
%           vector from patella tool to patella ACS origin)

% Tibia ligament insertion points, i.t.o. tibial tool
[ T_ALL_p2t, T_LCL_p2t, T_dsMCL_p2t, T_psMCL_p2t ] =
func_tibiaLigaments( A_data );
% T_ALL_p2t - ALL insertion point on tibia, i.t.o. tibial tool
% T_LCL_p2t - LCL insertion point on tibia, i.t.o. tibial tool
% The MCL form a thick band with to attachment points on the
tibia, a
% distal superficial MCL point and a proximal sMCL:
% T_dsMCL_p2t - dsMCL insertion point on tibia, i.t.o. tibial tool
% T_psMCL_p2t - psMCL insertion point on tibia, i.t.o. tibial tool
% ------------------------------


% Motion Data:

[ TT_t2w, RT_w2t, TP_t2w, RP_t2w, L ] = func_trackedMotion(T_data,
P_data);
% TT_t2w - Tibial tool position in terms of the world coordinate
system
% RT_t2w - Rotation matrix for tibial tool to world CS
```

```
% TP_t2w - Patella tool position in terms of the world coordinate
system
% RP_t2w - Rotation matrix for patella tool to world CS
% L - length/amount of motion data captured


for c = 1:(L)

    %% +++++ FEMUR TO TIBIA +++++

    % Rotations: **********************************
    % Rotation matrix of femur ACS to tibial ACS:
    R_Fa2Ta = RT_t2a * (RT_w2t(:,:,c)) * RF_t2a';

        %% Get joint coordinate system:
    % Tibial cartesian coordinate system, ijk (w.r.t. femur/world
CS):
    % v = conj(q) * V * q = R' * V [but R is w2t and we want t2w,
thus (R')']
    i = (RT_w2t(:,:,c)')' * (RT_t2a(1,:))';
    j = (RT_w2t(:,:,c)')' * (RT_t2a(2,:))';
    k = (RT_w2t(:,:,c)')' * (RT_t2a(3,:))';

    % Femoral cartesian coordinate system, IJK:
    I = RF_t2a(1,:);
    J = RF_t2a(2,:);
    K = RF_t2a(3,:);

    R_groode = [dot(I,i), dot(J,i), dot(K,i);
                dot(I,j), dot(J,j), dot(K,j);
                dot(I,k), dot(J,k), dot(K,k)];

%     R_groode = R_groode1';

    e3 = RT_w2t(:,:,c)*ZT_p2t;  % Column vectors
    e1 = XF_p2t;
    e2 = cross(e3,e1);

    R_JCS_t2a = [e1, e2, e3]';  % from world CS to joint coord
syst (JCS)

    flex(c) = 180-acosd(dot(J,e2));
    rot(c) = -asind(dot(e2,i));
    abd(c) = acosd(dot(I, k)) - 90; % abd(c) =
acosd(R_groode(3,1))-90;

%     rot(c) = atand(R_groode(2,1)/R_groode(1,1));
%     abd(c) = acosd(R_groode(3,1)) - 90;
%     flex(c) = atand(R_groode(3,2)/R_groode(3,3));

    % translations:
    % Tibia ACS origin during motion, i.t.o. world CS:
    TO_acs2w = TT_t2w(c,:,:)' + (RT_w2t(:,:,c)*TO_p2t);
    V_Fa2Ta = R_JCS_t2a*(TO_acs2w-FO_p2t);
```

```
    T_shift(c) = V_Fa2Ta(1) + V_Fa2Ta(3)*cosd(abd(c)+90);
    T_drawer(c) = V_Fa2Ta(2);
    T_distract(c) = -V_Fa2Ta(3)-V_Fa2Ta(1)*cosd(abd(c)+90);



    %% +++++ FEMUR TO PATELLA +++++

    % Rotations: **********************************
    % Rotation matrix of femur ACS to patella ACS:
    R_Fa2Pa = RP_t2a * (RP_t2w(:,:,c))' * RF_t2a';

    % Patella flexion rotation:
    P_flex(c) = atand(R_Fa2Pa(3,2)/R_Fa2Pa(3,3));
    % Patella tilt rotation:
    P_tilt(c) = atand(R_Fa2Pa(2,1)/R_Fa2Pa(1,1));
    % Patella twist rotation:
    temp2 = sqrt(1-R_Fa2Ta(1,3)^2);
    P_twist(c) = atand( abs(temp2/R_Fa2Ta(1,3)) )-90;

    % ****************************************

    % Translations: -------------------------------
    % Patella ACS origin during motion, i.t.o. world CS:
    PO_acs2w = TP_t2w(c,:,:)' + (RP_t2w(:,:,c)*PO_t2p);
    % Vector between femoral ACS to patella ACS, i.t.o. femur ACS:
    V_Fa2Pa = (RF_t2a')'*(PO_acs2w-FO_p2t);

    % Medial/lateral patella movement:
    P_medlat(c) = V_Fa2Pa(1);
    % Anterior/Posterior patellar movement relative to femur
    P_antpost(c) = V_Fa2Pa(2)*cosd(flex(c)) -
V_Fa2Pa(3)*sind(flex(c));
    % Proximal/distal patella movement relative to femur
    P_proxdist(c) = R_Fa2Pa(3,1)*V_Fa2Pa(1) +
R_Fa2Pa(3,2)*V_Fa2Pa(2) + R_Fa2Pa(3,3)*V_Fa2Pa(3);

    % -------------------------------------------



    %% +++++ LIGAMENT LENGTHENING PATTERNS +++++
    % The length patterns of the ALL, LCL and MCL ligaments during
flexion

    % First, use tibial rotation matrix to convert the vector from
tibial
    % insertion point to tibial tool, that is i.t.o. the tibial
tool, to
    % world/femur coordinate system:
    VT_ALL_p2t = RT_w2t(:,:,c) * T_ALL_p2t;
    VT_LCL_p2t = RT_w2t(:,:,c) * T_LCL_p2t;
    VT_dsMCL_p2t = RT_w2t(:,:,c) * T_dsMCL_p2t;
    VT_psMCL_p2t = RT_w2t(:,:,c) * T_psMCL_p2t;
```

```
    % Now, get insertion points, via tibial tool position
    % => (WCS to insertion point) = (WCS origin to tibia tool CS
origin) +
    %          (tibial tool CS origin to ligament insertion point
on tibia)
    V_ALL_w2p = TT_t2w(c,:)' + VT_ALL_p2t;
    V_LCL_w2p = TT_t2w(c,:)' + VT_LCL_p2t;
    V_dsMCL_w2p = TT_t2w(c,:)' + VT_dsMCL_p2t;
    V_psMCL_w2p = TT_t2w(c,:)' + VT_dsMCL_p2t;

    z_temp = (V_dsMCL_w2p+V_psMCL_w2p)/2;

    V_ALL = F_LCL_p2t - V_ALL_w2p;
    V_LCL = F_LCL_p2t - V_LCL_w2p;
    V_dsMCL = F_MCL_p2t - V_dsMCL_w2p;
    V_psMCL = F_MCL_p2t - V_psMCL_w2p;
    V_MCL = (V_dsMCL+V_psMCL)/2;    % MCL is a thick ligament band

    ALL(c) = sqrt(V_ALL(1)^2 + V_ALL(2)^2 + V_ALL(3)^2);
    LCL(c) = sqrt(V_LCL(1)^2 + V_LCL(2)^2 + V_LCL(3)^2);
    MCL(c) = sqrt(V_MCL(1)^2 + V_MCL(2)^2 + V_MCL(3)^2);

end

%

% smooth(rot,0.3,'loess')
% Apply butterworth filter to all results:
flex = filtfilt(b,a,flex);
rot = filtfilt(b,a,rot);
abd = filtfilt(b,a,abd);
T_shift = filtfilt(b,a,T_shift);
T_drawer = filtfilt(b,a,T_drawer);
T_distract = filtfilt(b,a,T_distract);
LCL = filtfilt(b,a,LCL);
ALL = filtfilt(b,a,ALL);
MCL = filtfilt(b,a,MCL);
P_flex = filtfilt(b,a,P_flex);
P_tilt = filtfilt(b,a,P_tilt);
P_twist = filtfilt(b,a,P_twist);
P_medlat = filtfilt(b,a,P_medlat);
P_antpost = filtfilt(b,a,P_antpost);
P_proxdist = filtfilt(b,a,P_proxdist);
quadForce = filtfilt(b,a,quadForce);

% Further, apply some smoothing:
SPAN = 0.2; % Span % of data
rot = smooth(rot,SPAN,'loess');
abd = smooth(abd,SPAN,'loess');
T_shift = smooth(T_shift,SPAN,'loess');
T_drawer = smooth(T_drawer,SPAN,'loess');
T_distract = smooth(T_distract,SPAN,'loess');
LCL = smooth(LCL,SPAN,'loess');
ALL = smooth(ALL,SPAN,'loess');
MCL = smooth(MCL,SPAN,'loess');
```

```
P_flex = smooth(P_flex,SPAN,'loess');
P_tilt = smooth(P_tilt,SPAN,'loess');
P_twist = smooth(P_twist,SPAN,'loess');
P_medlat = smooth(P_medlat,SPAN,'loess');
P_antpost = smooth(P_antpost,SPAN,'loess');
P_proxdist = smooth(P_proxdist,SPAN,'loess');
quadForce = smooth(quadForce,SPAN,'loess');

% Write variables to Excel file
% filename = 'Patella Tests.xlsx';
% sheet = 'Normal';
%
% xlswrite(filename,flex',sheet,'A1');
% xlswrite(filename,rot,sheet,'B1');
% xlswrite(filename,abd,sheet,'C1');
% xlswrite(filename,T_shift,sheet,'D1');
% xlswrite(filename,T_drawer,sheet,'E1');
% xlswrite(filename,T_distract,sheet,'F1');
% xlswrite(filename,LCL,sheet,'G1');
% xlswrite(filename,ALL,sheet,'H1');
% xlswrite(filename,MCL,sheet,'I1');
% xlswrite(filename,P_flex,sheet,'J1');
% xlswrite(filename,P_tilt,sheet,'K1');
% xlswrite(filename,P_twist,sheet,'L1');
% xlswrite(filename,P_medlat,sheet,'M1');
% xlswrite(filename,P_antpost,sheet,'N1');
% xlswrite(filename,P_proxdist,sheet,'O1');
%  xlswrite(filename,quadForce,sheet,'P1');

%%
% Plot parameters vs time/sample
% ..........................................................
figure(1)
% Rotations:
subplot(2,3,1);
plot(flex)
title('Flexion-extension');
ylabel('Degrees');
xlabel('Samples');
subplot(2,3,2);
plot(rot)
title('Tibial rotation');
xlabel('Samples');
subplot(2,3,3);
plot(abd)
title('Add-abd');
xlabel('Samples');

% Translations:
subplot(2,3,4);
plot(T_shift)
title({'Medial/lateral tibial shift','along femoral x-axis'});
ylabel('Millimeters');
subplot(2,3,5);
plot(T_drawer)
title({'Displacement of tibial origin','along floating axis'});
```

```
subplot(2,3,6);
plot(T_distract)
title({'Height of femoral origin','above tibial transverse
plane'});

%%
% Plot parameters vs flexion angle:
% ..........................................................
figure(2)
% Rotations:
subplot(2,3,1);
plot(flex)
title('Flexion-extension');
ylabel('Degrees');
xlabel('Samples');
subplot(2,3,2);
plot(flex(1:L/2),rot(1:L/2))
title('Tibial rotation');
xlabel('Flexion (degrees)');
subplot(2,3,3);
plot(flex(1:L/2),abd(1:L/2))
title('Add-abd');
xlabel('Flexion (degrees)');

% Translations:
subplot(2,3,4);
plot(flex(1:L/2),T_shift(1:L/2))
title({'Medial/lateral tibial shift','along femoral x-axis'});
ylabel('Millimeters');
subplot(2,3,5);
plot(flex(1:L/2),T_drawer(1:L/2))
title({'Displacement of tibial origin','along floating axis'});
subplot(2,3,6);
plot(flex(1:L/2),T_distract(1:L/2))
title({'Height of femoral origin','above tibial transverse
plane'});

%% Ligament lengthening patterns:

figure(3)
subplot(1,3,1);
plot(flex(1:L/2),LCL(1:L/2))
title('LCL lengthening pattern');
ylabel('mm');
xlabel('Flexion (degrees)');

subplot(1,3,2);
plot(flex(1:L/2),ALL(1:L/2))
title('ALL lengthening pattern');
ylabel('mm');
xlabel('Flexion (degrees)');

subplot(1,3,3);
plot(flex(1:L/2),MCL(1:L/2))
title('MCL lengthening pattern');
```

```
ylabel('mm');
xlabel('Flexion (degrees)');


%% Patella Motion
figure(4)
subplot(1,3,1);
plot(flex(1:L/2),P_medlat(1:L/2));
title({'Medial/Lateral Patella Movement','relative to femur'});
ylabel('mm');
xlabel('Flexion (degrees)');

subplot(1,3,2);
plot(flex(1:L/2),P_antpost(1:L/2));
title('Anterior/Posterior Patella Movement');
ylabel('mm');
xlabel('Flexion (degrees)');

subplot(1,3,3);
plot(flex(1:L/2),P_proxdist(1:L/2));
title('Proximal/Distal Patella Movement');
ylabel('mm');
xlabel('Flexion (degrees)');

%% Quadriceps force
figure(5)
subplot(1,2,1);
plot(quadForce);
title('Quadriceps force during squat motion')
ylabel('Newtons')
xlabel('Samples')

subplot(1,2,2);
plot(flex,quadForce);
title('Quadriceps force during squat motion')
ylabel('Newtons')
xlabel('Flexion (degrees)')


%%
% A = [-6.216, -34.478, 292.233];
% C = [-5.423, -15.369, 377.029];
%
% V = C-A;
%
% Q1 = [0.9933657, -0.1127529, 0.0068373, 0.0215567];
%
% R1 = quat2rotm(Q1);
%
% V1 = V/norm(V)
% Z1 = R1*[0 0 1]'
% Z2 = R1'*V1'
```

Func tibiaProbe

```
function [ RT_t2a, TO_p2t, ZT_p2t ] = func_tibiaProbe(A_data)
%Functn_tibiaProbe - Get constant rotation matrix from tibial tool
to
% tibial anatomic coordinate system.
%   This function uses the probe/virtual marker points to
establish
%   a coordinate system at the proximal tibia with the identified
%   anatomic bone landmarks. The anatomic coordinate system (ACS)
is
%   relative to the tibial tool 339. This function ensures that
the tibia
%   does not have to be kept fixed/stationary when the anatomic
landmarks
%   are identified with the probe.

% p2t - probe points referenced 2 tool
% t2w - tool to world
% p2w - probe points referenced 2 world
% TO_p2t - Proximal tibia point (tibia ACS origin), relative to
tibial tool

% -----------------------------------------------
xT_lateral_p2w = A_data(12, 11:13)'; % => Column vector
xT_lateral_t2w = A_data(12, 6:8)'; % Position of tibia tool
% relative to the world at time of taking the lateral tibia point
reading.

% Quaternion rotation from world to fixed tool on tibia at time of
taking
% lateral digitized/probe point:
QT_lateral_w2t = A_data(12, 1:4);
RT_lateral_w2t = quat2rotm(QT_lateral_w2t); % Rotation matrix of
quaternion
% -----------------------------------------------
xT_medial_p2w = A_data(14, 11:13)';
xT_medial_t2w = A_data(14, 6:8)';

QT_medial_w2t = A_data(14, 1:4);
RT_medial_w2t = quat2rotm(QT_medial_w2t);
% -----------------------------------------------

zT_distal_p2w = A_data(10, 11:13)';
zT_distal_t2w = A_data(10, 6:8)';

QT_distal_w2t = A_data(10, 1:4);
RT_distal_w2t = quat2rotm(QT_distal_w2t);
% -----------------------------------------------

zT_proximal_p2w = A_data(15, 11:13)';
zT_proximal_t2w = A_data(15, 6:8)';

QT_proximal_w2t = A_data(15, 1:4);
RT_proximal_w2t = quat2rotm(QT_proximal_w2t);
% -----------------------------------------------
```

```
% Write all probe points i.t.o. tool coordinate system; apply
rotation
% => Creates constant vectors from fixed tool to digitized/probe
points,
% i.t.o. tool system of axes:
xT_lateral_p2t = RT_lateral_w2t' * (xT_lateral_p2w -
xT_lateral_t2w);
% q = QT_lateral_w2t;   qn = quatconj(QT_lateral_w2t); R =
(xT_lateral_p2w - xT_lateral_t2w)
% xT_lateral_p2t = quatmultiply(quatmultiply(qn,R),q);      => r =
(q*)R(q)
xT_medial_p2t = RT_medial_w2t' * (xT_medial_p2w - xT_medial_t2w);
zT_distal_p2t = RT_distal_w2t' * (zT_distal_p2w - zT_distal_t2w);
zT_proximal_p2t = RT_proximal_w2t' * (zT_proximal_p2w -
zT_proximal_t2w);

% Tibia ACS
% => Creating the bony system of axes from digitized points:
Ztt = zT_proximal_p2t - zT_distal_p2t;
xT_temp = xT_lateral_p2t - xT_medial_p2t;
Ytt = cross(Ztt, xT_temp);
Xtt = cross(Ztt, Ytt);
% Unit Vectors (Normalized):
XT_p2t = Xtt/norm(Xtt);
YT_p2t = Ytt/norm(Ytt);
ZT_p2t = Ztt/norm(Ztt);

% XT_p2t - Unit vector of x-axis on tibia anatomic CS, medial to
lateral
% YT_p2t - Unit vector of y-axis on tibia ACS, posterior to
anterior
% ZT_p2t - Unit vector of z-axis on tibia ACS, distal to proximal
% RT_t2a - Rotation matrix of tibial tool to ACS - constant value

% Rotation matrix to go from tibial tool to tibial anatomic coord
system
RT_t2a = [XT_p2t, YT_p2t, ZT_p2t]';  % => [XT_p2t, YT_p2t, ZT_p2t]
=
%                                          [XT_p2t(1) YT_p2t(1)
ZT_p2t(1);
%                                          XT_p2t(2) YT_p2t(2)
ZT_p2t(2);
%                                          XT_p2t(3); YT_p2t(3)
ZT_p2t(3)]

% TO_t2p - Proximal tibia point (tibia ACS origin), relative to
tibial tool
TO_p2t = zT_proximal_p2t;

end
```

func_trackedMotion

```
function [ TT_t2w, RT_w2t, TP_t2w, RP_w2t, L ] =
func_trackedMotion(T_data, P_data)
%func_trackedQuat This function reads the quaternion data received
from the
%sensor. The femoral tool is used as the reference/world
coordinate system.
%   T - Tibia
%   t2w - tool 2 world
%   w2t - world to tool
%   QT_t2w - Quaternion orientation/rotation for tibial tool to
world CS
%   RT_t2w - Rotation matrix for tibial tool to world CS
%   L - length/amount of motion data captured
%   TT_t2w - Tibial tool position in terms of the world coordinate
system

%% Tibia Tool:
% Orientation
Q_wt = T_data(:,1) ; Q_xt = T_data(:,2) ; Q_yt = T_data(:,3) ;
Q_zt = T_data(:,4) ;
QT_w2t = [Q_wt, Q_xt, Q_yt, Q_zt];

RT_w2t = quat2rotm(QT_w2t);
L = length(QT_w2t);

% Position
T_xt = T_data(:,6) ; T_yt = T_data(:,7) ; T_zt = T_data(:,8) ;

TT_t2w = [T_xt, T_yt, T_zt];

%% Patella Tool:
% Orientation
Q_wp = P_data(:,1) ; Q_xp = P_data(:,2) ; Q_yp = P_data(:,3) ;
Q_zp = P_data(:,4) ;
QP_w2t = [Q_wp, Q_xp, Q_yp, Q_zp];

RP_w2t = quat2rotm(QP_w2t);

% Position
T_xp = P_data(:,6) ; T_yp = P_data(:,7) ; T_zp = P_data(:,8) ;

TP_t2w = [T_xp, T_yp, T_zp];

end
```

Func_femurProbe

```
function [ RF_t2a, FO_p2t, F_LCL_p2t, F_MCL_p2t ] =
func_femurProbe( A_data )
%func_femurProbe - Get constant rotation matrix from femur/world
tool to
% femoral anatomic coordinate system.
%   This function uses the probe/virtual marker points to
establish
%   a coordinate system at the distal femur with the identified
%   anatomic bone landmarks. The anatomic coordinate system (ACS)
is
%   relative to the femur tool 339. This function ensures that the
femur
%   does not have to be kept fixed/stationary when the anatomic
landmarks
%   are identified with the probe.

% p2t - probe points referenced 2 tool
% t2w - tool to world
% p2w - probe points referenced 2 world
% FO_p2t - Distal femur point (femur ACS origin), relative to
femoral tool
% ------------------------------------------------
xF_lateral_p2w = A_data(2, 11:13)'; % Column vector

% ------------------------------------------------
xF_medial_p2w = A_data(3, 11:13)';

% ------------------------------------------------
zF_distal_p2w = A_data(1, 11:13)'; % Femoral ACS origin point

% ------------------------------------------------
zF_proximal_p2w = A_data(4, 11:13)';

% ------------------------------------------------

% Femur ACS
% => Creating the bony system of axes from digitized points:
Zff = (zF_proximal_p2w - zF_distal_p2w);
xF_temp = (xF_lateral_p2w - xF_medial_p2w);
Yff = cross(Zff, xF_temp);
Xff = cross(Zff, Yff);
% Unit Vectors (Normalized), in world coordinate system:
XF_p2t = Xff/norm(Xff);
YF_p2t = Yff/norm(Yff);
ZF_p2t = Zff/norm(Zff);

% XF_p2t - Unit vector of x-axis on femur anatomic CS, medial to
lateral
% YF_p2t - Unit vector of y-axis on femur ACS, posterior to
anterior
% ZF_p2t - Unit vector of z-axis on femur ACS, distal to proximal
% RF_t2a - Rotation matrix of femoral tool to ACS - constant value
```

```
% FO_p2t - Distal femur point (femur ACS origin), relative to
femur/world
% tool:
FO_p2t = zF_distal_p2w;

% Rotation matrix to go from femoral/world tool to femoral ACS
RF_t2a = [XF_p2t, YF_p2t, ZF_p2t]';

F_LCL_p2t = xF_lateral_p2w;
F_MCL_p2t = xF_medial_p2w;

end
```

func_patella

```
function [ RP_t2a, PO_t2p ] = func_patella(A_data, RF_t2a)
%func_patella: SFunction that determines coordinate system on
patella
%   Detailed explanation goes here

% Rotation matrix of patella sensor to world coord system at
reference pos
QP_ref = A_data(6, 1:4);
RP_ref = quat2rotm(QP_ref); % Rotation matrix from patella sensor
to source at ref position

P_post_p2w = A_data(7, 11:13);  % Probe position at posterior
patella, or patella ACS origin
P_post_t2w = A_data(7, 6:8);    % Patella tool 338 position when
probe point taken
QP_post_w2t = A_data(7, 1:4);   % Orientation quaternion of
tool338 when probe point taken
RP_post_w2t = quat2rotm(QP_post_w2t); % Rotation matrix tool338 to
world; Rsepo

% Constant vector from patella tool to patella ACS origin, i.t.o.
patella
% tool system of axes:
PO_t2p = RP_post_w2t*(P_post_p2w - P_post_t2w)';    % Cpo

% Assuming that the patella ACS and femur ACS have parallel axes
at
% reference position, RP_t2a is rotation matrix from patella tool
to
% patella ACS at reference orientation (full extension).
% RP_t2a stays constant:
RP_t2a = RF_t2a*RP_ref; %Rpo

end
```